Dissertation

submitted to the

Combined Faculty of Natural Sciences and Mathematics

Ruprecht-Karls University Heidelberg, Germany

for the degree of

Doctor of Natural Sciences (Dr. rer. nat.)

Presented by

M.Sc. Bio-Phys. Tawheed H. A. Mohamed

Born in Alexandria, Egypt

Oral examination: 18-07-2014

In-situ and *ex-situ* studies of barnacle proteinaceous cements settled at earlier time points using μ-Raman spectroscopy and synchrotron based X-ray microprobe fluorescence techniques

This dissertation was carried out at the
Department of Applied Physical Chemistry
University of Heidelberg

Referees:
Prof. Dr. Michael Grunze
apl. Prof. Dr. Hans-Robert Volpp

Abstract

Among the different biofouling species, barnacles resemble a specific threat as they are difficult to remove, able to damage fouling release coatings and increase the drag force of ships. Additionally, barnacles are a good model system for research on permanent underwater adhesion strategies. This study aims to understand and compare the spatial organization and the chemistry of the adhesive secreted by two different species (*Balanus amphitrite* and *Balanus improvisus*) of cyprid larvae and juvenile barnacles for settlement. Raman spectromicroscopy and synchrotron based X-ray microprobe fluorescence analysis have been applied for the *in-situ* and *ex-situ* investigation of juvenile barnacle cement chemistry. Confocal Raman spectromicroscopy revealed the chemical heterogeneity of the barnacle baseplate and allowed to distinguish three regions of various chemical compositions. The adhesive of cyprids was different from the one of larvae and analyzed in detail from the metamorphosis to the age of fourteen days. The results of these studies provided information on the chemical composition and morphological structure of both barnacle species at different life stages.

Kurzfassung

Unter den verschiedenen *Biofoulern* stellen die Seepocken ein besonderesgroßes Problem dar. Es ist schwer sie von Oberflächen zu entfernen, sie sind dazu in der Lage *Fouling-Release* Oberflächen zu beschädigen, und wenn sie an Schiffsrümpfen vorkommen, erhöhen sie die Reibung des Schiffs im Wasser. Ausserdemstellen die Seepocken ein hervorragendes Modellsystem zur Untersuchung von Unterwasserhaftungsstrategien dar. Diese Studie zielt darauf ab die räumliche Organisation und die chemische Zusammensetzung des Klebstoffs zu verstehen, der von Seepockenlarven und adoleszenten Seepocken zweier verschiedener Gattungen (*Balanus amphitrite* und *Balanus improvisus*) abgesondert wird. Raman Spektromikroskopie und Synchrotron basierte Mikrofokus-Röntgenfloreszenzanalyse wurden zur *in-situ* und *ex-situ* Analyse des Klebstoffs adoleszenter Seepocken angewendet. Konfokale Raman Spektromikroskopieoffenbarte die chemische Heterogenität der Seepockengrundplatte und ermöglichte die Unterscheidung dreier Regionen unterschiedlicher chemischer Zusammensetzung. Der Klebstoff der Larven unterscheidet sich von dem Klebstoff der jungen Seepocken, welcher enDétail für Seepocken verschiedener Entwicklungsstufen, von der Metamorphose hin zu 14 Tage alten Seepocken, untersucht wurde. Die Ergebnisse dieser Untersuchungen liefern Informationen über die chemische Zusammensetzung und die Morphologie beider Seepockenspezies während verschiedener Lebensabschnitte.

Contents

Abstract I

1. Introduction 1

2. Theoretical background 3

2.1. Biofouling 3

2.1.1. Classification of marine biofouling organisms 4

2.1.2. Colonization process 5

2.1.3. Consequences of biofouling settlement 5

2.1.4. Antifouling approaches 6

2.1.5. Dispersal stage 7

2.2. Barnacle 8

2.2.1. Barnacle life cycle 11

2.2.2. *B. amphitrite* vs *B. improvisus* 14

2.3. Barnacle adhesives 15

2.3.1. Temporary adhesive "Footprint" 16

2.3.2 Cyprid cement 19

2.3.3. Adult barnacle cement 20

2.3.3.1. Morphological structure 21

2.3.3.2. Mechanical properties 22

2.3.3.3. Chemical characteristics and spectroscopic studies 23

2.4. Barnacle cement as biomimetic material 25

3. Motivation 27

4. Analytical techniques 29

4.1. Raman spectromicroscopy 29

4.2. µ-X-ray microprobe fluorescence (µ-XRF) 31

4.3. Scanning Electron Microscopy (SEM) 33

4.4. Confocal 3D laser scanning microscopy 34

5. Experimental procedure 36

5.1. *In-situ* studies 36

5.1.1. Raman spectromicroscopy 36

5.1.2. µ-X-ray microprobe fluorescence (µ-XRF): 38

5.2. *Ex-situ* studies 39

5.2.1. Scanning Electron Microscopy (SEM) 39

5.2.2. 3D scanning laser microscopy 40

5.3. Strategies of sample preparation 41
5.4. Reference substances 43
6. Results and discussion 44
6.1. Raman spectroscopy results 44
6.1.1. *In-situ* results of µ-Raman spectroscopy 44
6.1.1.1. Chemical variations across the juvenile barnacle baseplate 44
6.1.1.2. Reproducibility of spectra 49
6.1.1.3. Comparison of cyprid footprints and juvenile barnacle cement 50
6.1.1.4. Protein secondary structure of cyprid cements at different time points 51
6.1.1.5. Calcification process 54
6.1.2. *Ex-situ* Raman spectroscopy results 56
6.1.3. Discussion of *in-situ* and *ex-situ Raman results* 61
6.1.3.1. Comparison of spectra recorded at antennule region (*in-situ*), remaining cement (*ex-situ*), and cyprid footprints 61
6.1.3.2. Confocal Raman spectroscopy maps 67
6.2. µ-X-ray microprobe fluorescence results 69
6.2.1. *In-situ* results of µ-X-ray microprobe fluorescence 69
6.2.2. *Ex-situ* µ-X-ray fluorescence mapping of cyprid cement 72
6.2.3. Discussion of *In-situ* and *Ex-situ* µ-XRF mapping 74
6.2.3.1. The comparison between *in-situ* and *ex-situ* results 74
6.2.3.2. Possible explanations of the role of the detected elements 75
6.3. Similarity of juvenile cement of different barnacle species (*B. amphitrite* and *B. improvisus*) 76
6.3.1. Raman spectroscopy 77
6.3.2. Confocal µ-Raman spectroscopy 79
6.3.3. Calcification process 81
6.3.4. µ-X-ray microprobe fluorescence 82
6.4. Conclusion 83
7. Summary and outlook 86
List of abbreviations and shortenings 90
List of publications 91
List of conferences 92
Bibliography 93

1. Introduction

Have you ever seen a beautiful assembly of different shells and seaweeds on the waterline at pier or on the bottom of boats pulled out of water to the beach? Is not it amazing (Figure 1), the way these organisms form a solidary community and attach to the surface? However, the ordinary life of these marine dwellers conceals a number of undesirable drawbacks. Marine biofouling is an abundant conglomeration of marine organisms on immersed substrata and is one of the significant problems that subaquatic surfaces suffer from [1]. Just a few detrimental impacts that biofouling leads to are metal corrosion and decrease in efficiency of underwater constructions and equipment, e.g. ships and water cooling systems [1–3].

Figure 1: Variety of marine biofouling organisms [4–8]

Study of adhesive material of one of these sessile marine biofoulers, a barnacle, is the main aim of this research work. Barnacles are one of the most frequently observed calcareous biofouling organisms that attach to submersed surfaces by secreting a special, still obscure in composition, adhesive material, usually named ‘cement’ [9–11]. A number of scientific groups study this field intensively, trying to reveal the secrets of underwater adhesion and to find a solution for the economic and environmental problems caused by biofouling [11–13]. To prevent biofouling a detailed understanding of the barnacle adhesive cement, changes in its chemical composition and its interaction with different substrata will be very helpful. New knowledge about subaquatic adhesion mechanism will further help to develop new techniques to detach adult organisms from infected surfaces.

Barnacles produce several types of cement, [12] but not all of them are to date well studied. In contrast to adult cement, a detailed understanding of the temporary adhesive (footprints), and adhesives involved in the early stages of settlement (cyprid cement) is still lacking due to small amount of material and complexity of the experiments needed to be

conducted. Thus, there are still numerous questions which have not been answered yet. What is the difference between the temporary (footprint) and the permanent adhesives? Is the juvenile barnacle cement proteinaceous as the adult cement and if so, does it have the same type of protein with a similar secondary structure as the adult? Do different species have the same adhesive composition? How do the different chemical components distribute throughout the baseplate? Does the cement adhesive keep the same chemical composition throughout its life cycle, or does it change with time? What is the origin of the carotenoid signals? When do barnacles start to form their calcareous shells?

To answer these questions, this study focuses mainly on the determination of functional groups contained in juvenile barnacle cement and at the beginning of shell calcification, finding the origin of carotenoid signals in cement, and obtaining a elemental distribution map. Comparison between different barnacle species is important since not all barnacle species live in similar environmental conditions, which means that such environmental factors as temperature and salinity may cause differences in chemical composition and in the curing mechanisms of barnacle adhesives. The study of adhesives at the early life stages will show what changes, if any, occur in chemical composition and therefore may give a hint for developing antifouling techniques to prevent adhesive curing.

To date, the majority of research on barnacles was conducted *ex-situ*, which means that some specific information about the cement chemical composition could be lost after the death of the organism, its drying or treatment as a part of sample preparation, e.g. removal of the calcarious baseplate or bacterial contamination. Though experimentally more demanding, *in-situ* studies are a sensible way out. Thus, the aim of this work is to study the chemical composition of the temporary adhesive (footprint), as well as the time depending chemical distribution within juvenile barnacle baseplates of different species (*Balanus amphitrite* (*B. amphitrite*) and *Balanus improvisus* (*B. improvisus*)) using *in-situ* microanalysis techniques such as Micro-Raman spectroscopy, IR spectroscopy, and X-ray microprobe fluorescence analysis. Auxiliary results provided in this study, such as calcification starting time point; *in-situ* adhesive cement morphological information, including size and shape, at the early time points; and origin of the carotenoids found in the cement will help to add new pieces of information to the overall picture of barnacle cement enigma.

2. Theoretical background

2.1. Biofouling

Marine biofouling is an undesirable accumulation of organisms on immersed substrata (Figure 2), that is formed due to the special adherence to the surface. The highly adapted processes for temporary or permanent surface attachment that these organisms use [14] are usually referred to as "bioadhesion". Biofouling occurs naturally in a wide range of surfaces, either natural or man-made [1], and plays a vital role in organisms' life cycles and survival [14, 15]. Viscous substances, secreted by marine biofoulers, enable permanent or temporary adhesion, the mechanisms of which are not yet entirely understood. It is believed though, that two main steps determine the interaction between the adhesive, produced by biofouling organisms, and the surface [16]. The first step is wetting of the surface by the adhesive, while its curing process is the second step. The actual area of contact between the adhesive material and the substrate is defined during the wetting process, which is determined by the interaction force between the adhesive and the substrate. In the meanwhile, the curing process influences mechanical properties and strength of adhesion and is important for the solidified layer microstructure [16].

Figure 2: Different species of marine biofouling organisms settled on immersed substrata [17, 18]

Artificial objects that marine biofoulers choose are ship walls, underwater pipes, bulky subaquatic industrial equipment and water purifying or cooling systems at plants and power stations [16, 19]. Biofouling typically occurs in shallow coastal and tidal marine areas due to the comfortable conditions these waters provide for fouling invertebrates to grow [16, 20]. However, a great number of parameters may influence the degree of biofouling. Among all the factors temperature can be put into the first place. Even though extremely severe

biofouling majorly takes place in tropical areas, any warm waters and especially near-surface substrata, heated by the sun, are potential areas for fouling development. At present more than 4000 [21] biofouling species are known but their favorable conditions for settlement differ substantially.

2.1.1. Classification of marine biofouling organisms

Marine biofouling organisms can be divided into two main groups, micro-fouling and macro-fouling (Figure 3) [16]. Micro-fouling organisms include primarily bacterial and other microbial organisms which form biofilms on the submerged surfaces. Macro-fouling organisms such as, mussel, barnacle, sponge and tubeworm are more detrimental for offshore structures, ships, oceanographic instruments, etc. than micro-fouling due to its larger contribution to weight or hydrodynamic loading. This grouping includes abundant large plants and animals (100 µm to few centimeters), that may settle as independently or in large colonies. Macro-fouling organisms are generally classified into "hard" and "soft" fouling [16]. Calcareous shell-shaped hard skeleton is a distinguishing characteristic feature of hard fouling organisms and is designed to protect the organism's body from invasions or aggressive ambient media such as waves and water streams. The soft species such as sponges, anemones, bryozoans, contrariwise lack this kind of protection but have developed sophisticated protection mechanisms, for instance, toxicity.

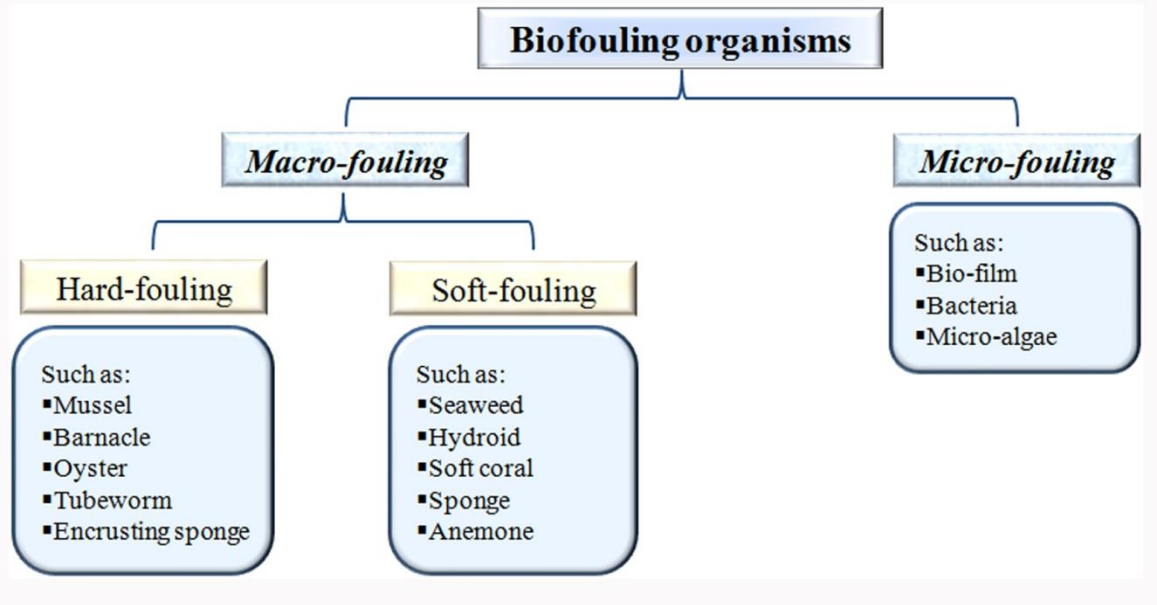

Figure 3: Classification of marine biofouling organisms.

2.1.2. Colonization process

In general, biofouling process starts instantly after the surface is immersed in water, no matter whether it is marine or fresh. When a clean surface is submerged in water, it adsorbs a number of organic macro-molecules, such as proteins, humic acids and carbohydrates that are present with minerals in the ambient water in order to build the initial form of the biofilm which is known as a conditioning layer [22–24]. Colonization of the conditioned substrata, being a highly dynamic process, depends on the surface characteristics, availability of the colonizing stages, speed of organisms surface exploration and attachment, season and geography of the place, and bio-ecological factors like predation and competition [25].

For quite a while it was reported that surface colonization occurs in a succession of steps, meaning that firstly the biofilm is formed on the substrata and within a week various fungi, protozoa and seaweed attach to it, which in several weeks is followed by settlement of larva of different invertebrate biofoulers, like barnacles. However, this is an oversimplification and a rather rough description model, since mobile spores of seaweeds and larvae of some bryozoans, hydroids and barnacles may settle in several minutes and in several hours, respectively, after immersion of the substrata. In comparison to linear succession model, the "dynamic" model gives a more balanced understanding of the surface colonization process, even though it is still misleading to assume that there is any direct relationship between the steeps following each other and that biofouling can easily be stopped by decreasing the extent or even completely eliminating one of the colonization stages. It has been observed in controlled laboratory experiments that attachment of larvae and spores can be affected by colonization of other organisms in positive, negative and neutral way [25].

2.1.3. Consequences of biofouling settlement

To date the problem of biofouling has become a matter of human concern in waters with widely varying salinity, streams and state of pollution [20]. Some percent of these species particularly selects vessel hulls as their target colonization place. In this case organisms, appearing as biofoulers, must be able to adapt to altering ambient conditions [20]. This becomes possible for those species that secrete special adhesives, i.e. barnacles, diatoms, tubeworm, mussels, green and brown algae. Furthermore, this adhesive substance is able to cope with constant changes in water salinity, temperature and vorticity of water flows around the hull. Despite these harsh conditions, invertebrates fouling have become a significant problem, which leads to diminishing the efficiency of subaquatic acoustic systems, e.g. sonic sound devices, corrosion or even destruction of underwater constructions [26–28].

Especially for marine vessels, barnacles resemble a tremendous challenge for shipping and industry [14, 29, 30]. Generally biofoulers tend to form an extensive colony, tightly attaching one to another. The weight of biomass, inhabiting 100 cm^2 of surfaces, cans increase to 0.7 kg in just five months after first settlement [19]. Moreover, accumulating organisms increase hull roughness and thus ship's frictional resistance, and reduce the power of water vortexes around the hull, thus helping new organisms to settle much easier with faster progression.

Consequential decrease in speed and maneuverability, e.g. loss of 86% efficiency at cruising speed to medium-sized naval combatant [31], may lead to increase of fuel consumption to 40% [20, 32], thus causing overall voyage costs augmentation to 77% [20, 33] and increased greenhouse gas emissions [20, 30]. Additionally, long-distance voyaging ships may cause occupation of different marine communities by non-native invaders, thus greatly affecting local ecology [20, 34, 35].

Due to the detrimental impacts biofouler colonization has to various aquatic structures, annually enormous efforts are put into development of innovative, environmentally benign antifouling solutions [36]. Each year world marine husbandry spends overall billions of dollars for various antifouling procedures, including preventive surface treatments, repair, and cleaning [14].

2.1.4. Antifouling approaches

The competition between ship's biofouling invaders and humans lasts since 2000 years. Since the beginning of navigation, different methods to avoid the undesirable effects of biofouling are being sought and specific antifouling approaches has been developed in science. Two main approaches, marked out through the centuries, are removal of adult organisms after substrata are abundantly fouled and preventing or diminishing the settlement from the beginning.

First approach turns out to be rather costly but is sometimes the only possible solution. Calcareous foulers may be dislodged by applying immense mechanical force, i.e. scraped off with a excavator bucket [20]. Another way of biofouling removal is application of different chemicals, most of which are toxic, in order to dissolve the calcareous shells and proteinous remains of organisms. Additionally, high voltages, UV, ultrasonication and laser treatment have been applied [20]. All these antifouling technologies require a significant increase in frequency of dry docking operations, which in turn includes time loss, waste of resources, and toxic wastes that has to be individually disposed.

The second approach is prevention of biofouling from the beginning and development of techniques that can restrain its rapid extension. Generally modern ways to maintain this are special antifouling coatings, emitting special chemical substance that deter attachment or secure settlement and specific surface morphology, uncomfortable for marine organisms to populate. Typically water flow around moving ship hulls is not strong enough to remove biofoulers that settle on biocidal antifouling paints [37].

In the middle of 1800s an idea of dispersing a toxicant in a polymeric carrier was employed in the development of paints [3]. Among the toxic antifouling paints modernly used are conventional paints based on paints pigmented with copper, usually cuprous oxide (Cu_2O), or soluble matrix paints; ablative paints, that are modern versions of conventional paints, and self-polishing systems, that clean themselves from organism by emission of toxicant that kills the settled organisms and surface becomes polished. The highly toxic component of self-polishing copolymer paints, introduced in 1974, tributyltin (TBT), turned out to cause diseases and genetic mutations in non-target organisms, and therefore is

currently prohibited worldwide and awoke special regulations to be applied to antifouling biocides. Just a few of biocide paints are contemporary in use, i.e. Sea-Nine 211 (an isothiazolone), zinc pyrithione (an fungicide also used in anti-dandruff shampoos) and Irgarol 1051 (a triazine herbicide) [16].As an alternative to biocide-containing paints, silicone release antifouling coatings have been developed. They minimize the adhesion strength of attached organisms, but are expensive and prone to tearing, and thus are employed only in specific applications, for instance, in locations where toxic paints cannot be used or on high speed vessels where release of biofouling is effective [16]. Additionally, biofouling organisms give their preference to ship hulls painted in dark or calm colors [20], whereas bright, toxic-colored surfaces are inhabited less frequently, therefore even this easy type of antifouling procedures can be effective. Furthermore, there are some works that suggest to stop fouling from the early life stages of biofoulers, for instance [38], that introduce Alcalase that inhibits barnacle cyprid settlement in a non-toxic way. Although all these approaches are quite different, the study of marine biofouling organisms is required for their optimization. A close collaboration of materials scientists, coatings specialists, chemists and biologists may result in development of innovative solutions or improving existing technologies. The knowledge about the settlement behavior of biofouling organisms is important for implementation of new antifouling ideas, but the mechanisms of underwater attachment remain poorly understood [36].

2.1.5. Dispersal stage

To solve the biofouling problem requires control of the dispersal life cycle stage. Biological dispersal is a dissemination process of various life forms, such as animals, plants, fungi, bacteria, etc., intended to find a new area for living and reproduction. The dispersal process of an organism can be divided into three main phases: larva release, transfer and settlement. During each of these phases different fitness costs and benefits are expected. Dispersal stage can be truly treated as the key life stage of sessile organisms, as molds conditions of organisms and the subsequent development stages by specifying its place of settlement, or to be precise, a place for all its future life. The abundance of adult biofouling species is strongly affected by the percentage of the successful larva settlement, which in turn is a direct consequence of successful larvae dispersal [39]. According to McQuaid studies, dispersal distance and successfulness of settlement will greatly influence not only a life cycle of an individual organism, but a whole population in general: neighborhood size, area where breeding geographically occurs, and ecological effects, e.g. genetic diversity [39]. Even a slight swimming ability of some animal biofouling species may have a dramatic influence on dispersal. Dispersal is hard to be assessed in a direct way that is why different modeling techniques and indirect estimation methods are generally used. In general dispersal can be discriminated into localized (for algae spore lings the distances may reach hundred meters) and long-distance types (animal larvae travelling distances may vary from tens of meters to thousands of kilometers) [39]. In order to complete this important life history process invertebrate larvae and algae spores must rapidly find an appropriate place for attachment and

safely bind to the surface. Upon the average, the duration of this process last for seconds, within which these organisms adhere to Subaquatic substrates under a wide range of relevant environmental parameters, e.g. water temperature, salinity and vorticity. Adhesion may become permanent from the beginning, but some species take some time to explore the surface to find the best settlement area and in this case the first attachment is not final and several places can be tested until the best one is found. Initial, first-contact adhesion is known as 'first-kiss' and is typical for different single- and multi-cellular fouling organisms, e.g. barnacles and tubeworms [16]. Contemporary marine fouling studies aim to conceive the cellular and molecular processes occurring within the materials involved. Dispersal stage is the perfect moment to prevent the fouling process from the start and therefore avoid all the undesirable impacts biofouling may cause. Therefore, further investigation of this early life stage of fouling organisms is highly desired.

2.2. Barnacle

The taxonomy of the barnacle family puts them in the phylum Arthropoda ("joint footed"), the class Crustacea ("the shelled ones") and the order Cirripedia ("curl-footed"), and barnacles are related to crabs and lobsters [40]. These cirripedia, whose around 1,220 species are known to date, are the most frequently observed biofouling organisms (Figure 4) [41]. Existing since Jurassic times, barnacles are thought to be one of the oldest surviving creatures on the planet, and their ancestry can be traced back nearly 500 million years [42]. Although there will have been some adaptations, the barnacle is thought to have changed very little over that time [43].

Figure 4: Consequences of barnacle invasion on boat hulls and pier structures. Images have been taken in Dekheila port, Alexandria, Egypt.

There are two general kinds of barnacles: stalked, that attaches to surface with a stipe, and the non-stalked barnacle (acorn, or sessile barnacle), growing their shells directly onto the substrate [49]. The majority of barnacles is hermaphroditic; however, most barnacles should be fecundated by a neighboring individual, that is why they tend to form extensive colonies. The average life span of most barnacles is from three to five years, sometimes up to ten, but some of the larger species are known to be much older. The most common barnacle belongs to the order Balanus.

Barnacles exclusively occur in the marine environment and prefer to inhabit shallow waters, three fourth of all species favor depth of less than 100 m, the rest are comfortable in the intertidal zone, although sometimes these marine biofoulers may settle up to 600 m deep [44]. Breaking waves may sometimes uncover the coastal line even for a significant period of time, but barnacles are well protected from drying out and water loss – they are capable to tightly close their shell, so the necessary amount of water is kept inside until the new tide comes [44].

Barnacles are most often seen as roughly circular sessile invertebrates, and are permanently attached to the substrate they live on. In their larval form they are free-floating, but eventually they attach themselves to any nearby rock, shell, or other object, even turtles or whales (Figure 5), and stay there for the rest of their lives [16]. Barnacles suffer from numerous predators, particularly at the larvae stage, when they float in the water searching for the most benign attachment site. At the adulthood, when their hard calcite shells are formed, they are well protected from the majority of predators, although whelks are capable

to break the shell. Some barnacle species are edible for humans, for instance, goose barnacles that are eaten in Spain and Portugal and *Balanus nubilus*, found in Puget Sound, which can grow as big as a foot in diameter [45].

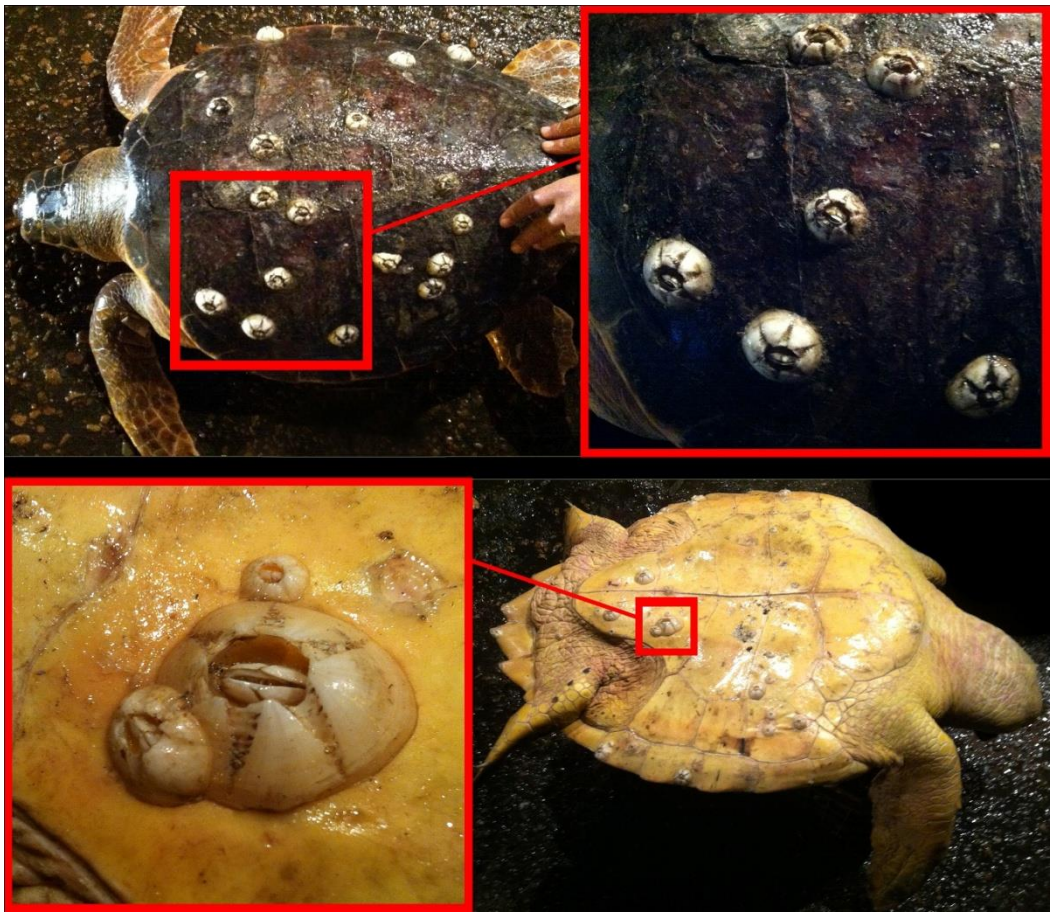

Figure 5: Barnacles settled on top and bottom sides of a turtle. Images have been taken in Dekheila port, Alexandria, Egypt.

The calcareous carapace of a barnacle consists of several plates, usually six: lateral and carino-lateral, two of each kind, a rostrum and a carina [46], which are allocated in the form of a ring and can be firmly intercoalesced or held together by muscles or other means. The inner surface of carapace is dissolved with a special chemical secreted when the shell becomes too tight for the growing barnacle, and new calcareous layer is simultaneously augmented from the outside. An operculum, possibly recessed into the carapace, covers barnacle's body from the top, which is oriented upside down, with limbs neighbouring the opening in the shell. Barnacle filter out food from the ambient water and move it closer to the mouth with help of "cirri"– six pairs of long (Figure 6), feathery thoracic limbs, being very sensitive, since barnacles' main sense is touch. It is hard to distinguish between different parts of barnacle's body, but generally it is subdivided into two major parts - a head, with several appendages, one of which is a vestigial pair of antennae attached to the cement gland and thorax, sometimes with the negligible abdomen present. Barnacles possess a minimal

cardio-vascular system, with a cavity close to the gullet, fulfilling the functions of heart. The oxygen is absorbed by barnacles from water through cirris and inner membrane of the shell. Maxillary glands serve as execratory organs. Barnacle may distinguish the difference between darkness and light with help of a single eye, originating from primary one of naupilius [47, 48].

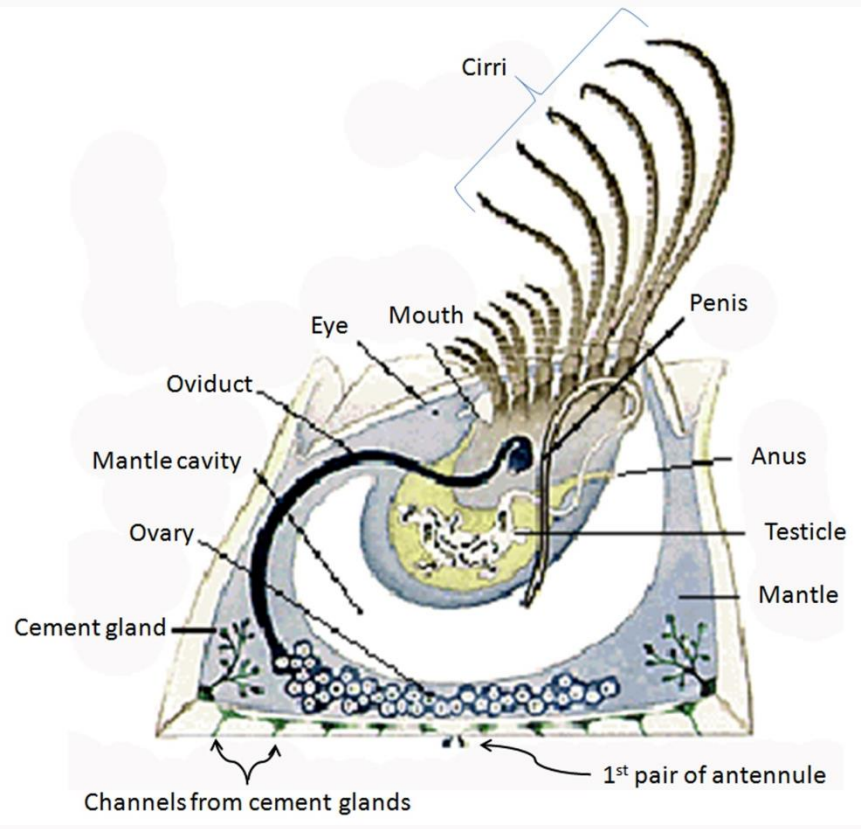

Figure 6: Anatomy of an adult barnacle [49]

Barnacles play an important role in structuring marine communities, and therefore are a matter of interest to community and behavioral ecologists [50, 51]. The key question these specialists are trying to solve is the chemistry that makes barnacles form gregarious settlement sites [10].

2.2.1. Barnacle life cycle

Barnacles, being among the most widespread intertidal organisms, undergo several transformations before they turn into harmful biofoulers. In general, the barnacle life cycle can be divided into three main phases: planktonic (pelagic), plankto-benthic and benthic [10, 46, 52]. The typical life-cycle of a barnacle is depicted in Figure 7, where the aforementioned major life stages are marked with capital letters A, B and C and sub-stages are references throughout the chapter. Successful conversion from a freely swimming naupli (A) into sessile

juveniles (C_1) is crucial not only for organisms development, but is also important for the overall colony development and species spreading [12].

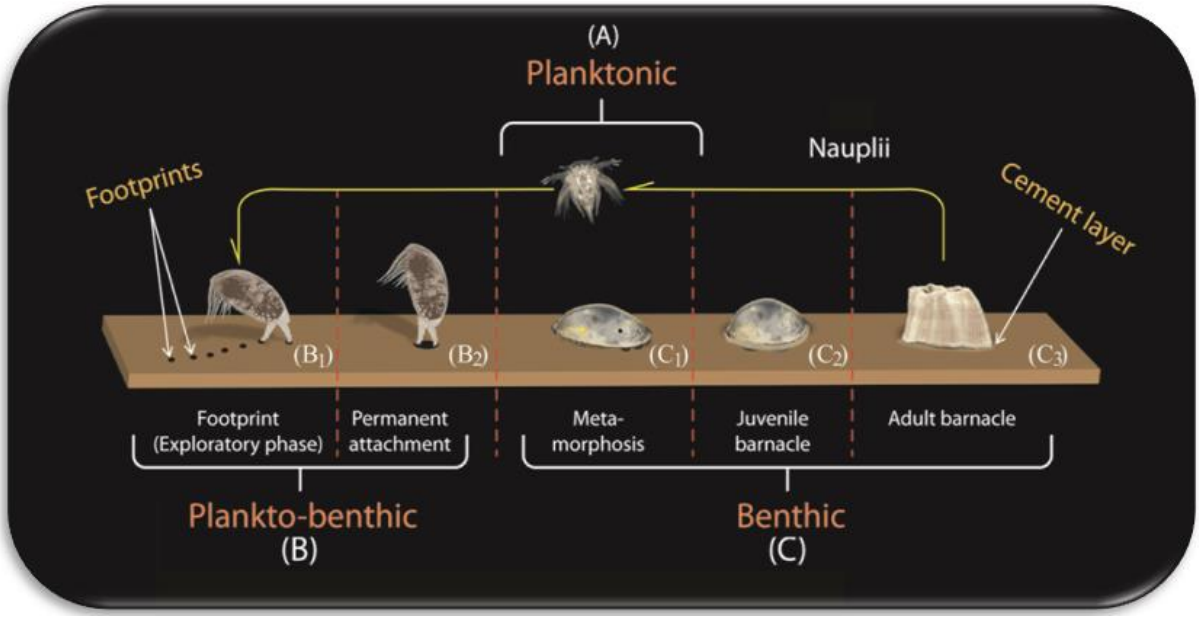

Figure 7: Main stages of the barnacle life cycle: *planktotrophic nauplius* (A), with the main function to store energy for the next phase; *lecithotrophic benthic* phase (B), exploration process (B_1), permanent settlement (B_2), and benthic phase (C): metamorphosis (C_1), juvenile barnacle (C_2), adult (C_3).

The first phase of the barnacle life cycle includes six pelagic nauplius stages (A), and plankton is the major food for this organism during the last five of these stages [12]. The main aim of this period in barnacle life is to devour/consume as much food as it possibly can in order to store enough energy for the future metamorphosis process (C_1).

After six naupilar substages [53], barnacle nauplii transform into a cyprids (B). Under laboratory conditions at 28°C it takes 5 days for *B. amphitrite* to complete all the stages from nauplius to the cyprid [12, 54]. Within cyprid phase the organism explores the surface and selects the most suitable area for settlement, and afterwards is competent to attach on a suitable substratum and undergo metamorphosis into the sessile juvenile stage [12, 53, 55, 56]. This attachment step is considered to be one of the most important in barnacle's life cycle. Instant settlement immediately after moult is possible for cyprids due to their peculiar adaptations, i.e. compound eyes that are developed in the nauplius stage VI [12].

Not all surfaces are, though, suitable for permanent barnacle settlement, and cyprids have a rather critical approach for making the final decision in order to ensure their survival and reproduction [12]. The substratum must have a specific microtopography, wettability, local hydrodynamics, surface colour, and presence of any other properties [16, 20, 57–61]. Moreover, recent research shows that there is a specific surface chemistry involved in barnacle choice of surface, particularly, cyprids of *B. amphitrite* prefer hydrophobic surfaces [56]. Furthermore, there are some additional factors that can influence colonization of the

chosen surface. For instance, low concentration of external Ca^{2+} can inhibit *B. amphitrite* larval settlement [52, 61, 62]. In order to ensure a successful metamorphosis into a sessile juvenile barnacle, cyprids must settle within days to weeks depending on culture conditions [12].

In order to find the most appropriate place for settlement, the cypris larvae initiate exploring process. At first cyprids descend from the water column, by navigating with paddle-like appendiges to potential settlement sites and for careful exploration [63, 64], but can return to the water column if substrata are found to be unsatisfactory [12]. Cyprid may develop maximum speed up to 60–95 body lengths per second, depending on species, and thorapod beat frequencies are approximately 15Hz for *B. amphitrite* [64–67]. If the surface is considered suitable, cyprid attaches to it using temporary adhesive, secreted from two specialized antennules, present already in nauplius, but transformed by cyprid stage to bear sensory structures located in an adhesive disc [12, 68, 69]. This initial, first contact attachment to substratum is known as "first kiss" [16]. Usually the place of initial attachment does not satisfy the cyprids completely and it needs to inspect the vicinity of the first attachment area by walking on their antennules as on stilts [63] (B_1) and thereby terminating the exploration process. Thus, cyprids take some additional effort to wander across the surface in a bi-pedal fashion at a maximum rate of two body lengths per second before they adhere permanently [12, 56, 69]. As an organism walks on the surface it leaves blobs of temporary adhesive, termed "footprints" (B_1), that have to date an unknown proteinaceous composition. Barnacles tend to form gregarious colonies, expansion of which is reinforced by settlement-inducing protein complex (SIPC), a large glycoprotein acting as a pheromone attracting new cyprids to inhabit the neighborhood [12, 70–72]. Both SIPC and footprint protein are possibly related, since footprints exhibit some pheromonal activity and they both are likely to be epidermal in origin [12, 50, 72, 73].

When the most appropriate settlement site is found, cyprid secures itself in a vertical position (B_2) and starts the process of permanent adhesion via secretion of permanent cement. This permanent adhesive is stored in secretory granules in a pair of specialized glands within the body of the cyprid [38]. Antennules, excited by neurotransmitter simulation [74], exude two cement components via exocytosis [69]. These components embed cyprid antennules into a globular disc less than 100 μm in diameter [12] by curing after being mixed together, and, therefore, adhere cyprid permanently to the selected substratum [63]. For *B. amphitrite* total curing time is estimated to be approximately 15 hours for the entire permanent cement plaque, and two hours for just the cement surface [12, 75].

After permanent settlement is successfully accomplished, cyprids start metamorphosis (C_1) into juvenile barnacles (C_2) that lasts around 12 hours [12]. During this process several major morphological changes take place: cyprid carapace is decorticated and a new chitinous layer is formed, compound eyes and setae degenerate, naupilar eye migrates and feeding cirri are developed [76].

Juvenile barnacles (C_2) grow secreting the permanent cement to enhance anchoring on the substratum and develop into adults with repetitive moulting, calcification of the outer shell and baseplate, and cementing [63,77]. Within a few months barnacles will be sexually mature

to bear eggs within the mantle cavity, that will eventually hatch and new nauplii will continue the life cycle in the water column [12].

Adult cement is secreted by adult cement glands 40 days after the metamorphosis [63, 78]. As adult barnacle grow, calcified material is deposited on the bottom of a set of interconnected side (parietal) plates, so the size of the organisms increases radially, expanding from the periphery [14] and thus, creating a series of concentric rings, visible underneath the barnacle and evolving from sequential growth involving molt cycles [13]. The enlarged marginal area in the calcareous base should be further fixed to the substratum, so it is assumed that the timing of cement secretion is tuned to the molting cycle [38, 63]. The rings are formed by extension of the cuticular membrane [89] followed by calcification; the adhesive is secreted and cured in place under the protection of the barnacle shell and continuous secretion throughout the life increases adhesive strength to the surface to reinsure organisms survival and successful continuation of the life cycle [13].

Thus, barnacles pass through three attachment processes in its life cycle: temporary attachment during the cyprid behavior, attachment with cyprid cement for settlement, and permanent fixation by adult cement [63, 77].

To date compositions of both, cyprid temporary and permanent adhesives, are high interest and investigation of them may allow to find innovative solutions for antifouling techniques, as well as integration of new biomimetic materials in human everyday life, i.e. dental service.

2.2.2. *B. amphitrite* vs *B. improvisus*

In this chapter the two barnacle species, *B. amphitrite* and *B. improvisus*, chosen in the current research work for cement properties comparison, are shortly described. Both species were first identified and characterized by Darwin in the middle of the 19th century [80, 81].

Balanus amphitrite, shown in Figure 8 (a), is a striped worldwide spread fouling barnacle, found in harbours and favouring the hulls of ships, rocks, pilings, seawalls, the shells of living oysters, mussels and crabs and can be found only in salty water. This species has a calcareous shell in conical shapes which consist of six red-brown rough integrated plates. The adult of this species can grow with a maximum diameter of about 20 mm. *B. amphitrite* may tolerate water temperature down to 12°C, but temperatures of at least 15–18°C and salinities of at least 10–15 ppt are required for it to breed [82]. In the Netherlands and Britain, barnacles settle in waters heated by the flow from sewers of power plants [82].

B. improvisus, shown in Figure 8 (b), is a sessile crustacean with a smooth white calcareous shell consisting of six integrated plates with diamond-shaped slightly toothed opening [81]. Adults of these species can grow up to 17 mm in diameter and 10 mm in height. It inhabits marine and brackish environments and does not reproduce in fresh water. The temperature range benign for *B. improvisus* is 0–30 °C, but optimum conditions for free swimming larvae are ~14°C. These species inhabit waters with a wide salinity range but major larval settlement is observed at medium salinities of 3–10 ppt. Large colonies of *B. improvisus* can be found attached to surfaces at six-meter depths, but these animals also

prefer waters up to the splash zone, although any long-run deaquation will be lethal to them [81].

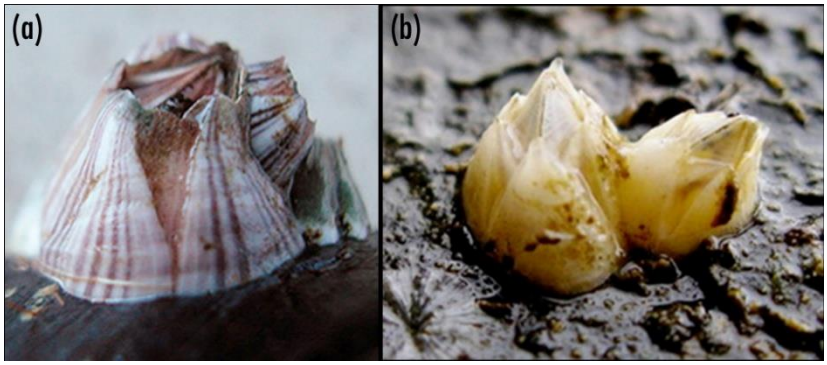

Figure 8: a) *Balanus amphitrite*, courtesy of Andrew N. Cohen, Center for Research on Aquatic Bioinvasions. [6] and b) *Balanus improvisus,* [83].

Native range of *B. improvisus* is Atlantic Ocean, most likely from American coast, but currently they have invaded Atlantic coast of Europe, Baltic, Caspian, Azov and Black Seas, Hawaii, African coast, Japan, Australian East Coast, New Zealand, Pacific coast of USA, Mexico, Columbia, Peru [84]. The native range of *B. amphitrite* is uncertain, but may be located in the Indian Ocean in the southwestern Pacific [85]. It has now spread to most of the warm and temperate seas of the world [86].

Both species are hermaphrodites, and reproductive individuals may simultaneously produce male and female gametes. However, the fertilizing generally occurs throughout crossing with neighbouring individuals that happen through sperm depositing into the mantle cavities of neighbouring barnacles via a long intermittent tube and following internal fecundation of eggs. Nevertheless, self-fertilization is also reported to occur [86–89]. Spawning for both species seasonality varies by location, averaging to two spawns in temporal areas, whereas barnacles living in tropical waters may spawn throughout the year, releasing 1,000–10,000 eggs/brood during maximum 24 broods/year [89].

The comparative study of both species (*B. amphitrite* and *B. improvisus*) may help to reveal any relationship between the environmental factors, such as temperature and salinity, and difference in chemical composition and adhesives' curing mechanisms of different barnacle species, if any exists. Moreover, this study may provide further information about applicability of the same antifouling techniques for different species.

2.3. Barnacle adhesives

The sophisticated attachment mechanism of Barnacle cirripedia includes several types of adhesives, that are represented in Figure 9. The first classification distinguishes temporary adhesive, that assumes reversible attachment, [16, 90] and permanent adhesive, designed for secure perpetual settlement [77]. Temporary adhesive, known as footprints and used by

cyprids during surface exploration, will be discussed in subsection 2.3.1. The notion of permanent adhesive includes cyprid cement, that is secreted during the first 5 weeks of barnacle life and is intended to safely anchor the organism on chosen surfaces and which is exuded [78], and adult cement, that corresponds to the whole bulk of material, coupling invertebrate to substrata, and new portions that are secreted during the growth of the organism [13]. Permanent cement in turn can be divided into primary and secondary adhesive. Secondary cement is secreted out when barnacle is dislodged from the surface, and the layer formed is much thicker than of primary cement. Despite the structural differences secondary cement allows repeated attachment [12, 63, 91]. Both cyprid and adult cements are reviewed in subchapters 1.3.2 and 1.3.3, respectively.

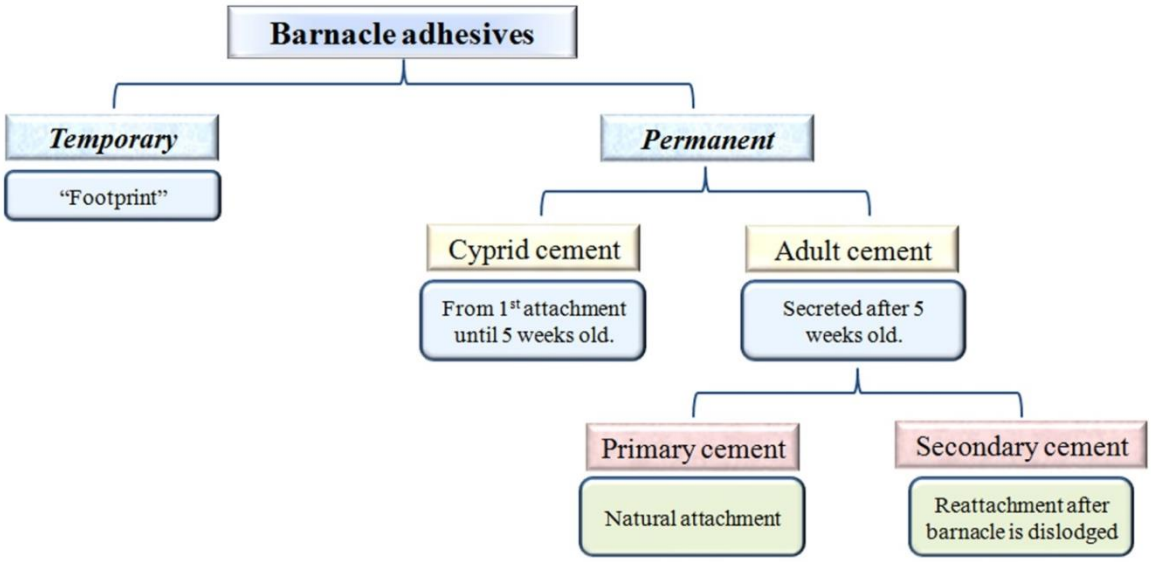

Figure 9: Classification of barnacle adhesives.

Barnacle cement study is a hard nut to crack, due to low amount of the material available at the earlier time points and underwater conditions that complex the *in-situ* analysis. However, there are a number of techniques applicable for barnacle cement physical, mechanical and chemical properties study. In this chapter major techniques will be mentioned in respect to their application.

2.3.1. Temporary adhesive "Footprint"

To date the majority of barnacle fouling studies are devoted to the adult barnacles, leaving out the exploration stage of cypris larva, that is an indisputable neglect, because this phase of Lifecycle can be truly treated as a key one. As described in subsection 2.2.1, after "first-kiss" affiliation to the supposedly benign neighborhood, cypris larva initiates an exploratory process, by walking in a stilt-like fashion along the surface [38]. While the organism examines the settlement suitability of a yet foreign substrata, it leaves behind blobs of a

proteinaceous secretion, known as "footprints", that can be detected by staining with the protein dye reagent Coomassie Brilliant Blue (CBB) [68, 90], particularly on a high protein-binding surface such as nitrocellulose membrane [50, 71]. Function and chemical content as well as physical properties of the footprint material is yet poorly understood due to the small amount of substance available for analysis. This substance is thought to function as temporary cement, granting cyprid the ability to adhere temporarily while 'walking' over the substratum, and secondary cue in entry-level settlement interactions [50]. In this chapter the major results of recent studies are reviewed.

The first attempts to interpret the mechanism of reversible, or temporary, attachment of cyprids started to appear in 1980s [12]. Due to the high inherent viscosity, the proteinaceous cyprids' footprint material has always been thought to maintain the adhesion between substrata and attachment disc, and thus considered as a 'wet' adhesive [12]. It is yet uncertain, if the adherence to surfaces is maintained only due to high viscosity of cement or barnacle can itself regulate and influence the adhesion [92]. Previously there existed a hypothesis that attachment may occur due to suction, created by encircling cuticular velum [93], but it was questioned by the fact that cyprids may explore even those areas where their antennular discs are not wholly connected to the surface, i.e. fine surface edges [78]; and finally refuted by Barnes 1970 [94], and Lagersson 2002 [95], who proved that low pressure underneath the adhesive disc cannot be created by the existing musculature of antennule. Later it has also been speculated [6] that the temporary adhesive may have several applications, e.g. it may act as a release agent or a substitute for water, favouring van der Waals interactions between the surface and the cuticular villi, due to a low dielectric constant environment created [38]. Phang 2008 [96], suggested that cuticular villi of the barnacle's attachment disc may adhere alike spatulae of geckos or pulvilli of flies [97], through increasing adhesion by contact cleaving [12]. Additionally, work [96] states the hypothesis that there might be other processes involved in viscosity of footprint, apart from the attachment tenacity of cyprids [12]. Thus, latest studies reveal that barnacle footprint cement is not just an adhesive, acting by wetting the substrata, but it can be a part of a complex adhesive system, that might consist of muscular behavior of the organism, chemical interactions between cement and substrata and other yet unknown factors [36].

Proteinaceous footprint cement is thought to be exuded on the coupled attachment discs of the ambulatory antennules by modifying tegumental glands, located in one of the segments of the antennules [50, 69, 98]. Two interfaces are characteristic to the deposited cyprid footprints: the protein-substratum and the protein-seawater interfaces; the latter of which is in contact with the cyprid antennular disc during adhesion [12, 36]. In the previous works [10, 38, 96, 99] cyprid footprints are referred to as a characteristic halo or oval doughnut shaped deposit, with a central circular area of approximately 10 μm in diameter, containing slight glycoprotein secretion. The sizes of individual footprints are measured to be 34.8±6.5 μm [50, 68, 71]. Examination of cyprid wide exploratory behaviour [95, 100] showed that average step between footprints equals 361.4±52.5μm [50, 68]. The tenacity with which cyprids attach to the surface are estimated around 0.026 MPa [12] from theoretical calculations, while the empirically obtained values are around 0.068–0.076 MPa on glass for

Semibalanus balanoides [72] Even though researchers managed to acquire values for temporary adhesion strength, the mechanism of tenacity stays unclear [12].

It is believed that footprints may serve as a pheromone, because gregarious settlement occurs even for surfaces that have been just explored by cyprids and do not have any adult barnacles attached [68, 72]. As mentioned in subsection 1.2.2, presence of footprints induces the settlement of conspecific cyprids [50, 68, 72], for instance footprints of *Semibalanus balanoides* may continue to attract new neighbors for over three weeks of exposure to running natural seawater [50, 72].

To date it is believed [50, 71, 72, 101] that the inducing protein complex (SIPC) is somehow related to the footprint. Firstly similarities between footprints and SIPC were noticed by Yule and Walker 1985 [72], who reported that they both are proteinaceous and are related to cuticle. Work of Matsumura 1998 [71], proved that they are related immunologically and suggested SIPC might be a component of the footprint or equivalent to it. Studies of Dreanno 2006 [101, 118], and Matsumura 1998 [71], showed that for *B. amphitrite*, SIPC is expressed in the larval stage, as well as shell and soft tissues of an adult barnacle - cirri, egg mass, and penis, all of which are parts of cuticle[101]. Additionally, glycoprotein complexes, i.e. α_2-macroglobulin-like protein, are found in both SPIC and footprints. Studies have shown that footprint proteins left on the surface after it has been explored by cyprids are contained SIPC [71]. Research of Dreanno 2006 [50], suggested that both SIPC and footprints might have epidermal origin, and according to Dreanno 2006 [50], and Nott and Foster 1969 [36], are a secretion of exocrine and tegumentary glands, respectively. Thus, it is currently believed that SIPC is a large cuticle glycoprotein contact pheromone [101–103], and is a part of footprint material or very similar to it [71]. Since SIPC is expressed in an entire cuticle [101], it is possible that this substance may also serve as a waterborne cue if released into the ambient environment [101].

Cyprid behaviour on different chemically functionalized surfaces are of high interest, and it is expected that the physiochemical properties of the footprint adhesive could be conceived through investigation of the bioadhesive morphology of cyprids [56]. There has been several research works conducted to reveal to which surface type, hydrophobic or hydrophilic, footprint has a greater affinity [97], and both works state that footprints show a morphological difference depending on what kind of surface they are deposited on. The work of Phang 2009 [97], declares that if secreted on hydrophobic surfaces (CH_3-glass) footprints are “larger in size and porous, with thick microsized fibres spreading across the surface”. Structural investigation of temporary adhesive on $–NH_2$-glass [95, 97] showed that footprints are still porous, but are much more restricted/bound and highly condensed with proteinaceous fibers at various length scales from nano- up to a few micrometers, containing isolated chains and bundles of protein aggregates in their network [56].

Despite a number of works on footprints overviewed in this chapter, it is still under the question if the footprint material is actually an adhesive or not. Unfortunately, barnacle footprints, e.g. *B. amphitrite* [50] are rarely observed due to their tiny dimensions, translucency and sparse distribution. Even though these properties of footprints hinder to use them as a realistic analytical sample, but currently they can be stained and examined with the help of AFM [38, 95] However, footprint adhesive material is a fruitful material for study, for

the reason that if the chemical composition of footprints is understood, the optimal solution to prevent fouling from the beginning might be found.

2.3.2 Cyprid cement

Alike temporary adhesive, described in section 2.3.1, that is not extensively described in literature, permanent adhesion of cyprids did not receive proper attention of researches due to the difficulty of its investigation [12]. The first study of cyprid barnacle cement, introduced by Walker in 1971 [104], opened the intricate study of young barnacle permanent adhesive. To date, more than 40 years later, total number of research articles about cyprid cement, studying its composition[10, 104], delivery [74, 105] and curing [12, 106], amounts to just 6pieces, latest published in 2009 by Schmidt [10].

Cyprid cement is a term usually referred to cementing exudate, secreted by cyprids at the antennule region during attachment and during the first 5 weeks of the organism's life until it becomes an adult [78]. As described in subsection 2.2.1, after the most suitable place for settlement has been found, cyprid secrets out of cement glands localized inside the body a liquid permanent adhesive, that is stored in secretory granules and is conducted through antennular cement ducts under nervous control [69, 104] and deposited on the surface in a globular disc around 100 μm (*B. amphitrite*) in diameter, that safely attaches cyprid to the substrata.

There has been stated a hypothesis that cyprid and adult cement are related, but there is still no solid evidence to prove it. Currently it is known that cyprid cement gland cells migrate and participle in the development of adult cement glands [104], but no adult cement genes were found in cyprids [107]. Work of Aldred 2008 shows that morphology of the cyprid cement studied with AFM differs dramatically from the adult adhesive, as examined in [108–110]. Protein chains of cyprid barnacle cement has been analyzed using the worm-like-chain model [13], but no novel information has been obtained and the protein structure of cyprid cement stays unrevealed. It is likely that adult and cyprid cement are not related according to molecular and morphological studies, described in [10, 12, 107–111].

Even though the exact composition of cyprid cement is still unknown, it is believed that it contains proteinaceous components and might be a highly tenacious heterogeneous glycoprotein material [10, 14, 38, 77, 104]. This fact is supported by presence of spatial distribution of the CH stretching (str.) bands in *in-situ* confocal Raman study of the juvenile barnacle cement confirming that cyprid cement has an organic matrix [10]. Furthermore, it is believed that proteins contained in this adhesive are initially water soluble, but cure underwater [69]. According to Phang 2006 [106], the cyprid cement of *B. amphitrite* cures within hours [75], or more precisely, within 70–120 minutes [38] after it has been secreted on the surface, which possibly can occur via quinine-tanning [10, 104], which is supported by the presence of diphenols and the enzyme polyphenoloxidase in the cement secreting apparatus.

The chemical composition of cyprid barnacle cement of *B. amphitrite* was examined *in-situ* with use of scanning confocal Raman microscopy [10]. The results of this study have

shown higher concentration of –OH groups present in the cement which supports an idea that water may influence the curing of the cyprid adhesive; that cyprid barnacle cement truly has an organic matrix what is proved by spatial distribution of C–H str. bands; but low signal for amide I band, which is anticipated to be contained in proteinaceous cement, but it is believed that a more careful experiment will reveal its spectra. Furthermore, according to the results of this Raman research, carotenoid signal is localized in the region where barnacle cement is expected, i.e. areas where cyprid cuticle contacts the surface, and carotenoids are mainly distributed in the outer boundary of the antennular discs and spreads to the sides from these organs [10]. In addition Martin Schmidt [10] suggested that the presence of highly intense carotenoid bands could be attributed to: a) the disc's cuticular villi and the vellum around the disc, or b) cyprids footprint adhesive blobs left behind after surface exploration. Furthermore, the structure of barnacles bodies have been reported to contain carotenoids. For example, the study of muscle fibers of the giant barnacle using Raman and resonance-enhanced Raman spectroscopic techniques has revealed two main bands of β–carotene at 1158 and 1520 cm^{-1} [112]. Carotenoids are in general known to play a role in antioxidation [113] and membrane reinforcement, e.g. cuticle [114]. In the current study, heightened attention to the presence of carotenoid in the material has been paid.

Additionally, some cyprid cement proteins were identified, for instance calmoduline (*B. amphitrite*), identical to one found in sea urchin, anemone, slug and copepod, that is suggested to be related to cement protein secretion [115].

Study of cyprid barnacle cement may elucidate the adhesion mechanism of barnacles, knowledge about its chemical composition may help in development of new antifouling materials and techniques.

2.3.3. Adult barnacle cement

In this subsection a short overview of the major up-to-date knowledge about one of the most lasting and a tenacious adhesive in the subaquatic environment [116], adult barnacle cement, is given. It is believed that permanent adult barnacle cement is started to be secreted by adult cement glands approximately 40 days after permanent attachment [78], although there are suggestions that it is obtained from the organism's circulatory system, since a number of blood proteins and cells was found in unpolymerized cement [9]. Burden et al 2012 [13], suggested that barnacle cement is exuded by at least two different secretions known as first barnacle cement secretion (BCS1) and second autofluorescent fluid (BCS2): BCS1 is released continuously during an animal's life, while the BCS2 is secreted only periodically.

As described in section 2.3, adult barnacle cement can be subdivided into two types – primary and secondary cement, based on differences in formation mechanism [91]. Primary adult barnacle cement is the material that occupies the place between substratum and baseplate, and its detailed study is a hard task, since this layer is normally not thicker than 5 μm [91]. On the contrary secondary cement samples can be collected much easier [117], since secondary cement is ascribed as hardened layer of white non-transparent material [117],

secreted after barnacle is detached from the surface. Delivery of primary adult adhesive is maintained through a network of ducts and capillaries, that could also provide extra adhesive material to repair the existing level by filling the gaps, or to conduct the new adhesive for reattachment after barnacle's dislodgement [13]. Both being proteinaceous in origin [118, 119], these cements are similar in amino acid composition [120] as well as peptide maps [119].

2.3.3.1. Morphological structure

In natural environment the thickness of dried layer of *B. amphitrite* primary cement is normally around 600 nm, but underneath a living organism it may reach up to several micrometers. In work of Sangeetha 2010 [28], it is reported that the overall structure of the primary barnacle cement layer is formed as shown in Figure 10. Thus, the layer consists of three parts: two smooth highly dense interface layers at baseplate-adhesive and adhesive-substratum boundary and the space between them is filled with mesh-like pattern of cement. It is believed that the dense layer neighbouring the substratum plays the role of etchant for metal surfaces and may act as a bacterial shield for the mesh-like layer [28].Work of Barlowet al 2010 [14], proved previous results of Wiegemann 2003 [121], that nanoscale morphology of primary barnacle cement is represented by fibrillar structures, what is also supported by Sangeetha [28].

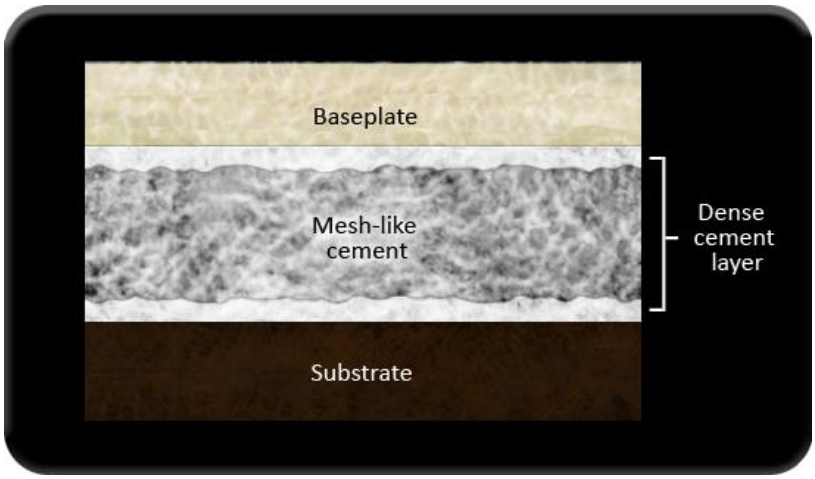

Figure 10: A schematic representation of solidified structure of barnacle cement over the substrate ([28] modified).

However, the thickness and morphology of barnacle adhesive layer differ dramatically depending on the nature of the substrata. On antifouling surfaces the layer is most likely to be thick and consist of non-transparent gummy material [14, 112–124]. According to Sangeetha 2011 [125], only 3mm of fibrous adhesive separate barnacle from the metallic substrata, whereas in order to attach to Poly(methyl methacrylate) (PMMA) surface 30 mm of porous sponge-like adhesive are needed. The explicit work of Berglin 2003 [110], shows that the

layer of primary barnacle cement on PMMA is hard and difficult to deform, with streaks from center to the periphery of barnacle and thicker in the center of barnacle. Moreover, it represents a continuous layer with traces of individual granules, and possesses good adhesion and mechanical locking into substrata. The primary cement on Polydimethylsiloxane (PDMS) has densely packed ellipsoidal granules of 75 or 85 nm by 10 nm, that are likely to be a conglomeration of several proteins and most likely other components.

The secondary cement is believed to consist predominantly fibrils, which proves that the major structural components for primary and secondary cements correspond [9]. According to both of Sangeetha 2011 [125] and Sullan 2009 [37], secondary cement of *B. amphitrite* is ascribed as a blend of globular, rod- and mesh-like constituents at aluminum foil substrata. In work of Daniel Barlow 2010 [9], it was reported that secondary cement layer of reattached barnacles was thicker at the periphery with expressed dense fibrils and thinner to the center of the baseplate with rare individual fibrils. The fibrils observed had a different thickness (from 2 to 25 nm), which probably means the various stages of fibril formation and appeared in 50–100 nm length segments and maximum height of 25 nm. Sangeetha 2011 [125], reports that secondary cement of *B. crenatus* contains 0.5 nm pores. One of the main features of secondary cement is that these fibrils can cross each other and form cross sections of a greater height in comparison to non-contacting ones [9]. Layer formed on low surface energy materials such as silicone rubber and PDMS are usually concave without easily distinguishable concentric ring cement structure [125].Therefore, adult cement morphology depends strongly on the type of substratum and its surface energy, barnacle species and formation mechanism – primary or secondary cement [125].

2.3.3.2. Mechanical properties

Adult barnacle cement is a viscoelastic adhesive, which hardness and modulus values greatly depend on the adhering substratum [125]. Work of Sangeetha 2011 [125] and Sullan 2009 [37], reports the modulus of 0.0002–0.09 GPa for fibrous matrix, rod-like structures and unstructured agglomerations in the adult barnacle cement. In the work of Dougherty 1990 [126], it is said that pull-of strength for barnacle cement lies in range $(0.14–2.79)*10^5$ N/m^2 for polystyrene substrata and its bond strength is reported on the work of Bowlin 2008 [127], to be $0.48*10^5$ N/m^2 for wet plastic substrata.

It is believed that the mechanical stability of the interface may be accomplished due to physical or chemical anchoring of interface proteins to the substrata in interconnected fibers and phenolic compounds present in adult barnacle cement [14]. Furthermore, it is likely that toughness on the 1–100 nm length scale is created by some structures of mechanically mobile 100 kDa cement protein [18]. Mechanical interlocking is another important property of adult barnacle cement [128], and plays a significant role in adhesion by taking the advantage of surface roughness already at nm scale. On surfaces, easy for attachment, a rigid structure is formed that may endure high tensile and shear forces, while a rubber-like cement formed on release coating resists a peeling load well [128].However, the details of the physical and chemical mechanisms enhancing the mechanical properties still remain an open question.

2.3.3.3. Chemical characteristics and spectroscopic studies

The adult barnacle cement is predominantly a proteinaceous substance, consisting of more than 90% protein [117–119, 129]. The primary cement of the adult barnacle (*B. amphitrite*) is reported to contain 20–50% of water by weight, while secondary cement contains as much as 87% [14], but a series of experiments showed that water is weakly bound [14].

On the base of Walker 1972 [118], Naldrett 1993 [130], and Kamino 1996 [119] research that several barnacle species have similarities in amino acid composition, an average composition suggested by Nakashima 1990 [131], was supported, but a usual component of mussel foot proteins, 3,4-Dihydroxyphenylalanine (DOPA) was however not found in the barnacle cement [119, 130].

The biochemical analysis shows the presence of amino acid compounds in adult barnacle cement and several proteins, six of which, with sizes of 7–165 kDa, have been identified [37, 119, 130, 132, 133]. The proteins identified in adult barnacle cement are extremely insoluble [132, 133], while others are easily soluble, thus revealing the complexity of chemistry involved in the interactions of cement constituents to maintain its unique properties [63]. Furthermore, it is believed that hydrophobic interactions may be responsible for the self assembly of adult barnacle cement [37]. Studies of chemical composition and chemical interactions within the cement are of the high importance to understand the unique properties of this underwater adhesive.

Through AFM, FTIR, IR-excited Raman, confocal Raman and other spectroscopic techniques, it has been proved that adult barnacle cement is proteinaceous material that contains multiple protein secondary structures [10, 110, 134–136]. Some of *ex-situ* FTIR studies were analyzing the secondary cement of dislodged barnacles and showed that adult barnacle cement is proteinaceous material that has various composition and structure depending on the surface types that barnacles were grown on [2, 28, 110].

Other alternative modern *ex-situ* IR approaches have also been used to examine the adhesive *ex-situ*, thus avoiding sometimes encountered difficulties in dislodging barnacles and manual collection of adhesive, e.g. in works of Sullan et al. [37] and Barlow et al. [9]. Sullan et al., collected the secondary cement of reattached barnacles that after being removed from the first time became repeatedly strongly adhered on CaF_2 substrata, while Barlow et al., [9] using the same system, compared between primary and secondary cement that was left on CaF_2 surfaces. Both works of Sullan et al. and Barlow et al., are focused to study the amide-I bands for determining the protein secondary structure of adult barnacle cement with use of Fourier Self-Deconvolution (FSD) and peak fitting.

Works of Sullan et al., [37] described that the protein secondary structure of the secondary cement of adult barnacle showed one dominant peak assigned to random coil structure with relation peak area 75%, and other three inferior peaks assigned to β-sheet. While, the works done by Barlow et al., showed that both primary and secondary barnacle cements have similar protein secondary structure primarily β-sheet secondary structures, but also α-helix, turn and disordered structures [10, 110, 134–136], generally with peaks at 1620 cm^{-1}, 1640 cm^{-1},1654 $cm^{-1}$and 1685 cm^{-1} for amyloid β-sheet, disordered, α-helix and β-turn structure, respectively (Table 1). Further information from amide-I analysis reports that β-sheet

structure was consisted of both globular and amyloid cross-β-sheet components. The important protein structure found frequently in marine adhesives and other biomaterials is amyloid [9, 11, 37, 137,138], with lower-frequency of amide I band at 1610–1630 cm^{-1} [14, 139].Works of Naldrett et al., and Kaminoet al., [130, 132, 133, 140] suggest high cysteine content of adult barnacle cement. The amyloid content may be higher than 20% of the overall peak areas, content of cross β-sheet is estimated to be in the range 22–28%, considering pure amyloid cross β-sheet in 35–80% range [14].

Table 1: Assigned ranges for protein secondary structures in Raman spectroscopy

Protein secondary structure	Range (cm^{-1})	Mostly (cm^{-1})	References
Amyloid β-sheet	1610 – 1630	1622	[9, 13, 14, 134]
Non-amyloid β-sheet	1630 – 1640	1633	[9, 13, 14, 134]
Disordered	1640 –1650	1645	[9, 13, 14, 134]
α-helix	1650 – 1655	1653	[9, 13, 14, 134]
β-turn	1670 – 1695	1685	[9, 13, 14, 134]

Barlow et al 2009 [134] with use of ATR-FTIR spectroscopy were able to study buried undisturbed interfaces of live adult barnacle cement settled under different conditions on double-side polished wafers. Results of this study showed that the main interface is essentially a proteinaceous material, as specified by both amide-I and amide II bands at 1637 and 1531 cm^{-1} respectively. In addition to amide bands there was a small peak at 1081 cm^{-1}related to presence of some polysaccharide materials. This result is in concordance with former biochemical analysis [127]. Furthermore, this study showed the difference in water content between the hard cement of removed barnacle (20% – 50% by weight) and the gummy cement of the live barnacle (up to 87% water by weight) [141]. This difference related to exposure of baseplate in case of *ex-situ* study to dry nitrogen for 48 h that removed approximately all the water in the sample content. Knowledge about water content of the untouched interface is significant for understanding the action of water displacement in marine bioadhesion.

To provide a general analysis of barnacle cements composition, Raman spectroscopy is considered a useful technique among other complementary biochemical methods [10, 136]. IR-excited Raman spectroscopy has been used by Wiegemann et al. to investigate disulfide (S–S) bond in the adhesive of adult barnacle (*Balanus crenatus*) [136]. Interestingly, Wiegemann et al. did not find any sign for S–S bonding in their Raman spectra, bringing it into correlation with the impact of polydimethylsiloxane (PDMS) release substrate (that barnacles had been attached to) on the cross-linking chemistry [142] through prevention of S–S bonding. Additionally, these authors noted that Raman S bands might be weaker in natural bioadhesives [138] than in reference protein spectra of materials with a high–cysteine residue fraction.

Furthermore, the chemistry of cyprid permanent cement was investigated by Shmidt et al [10], by applying confocal Raman spectroscopy technique to live juvenile, right after metamorphosis, uncalcified barnacles. This study showed the chemical differences between the remaining cyprid cement plaque and area around it. Despite the fact that water is a relatively weak Raman scatterer, a broad peak for –OH str. of water (3000–3800 cm^{-1}) is

observed in this study in the cured cement. Quinone chemistries have also been reported to be involved intocyprid attachment adhesives [74, 106]. What is more, the results of this study showed a strong band of C=C str. vibration (1480–1580 cm^{-1}) related to carotenoid [14]. Results of *in-situ* Raman spectroscopy holds great promise for real-time analyses of the adhesive chemistries of both permanent and temporary bioadhesives.

2.4. Barnacle cement as biomimetic material

For decades, scientists have been investigating the up growing problem of marine bio-fouling that causes damage to various underwater constructions and, therefore, bring about enormous financial losses. Various barnacle species are among the most widespread bio-fouling crustaceans and numerous minds toiling at solving this problem through development of new antifouling coatings and removal techniques. On the other hand, despite the great annual expenses that barnacles as marine bio-foulers put to worldwide marine industry and vessel husbandry, these benthic animals should not be though considered as just pernicious organisms. History of science shows that human may borrow numerous splendid ideas from essential to naturalistic mechanisms of survival and adaptation.

Cirripedia are unique benthic dwellers, that can inspire scientists to create new materials, that can find application in building industry, applied sciences and medicine. Barnacles possess two main characteristic features, hard calcareous shell and advance submersible adhesive, investigation of which may lead to significant and beneficial results. One of the most promising fields for adoption of new barnacle-related technologies are biocompatible materials such as bone implants and dental coatings.

The rigid outer shell of barnacles consists mainly of calcite (more than 90% calcite and about 1–5% other organic material) [2], a carbonate mineral and the most stable polymorph of calcium carbonate ($CaCO_3$) [143]. Due to the higher porosity of calcite crystals, they could favor better bonding with bone and hence can be an alternative to nacre which has aragonite crystals of higher density [144]. Calcium carbonate ($CaCO_3$) in many respects resembles hydroxyapatite, found in bones and teeth and used as implant material, and thus is biocompatible and osteoconductive [145]. Therefore, investigation of calcareous shell structure, chemical composition, terms of its build-up and shaping may help in the development of new biocompatible materials, i.e. bone implants.

Additionally, barnacle adhesive may suppress a fresh departure in dental treatment. Stable to chemical and enzymatic degradation within a wide range of temperatures, barnacle cement is a material consisting of 90 % protein [146]. Being insoluble in water and famous for its mechanical properties, *B. amphitrite* barnacle cement is thought to possess properties, sufficient for it to serve as an adhesive and sealant in dentistry [6]. Studies on barnacle cement can lead to the development of innovative biomimetic materials which can be used in dental biomedical applications and this approach will be overviewed in more detail in this chapter.

Dental adhesives and sealants used in contemporary dental treatment are intended to be resistant and protect teeth from penetration of carious bacteria [147]. However, biomedical

engineers face a number of problems in developing new materials of this type. Placed in the oral cavity, they must endure constant saliva wetting and exposure to various acidities as well as temperatures. Major requirements that a dental adhesive or sealant must meet to be clinically successful are colour stability, biocompatibility, convenience in use and secure bonding to teeth surface, considering that surface energy of enamel and dentin is relatively low and may be rough from various debris and have contaminations [147].

Barnacle cement may potentially serve as a powerful dental adhesive, due to its insolubility, short polymerization times, especially possible under water, and easy adherence to a variety of subaquatic substrata. Moreover, bonding strength of barnacle cement can be favourably compared to other modern dental adhesives. According to Despain1973, [148] barnacle cement has some advantages over some dental adhesives, i.e. zinc phosphate cement, when placed on a wet surface. However the majority of researchers in this field considers the potential of barnacle cement in dentistry solely based on its mechanical properties and biochemical composition. Application of barnacle cement as a dental adhesive and sealant was studied in [147], where acid resistance, biocompatibility, speed of polymerization and aesthetic appeal have been studied.

According to this study, barnacle cement has been found to be non-toxic for human and other living beings. Applied to teeth it keeps them aesthetically appealing, having a tint close to the natural teeth colour [149]. The polymerization can be speeded up under infra-red radiation with use of Ca^{2+} catalysts. However, one of the main obstacles to usage of barnacle cement in dentistry is its low resistance to a long-term strong acidic exposure. Nevertheless, the innovative dental adhesives and sealants based on barnacle adhesive are still possible to develop if the way to enhance the acid-tolerance and polymerization rate of the cement can be found [147].

3. Motivation

Barnacles, being among the most predominant bio-foulers in the world, are widely used as a "model for research on underwater adhesion" [10]. The study of this organism may help to understand the settlement mechanism of marine invertebrates and therefore lead to the development of preventive antifouling strategies [115]. Barnacles should be interesting to those who would like to use their adhesives commercially [4, 11]. Despite the extensive knowledge published on barnacles, the reader is likely to come across numerous questions that are still left without an answer and numerous assumptions that lack trustworthy proof.

First of all, understanding the spatial organization of chemical components contributing to the bio-adhesion chemistry is of fundamental scientific relevance with significant potential for commercial underwater adhesives and to develop new antifouling strategies [10]. Changes in chemical composition at the interface with time will allow to understand the chemical interaction of the cement and the substrate [28]. Furthermore, very little is conceived about the chemical changes that happen when barnacles secret and cure their adhesives. Barlow and Wahl [14] noted that interfacial approaches that use time- and spatially resolved spectroscopy for chemical analysis are essential to understand the curing chemistry of subaquatic bio-adhesives, which is a likely trend in material science, i.e., supra-molecular chemistry [117, 150] A library of these physiochemical properties of macro-foulers adhesives should be established and utilized in the design of new antifouling surfaces [4].

To date, many studies of marine bio-adhesion employ *ex-situ* methods to understand the bio-chemical composition of marine bio-adhesives but just several [9, 10, 110, 130, 134] conduct *in-situ* studies that allow to make noninvasive analysis [151].

Research *in-situ* is intended to conduct the study in original environment or an environment similar to the original excluding any significant altering of the system or its parameters. This study gives the advantage to acquire information that is much closer to real data since changes occurring in the sample are negligible. However, the difficulty of conducting such studies can surely be counted as its disadvantage.

Ex-situ study gives great opportunities to investigate a wide range of parameters, but it is necessary to check the correspondence of these results to the results obtained from an unaffected interface. In order to do that use of vibrational spectroscopy is a possible solution, since the ability to study intact interface is one of the advantages of this technique. Despite the difficulty of conducting *in-situ* experiment, almost all aspects of live adhesive interface can be assessed closely to the real characteristics, avoiding false underestimation that might stem from altering the sample during *ex-situ* analysis or simplified model study. What is more, *in-situ* analysis may offer acquisition of information about a wide range of processes occurring in bio adhesives: from adsorption and water displacement, to adhesion and cohesion processes. Sometimes model characterization can be used for complex cases, but its validity should be verified by real-time *in-vivo* study. Furthermore, phenomena that take place on the surfaces, that are crucial for bioadhesion may be observed, e.g. wetting and surface conditioning [14].

3. Motivation

Cyprid stage is unarguably the critical phase in the barnacle colonization of surfaces [12], and in several works it is emphasized this settlement stage, cyprid's exploratory behavior and cements, despite their significance for antifouling means [12, 152, 153], has surprisingly not received a proper scientific insight [10, 4, 12, 38]. Work of Alred 2008, [12] suggests that the future barnacle research should focus on cyprid adhesion and surface selection, because if substrata can be made unfavourable to them or if their adherence mechanism can be intervened, avoiding their settlement, the barnacle fouling in general may be prevented from the beginning and adult barnacles will not be necessary to be dislodged. Moreover, the adhesion strategy used by cyprids is also interesting in terms of creating a synthetic reversible adhesion system [4].

Moreover, temporary adhesion, or reversible attachment, of barnacles is even less deeply understood and although the proteinaceous liquid they secret as footprints is thought to maintain temporary adhesion, its exact contribution to adherence is still unclear [4, 12, 38]. Studies of footprints morphology as well as the cyprid settlement beahviour may help to understand the spreading and adhesion of footprint adhesive to the surface [4]. The probable relation of footprint and SIPC is also to be carefully investigated in order to find the ways how gregarious settlement behavior may be controlled and new ecologically-sensitive anti-fouling technologies may be developed [102].

Furthermore, more profound insight into processes of calcification and cementing are required [117]. Further studies are necessary to identify the presence of carotenoids in footprint, that can be done using Raman spectroscopy to scan substrata previously explored by cyprids, and perhaps their putative function will be known [10].

Thus, Raman spectroscopy and μ-XRF techniques have been applied to conduct research of juvenile barnacle cement *in-situ* and *ex-situ*. Raman spectroscopy has been used to study the chemical composition of barnacle cement and to identify distribution of functional groups in barnacle baseplates, whereas μ-XRF has been used to identify elemental distribution, in them.

4. Analytical techniques

In this section the analytical methods which were used in the both *in-situ* and *ex-situ* studies included in the current thesis are described.

4.1. Raman spectromicroscopy

In structural studies of molecules, polymers and crystals the phenomenon of Raman scattering, i.e. an inelastic photon scattering from a monochromatic excitation source, is widely used [154]. For instance, Raman spectroscopy, a method to determine modes of molecular motions, particularly vibrations, is based on this effect and is generally utilized for quantitative and qualitative analysis molecules that are bound covalently [155].

This effect was discovered experimentally in 1928 by subsequent Nobel Prize laureate C.V. Raman and named after him. Raman scattering can occurs when incident photon is in elastically scattered in two possible ways: a) when incident photon deposits its energy by exciting a "static" bond to vibrating, and scattered photon yet possesses less energy; and b) when incident photon gains energy after being scattered off a vibrationally excited bond. These effects are called Stokes- and anti-Stokes-shifted Raman scattering, respectively [156]. Afterwards, the intensity of this scattered light is measured and information about composition types of chemical bonds present in the sample can be obtained through automatically plotted spectra. A Raman spectrum is a plot of Raman scattered radiation intensity as a function of its frequency differencefrom the incident radiation,usuallyreferred to as Raman shift and expressed in units of wavenumbers, cm^{-1}.In both scattering cases, described above, Raman shift will have the same absolute value, but different charge.

The Raman effect has only a small probability and 1 out of 10^7 incident photons are Raman shifted. For this reason, the Raman line intensity isabout 0.001% of the source intensity, which complicates their detection and measurement. However, in general intensity of a normal Raman peak is a complex function of molecule polarizability, intensity of the source, the concentration of the active groups, and increases with the fourth power of the frequency of the source and is usually directly proportional to the concentration of the active species [154, 157]. Thus, intensity of a Raman signal I_{Raman} can be expressed in the following way:

$$I_{Raman} = NL\Omega \frac{\hbar}{2m\omega_k} \left(\frac{\partial \alpha}{\partial r}\right)_0^2 \frac{\omega_l^4}{c^4} I_l = NL\Omega \left(\frac{\partial \sigma}{\partial \Omega}\right) I_l,$$

where I_{Raman} and I_l are the intensities of the Raman line and the excitation laser, respectively; N is the number of bonds; L is the length of the focal volume; Ω is the solid angle over which the signal is collected; α is the polarizability; ω_k is the frequency of a normal mode of vibration of the molecule; $(..)_0$ indicates the value at equilibrium; ω_l is the frequency of

induced dipole moment; *m* is the reduced mass of the vibrating molecule; and change in polarizability $d\alpha/dr$ can be equaled to the differential scattering cross-section $d\sigma/d\Omega$ [156].

Generally, according to rule of mutual exclusion, or so called selection rule, molecular vibrations symmetric with respect to the main axis of symmetry are forbidden in the IR spectroscopy, whereas antisymmetric and some symmetrical molecular vibrations are both allowed in Raman spectroscopy [158]. Thus, due to this contrasting feature Raman spectroscopy can be considered as a complementary technique to Infrared spectroscopy, since it allows to analyze vibration modes that are IR inactive according to the mutual excusion rule. Infrared absorbtion is related to the variation of the electric dipole moment, whereas Raman scattering is concerned with the variation of the polarizability due to vibrations [158]. If the polarizability α in a molecule is changed during the normal vibration, a Raman active vibration can be detected [159]. Thus, due to the selection rules, Raman spectroscopy is specifically applicable in characterization of the carbon backbone of organic substances and polymers.

The main components of the Raman setup are a laser illuminating the sample, optics collecting the backscattered radiation, a high-efficiency laser line rejection filter, a spectrometer with an entrance slit, a diffraction grating, and a CCD camera. During the experiment, the intensity of the inelastic scattered light arising from monochromatic light focused on the sample is detected. A Raman spectrometer is usually used in combination with an optical microscope, which gives benefit in high spatial resolution of a confocal optical setup. A basic scheme of a simple Raman spectrometer is shown in Figure 11 [160]. Confocal Raman micro-spectrometers are capable to produce blur-free images of thick samples at various depths depending on both of wavelength and the optics. For example, in case of using wavelength: 532 nm and 20X objective (NA 0.45), the depths will be much greater than 20 micrometers [157]. A comparison of the optics of a confocal and a conventional Raman microscope is shown in Figure 11 (b).

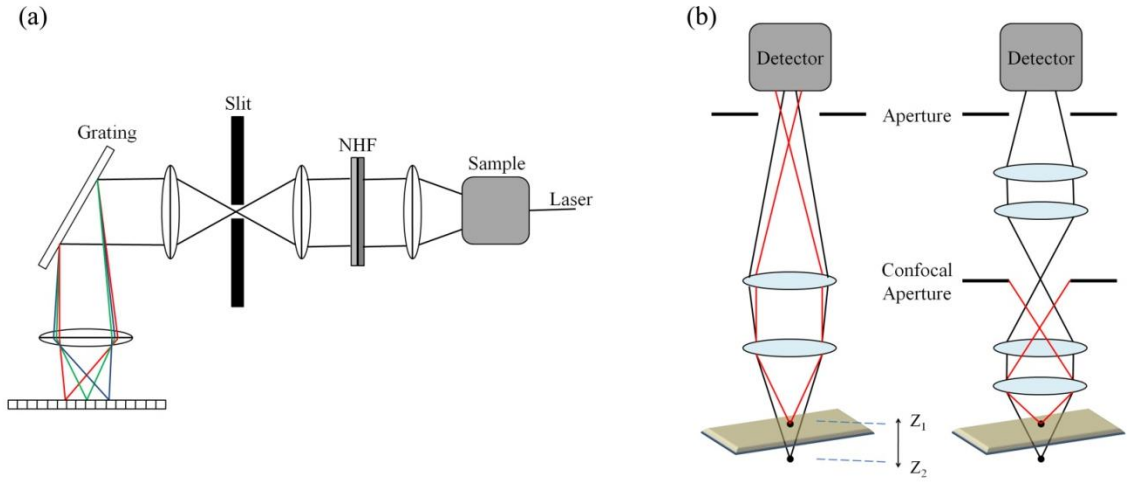

Figure 11: a) Scheme of a Raman spectrometer [160]. b) Conventional and confocal Raman microscope optics [161] (modified).

Raman spectroscopy as an investigation tool has several advantages. One of the major advantages of Raman spectroscopy is the possibility to study aqueous solutions or samples in aqueous media since water is a weak Raman scatterer [155]. It can be used to study a variety of samples, such as organic, inorganic or biological, in vacuum and in ambient conditions or even through different container walls. The possible of an *in-situ* analysis, is a great advantage over IR techniques [154]. In addition, minimal preparation is needed for gaseous, liquid and solid samples. An extensive Raman databases to date available to identify chemical components [155]. The region 4000 cm^{-1} to 50 cm^{-1} can be covered in a single scan without changing any bulky accompanying equipment, and small laser spot sizes allow to sample small areas [155] as the laser beam can be focused to 1 µm or less [157].

In comparison to IR spectroscopy, Raman spectroscopy provides information over a wider wavenumber range in a single measurement and its spatial resolution is much better due to the shorter wavelength of the probing light. Furthermore, the totally symmetric vibrations can be identified from the measurement of the depolarization ratios of Raman lines [154].

For decades Raman has been applied for protein analysis and has given an opportunity to study protein or peptide secondary structure and side-chain chemistries [162–164]. Vibrational modes of the protein amide band are used to observe secondary structure. Among amide bands of Raman spectroscopy amide I and amide III are those to which this technique is the most sensitive [165–166]. Furthermore, Raman spectroscopy is responsive to sulfur and ring structures of amino acid side chains [167].

However, Raman spectroscopy faces a number of problems. For instance, fluorescence and emission from hot samples may affect Raman spectroscopy. Furthermore, if the wavelength of the laser beam coincides with the absorption of the sample, than even an uncolored sample may be damaged during continuous irradiation by intense visible or near-ultra-violet laser beams [154].

4.2. µ-X-ray microprobe fluorescence (µ-XRF)

First proposed by Glocker and Schreiber in 1928, the use of fluorescent radiation excited by primary X-ray beam has become a powerful non-destructive analytical spectrometric technique. Attempts to confine the beam in X-ray fluorescence spectrometry taken over the last 20 years resulted into development of micro-XRF (µ-XRF) analysis, one of the modern beam impingement techniques. This method is based on the localized excitation and analysis of a microscopically small area on the surface of a larger sample, providing information on the distribution of major, minor, and trace elements in heterogeneous materials [168].

Laboratory X-ray sources are generally used for µ-XRF spectroscopy, but this technique becomes significantly more powerful when exploited with X-rays emitted from a synchrotron radiation (SR) source that is ideal for the generation of microscopically confined X-ray beams due to their high intensity and directionality. SR-based µ-XRF combines high sensitivity with high spatial resolution and possesses a number of advantages in comparison to other microprobe techniques. The extremely high-obtained brilliance, possibility to be used in atmospheric conditions, completely non-destructiveness and high intensity and

directionality are other particular advantages of SR µ-XRF if it is compared to conventional X-ray tubes. Currently, the intensities of X-ray micro beams exceed 10^{10} photons/s·µm^2. A high SR photon flux is another advantage to utilize it on microscopically small areas of samples as it allows multi-elemental XRF analysis of small amounts of material. SR is particularly useful for trace element detection at sub-ppm level, i.e. ~10ng/g for Sr in organic matrix [168–169].

To date, µ-XRF experiments are conducted on a large number of existing storage rings, which make it possible to combine the unique possibilities of SR with the advantages of XRF as an analytical tool [168]. The SR-µXRF spectroscopy experiments in this thesis were performed at ANKA synchrotron radiation source (Karlsruhe, Germany) at the FLUO beamline, the general scheme of which is shown in Figure 12 [169].

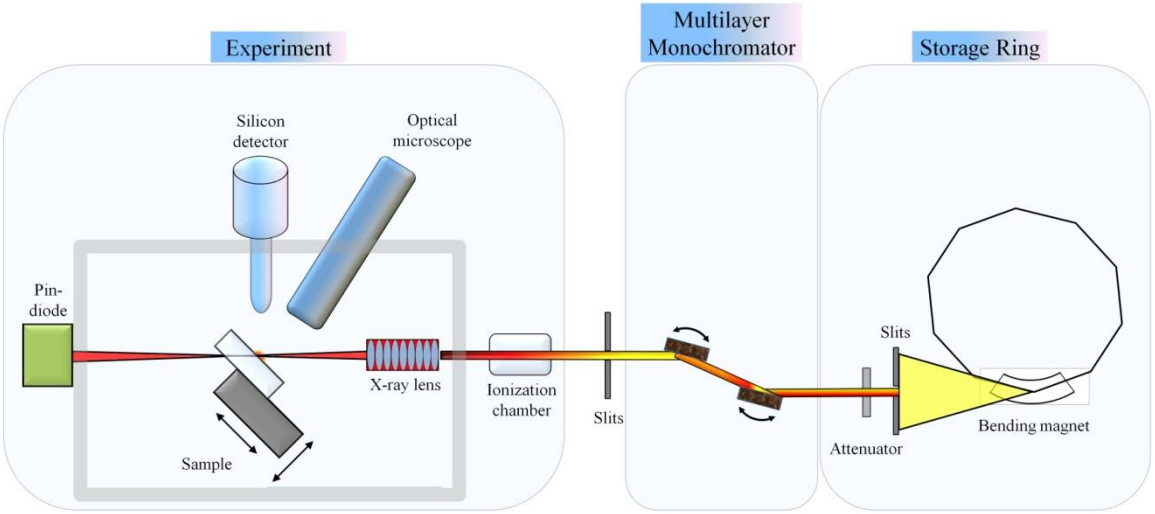

Figure 12: General scheme of SR-µXRF experiment at ANKA synchrotron source (Karlsruhe, Germany) [169] (modified).

The synchrotron radiation beam from a storage ring is monochromated by a double multilayer W-Si monochromator system with a fixed exit direction. Then, the beam passes through a monitoring ionization chamber, and enters the experimental vacuum chamber filled with inert gas and/or air under 10^{-2} mbar pressure. The energy of the photons can be selected between 1.5 keV and 33 keV with $\Delta E/E$ resolution of $2x10^{-2}$, which is sufficient for experiments close to the absorption edge. By X-ray lenses or polycapillaries the beam is focused onto the sample. The sample is placed on a mechanical sample stage with precision computer controlled micro stepping motors for X, Y, Z, that allow the sample to be moved over the beam path for acquiring the spectra for the measurement of elemental distribution maps. The size of the beam at sample can be adjusted from 5 mm x 2 mm down to 2 µm x 1 µm. The fluorescence radiation excited by the beam is measured by a semiconductor detector of the choice: energy dispersive Si(Li) detector, high purity Germanium detector or Silicon Multi-cathode Detector (SiMCD). PIN-Diodes (positive intrinsic negative diodes) at the exit

of the beam path are also used for monitoring the beam characteristics. Conducting experiments at FLUO beamline, it is possible to obtain 2D mapping of the sample with μm resolution and 3D information using confocal detector geometry or X-ray fluorescence computer tomography [169].

4.3. Scanning Electron Microscopy (SEM)

A scanning electron microscope (SEM), developed in USA in the beginning of the Second World War, is a type of electron microscope that scans the sample with a focused high energy electron beam and produces images containing information about the sample's surface topography and composition, that are computed from signals detected from electrons' interaction with sample atoms [170].

The region where the low energy secondary electrons can escape from is referred to as activated region and its size depends on the morphology of the sample surface. The deviation of the sample surface from flat topography induces a greater activated region and thus a greater number of secondary electrons that reach the detector what subsequently results in a higher signal [170].

A tungsten filament, a tungsten field-emission tip or Schottky emitter are typically employed in the SEM as electron source and the maximum accelerating voltage applied is typically 30 kV. Above the specimen, there two or three axially symmetric magnetic lenses, acting like condenser lenses, are placed (Figure 13). The diameter of the incident beam, also referred to as electron probe, in the SEM is usually10 nm, but can be reduced down to 1 nm or better if a field-emission source is used. Due to the method used to obtain the image, the performance of the final objective lens determines the spatial resolution of the instrument that can never be better than its incident-probe diameter. Specimens can be observed in high or low vacuum and in wet environmental conditions [170].

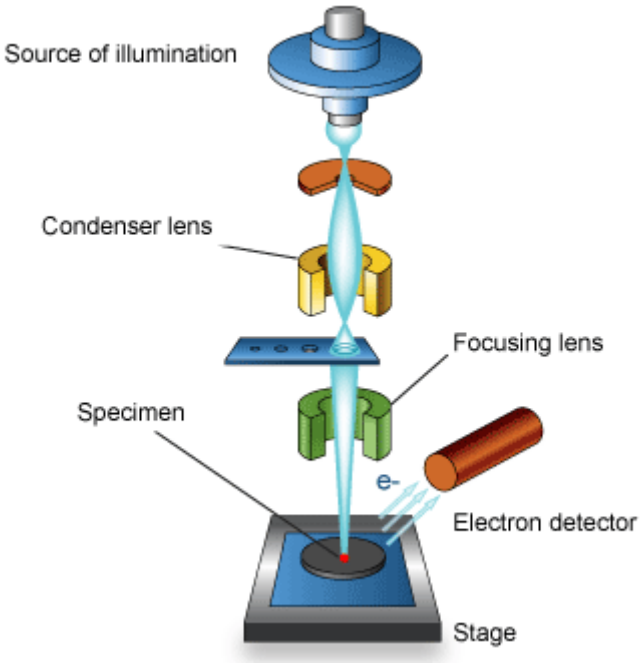

Figure 13: Schematic diagram of scanning electron microscope [171].

Interaction of the primary electron beam with sample atoms results in shell transitions, which lead to the X-ray emission with energy characteristics of the parental element, integrated detection and measurement of which provides the elemental analysis of the sample. This technique is called Energy Dispersive X-ray Spectroscopy (EDS or EDX) and can provide fast qualitative or quantitative analysis of elemental composition with 1–2 μm sampling depth and maps or line profiles of the elemental distribution of sample surface.

4.4. Confocal 3D laser scanning microscopy

Confocal 3D laser scanning microscopy (CLSM), is a valuable technique for obtaining high-resolution optical images and 3-D reconstructions (Figure 14 (a)) [172]. In a CLSM, the sample is irradiated by a laser beam, focused to a diffraction-limited spot, which illuminates one spot at a time and the specimen is therefore measured in a point-wise fashion [173]. A laser beam is focused by means of a microscope objective onto the specimen, where it excites fluorescence. A dichroic beam splitter efficiently directs the fluorescent radiation collected by objective to the detector. An emission filter is used to choose the fluorescence spectrum wavelength range of interest and also blocks the excitation laser line. The pinhole is arranged in front of the detector, on a plane conjugate to the focal plane. The radiation strikes the area surrounding the pinhole, when it is out of focus, and being excluded, therefore, does not contribute to image formation (Figure 14 (b)) [173].

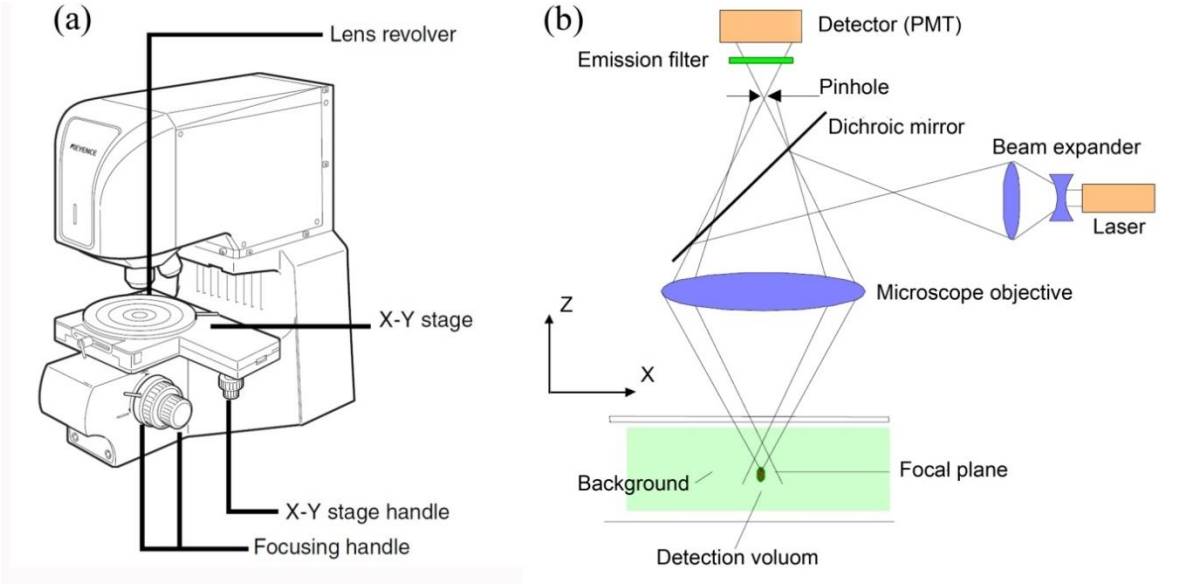

Figure 14: a) The general view of a 3D LSM [174], and b) Ray path in a confocal LSM [173].

LSM gives thepossibility to make an optical sectioning, that is to observe a single slice, less than 500 nm in thickness, out of a "thick", up to 100 µm, specimen in good contrast.The translation of the build-in controllers allows scanning the sample and obtaining information about the entire specimen. Therefore, confocal systems are also referred to as point-probing scanners. In confocal LSM a pinhole, or a confocal aperture, is arranged in a number of slices and recording them. The thickness of the slice and spacing between the successive slices affects the accuracy and quality. The speed of halfslice thickness is usually used as plane that is conjugate to the intermediate image plane and objectplaneofthe microscope. The confocal ray path implies that illuminated andobserved point are focused onto each other lying on conjugate planes. The confocal LSM is intrinsically depth-discriminating optical system, because varying the diameter of the pinhole allows to exclude the extraneous signal from object area outside the focalplane from the detection and moreover the degree of confocality can be adapted. The image becomes non-confocal when the aperture isfully open. Furthermore, the image contrast may be enhanced by suppressing the stray light by minimizing the pinhole diameter [173].

What is more the 3D information about the spatial structure of the object can be obtained by moving the sample to different Z planes, cutting out a great optimum Z-direction scanning rate [173].

The 3D data setobtained during scanning makes it possible to compute further information about the object, such as 3D reconstruction, sections of any spatial orientation, stero pairs, etc [173].

5. Experimental procedure

This section illuminates the details of conduct experiments and procedure of sample preparation for both barnacle species.

5.1. *In-situ* studies

Both, Raman spectromicroscopy and µ-X-ray microprobe fluorescence (µ-XRF) have been selected for the *in-situ* studies. On the other hand, to carry out *in-situ* studies a researcher faces several principal problems, and selection of surfaces to be used for each measurement technique is in the first place. The second significant issue is the way organisms (cyprids and juvenile barnacles) can be kept alive during the measurement. The solution of these two problems will describe in details for both techniques in the next subsections (5.1.1. and 5.1.2.).

5.1.1. Raman spectromicroscopy

A Senterra Raman spectrometer (Bruker Optics, Germany) (Figure 15 (a)) has been used *in-situ* to determine the chemical composition of both temporary and permanent barnacle adhesion at different life stages. In addition to chemical information on the molecules present, Raman spectroscopy provides information on the protein secondary structure [175]. Calcium fluoride disks (CaF_2 IR window 25±0.2 mm Ø X 1.5±0.1 mm polished, s/d: 80/50, Korth Kristalle GMBH, Kiel, Germany) have been used as substrates. Calcium fluoride has been chosen as a substrate for Raman studies due to its transparency which to identify the surface plane for depth profiling in confocal mode and give an intensive Raman band at ~320 cm^{-1} which can be used for normalization and allows, as well as its potential compatibility with future IR measurements. To conduct the *in-situ* measurements, a specific holder (Figure 15 (b)) compatible with the sample holder dimensions of the measurement device has been designed and manufactured from polytetrafluoroethylene (PTFE) (Figure 16). This configuration allows mounting samples with attached cyprids or juvenile barnacles in upside-down position and therefore, the cement layer will be the closest object for Raman investigation, while the organism is kept alive in its natural aquatic environment during the entire measurement (Figure 17 (c)).

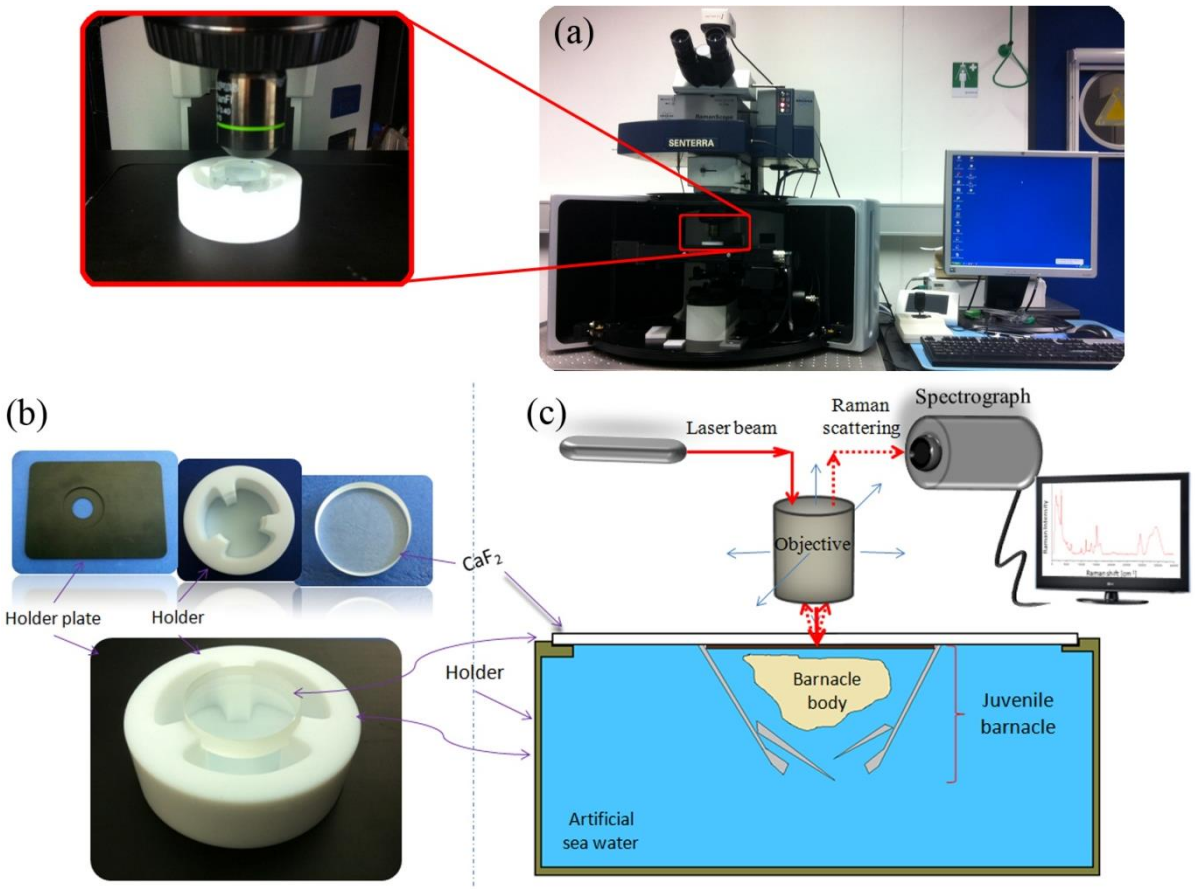

Figure 15: a) Real image of Senterra Raman spectroscopy, b) sample holders and CaF_2disck and c) general setup of *in-situ* Raman spectroscopy.

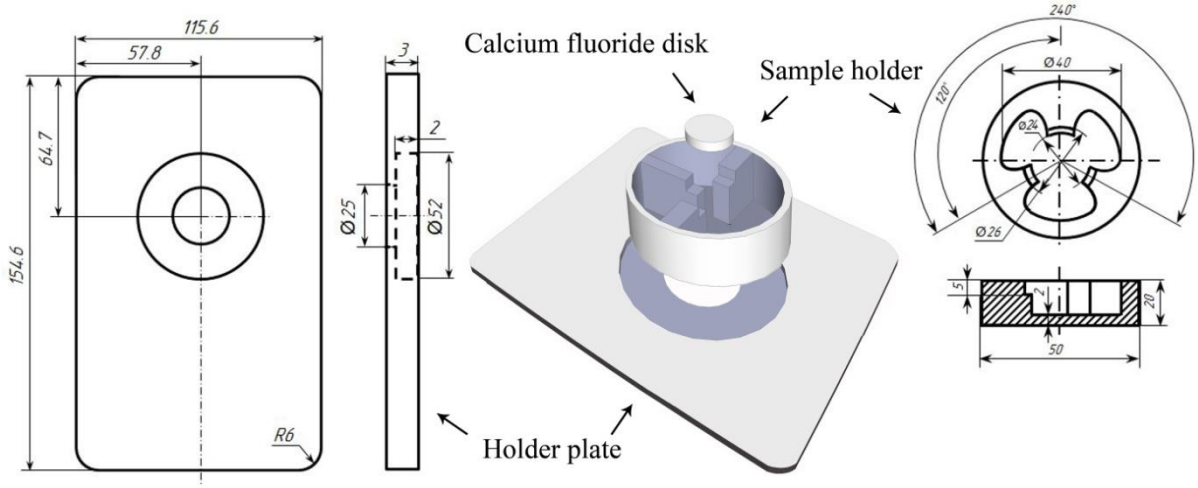

Figure 16: CAD drawing of sample holder and holder plate have been designed to support standard 25mm CaF_2 disk and has been manufactured in Heidelberg University workshop.

Raman spectroscopy has been excited by a frequency doubled diode pumped solid state Nd: YAG laser (wavelength: 532 nm) coupled into a 20X objective (NA 0.45) with spatial resolution of ~ 9–18 cm^{-1} resolution. Olympus BX51reflection confocal microscope that has been used to allow x-y movement (up to 2μm precision) and has trinocular head equipped with a CCD camera. The scattered light has been collected by the same objective and coupled into the spectrograph with reflection geometry 180ºC. The depth of the probed volume has been >20 μm. The spectra have been obtained with a resolution of 9 cm^{-1} in the range of 75 cm^{-1} to 4100 cm^{-1} at 20 mW laser power. The integration time of 4 minutes has been chosen for a single spectrum. For most positions, 4 morphologically similar points on the surface have been measured. At each measurement position, optical micrographs have additionally been recorded to document the exact position of measurement for each spectrum. Confocal Raman spectroscopy has been used *in-situ* to obtain 2D maps of juvenile barnacle base plates. Switching from Raman to confocal Raman is achieved by introducing an additional aperture into the beam path in order to allow only radiations collected in the focal plane to reach the detector. This allowed to obtain depth resolutions down to 20±5 μm instead of > 20 μm. As the intensity of the Raman bands can be affected by scattering, absorption, and changes in laser intensity as well as the different morphology of the sample, the absolute comparison of intensities in the spectra require normalization. This has been accomplished normalizing the spectra to the CaF_2 substrate signal at 320 cm^{-1}.The data were acquired using both of OPUS 6.5 and OPUS 7.2 software (Bruker Optics, Ettlingen, Germany).

5.1.2. μ-X-ray microprobe fluorescence (μ-XRF)

The μ-X-ray fluorescence measurements have been performed at the X-ray fluorescence beamline FLUO at the synchrotron radiation facility ANKA (KIT, Eggenstein-Leopoldshafen, Germany) using an excitation energy of 17.2 keV. A custom-made polycapillary (XOS, East Greenbush, NY, USA) has been used to focus the beam to a spot size of approximately 15 μm x 15 μm (FWHM). μ-X-ray microprobe fluorescence (μ-XRF) has been used in order to evaluate the 'distribution map' of the constituent elements of the interface area between the organism and the substrate. Kapton® (polyamide) foils (8 μm thickness and 64 mm diameter, SPEX Sample Prep, Metuchen, NJ, USA) have been selected for μ-XRF studies (Figure 17 (a)). Kapton® foil has been chosen as a substrate for μ-XRF because of its high transparency for the X-ray energy range and it has a very low level of metal impurities, which could interface with the X-ray fluorescence measurements. On the other hand, kapton® substrate shows a high bio-compatibility: marine biofoulers readily settle on this substrate, which is a prerequisite for the experiments. To work *in-situ* in artificial seawater, 40 mm disposable closed X-ray cells made of contaminant-free polypropylene (SPEX Sample Prep) were used (Figure 17 (a)). This kind of cells consists of a polyethylene snap-ring and cup with snap-post vent and reservoir. Beforehand the Kapton® foils have been checked for any contaminations of any elements apart from those forming Kapton® structures that can interfere with the μ-XRF results which might interfere with the μ-XRF measurements. After the cyprids settlement on kapton® foil the reservoirs were filled with

artificial seawater and the kapton® foil was placed on top of the cell. Afterwards, the cells were sealed with the snap-ring. Finally, the water tighted sample was placed in a sample holder and the µ-XRF microprobe scans can be performed (Figure 17 (b)). As mentioned in Figure 17 (b), the monochromatic X-ray beam (blue line) is focused on the organism settled on the Kapton® window film. The emitted X-ray fluorescence signal is detected at a right angle (green line) with a silicon drift detector. An optical microscope aligned to the X-ray micro-focus at an 45° angle (red line) is used to align the sample for the scans.

The window films show a high transparency for energies greater than 2 keV. Energies below this threshold are not relevant in this technique as they are not accessible with the silicon drift detectors used in the microprobe XRF analysis. Finally, Dr. Rolf Simon and Dr. David Batchelor have performed experiments of XRF, in addition that Mr. Tobias Senkbeil has analyzed all data obtained.

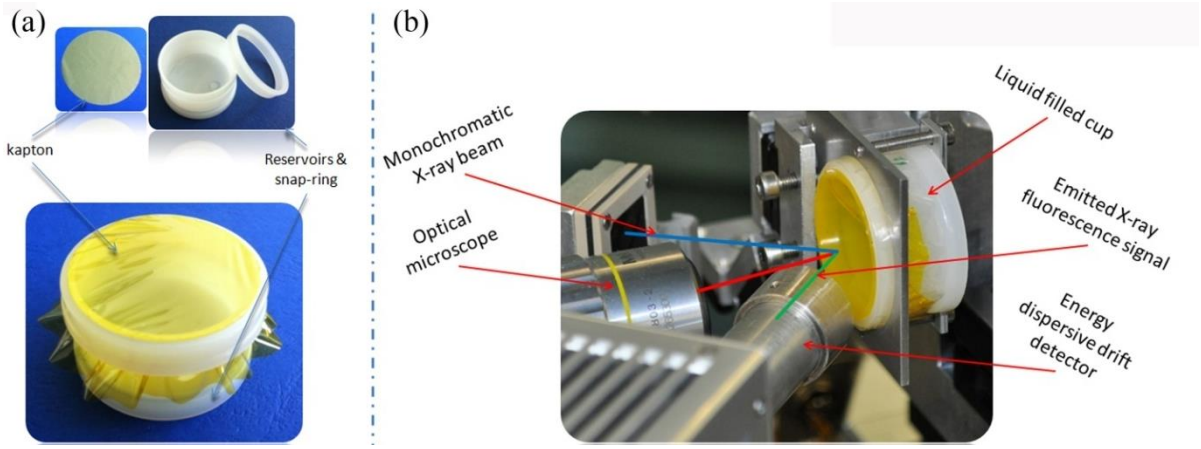

Figure 17: a) sample holders and kapton® foil and b) experimental setup of *in-situ* XRF (photo in Fig. 17 (b) provided by Tobias Senkbeil).

5.2. *Ex-situ* studies

Simultaneously with the *in-situ* studies, there have been a number of *ex-situ* studies made such as scanning electron microscopy (SEM), and 3D scanning laser microscopy.

5.2.1. Scanning Electron Microscopy (SEM)

The morphology of dried samples (adult barnacle shells and baseplates, cypris larva, juvenile barnacles, remaining barnacle cements as well as cyprid footprints) have been measured by SEM. All microscopic measurements are carried out in a FEI Philips XL 30 Field Emission Gun Environmental Scanning Electron Microscope (FEG-ESEM) (Figure 18

(a)). Samples under investigation were placed on carbon stubs and in order to avoid charging, insulating materials have been coated with a thin layer of conductive Gold/Palladium-film using coating system (3ΔL-TEC, MED 020) (Figure 18 (b)). Then the specimen were imaged under high vacuum conditions (10^{-5} Pa) using acceleration voltages between 5 and 20 kV. In adult barnacle shell and baseplate have been fixed directly on the carbon stubs without any additional surfaces, however, the other samples of barnacle larva, juvenile barnacles, remaining cements as well as footprints where placed first on 100 nm gold substrates that purchased from Georg Albert (PVD-Beschichtungen, Germany).

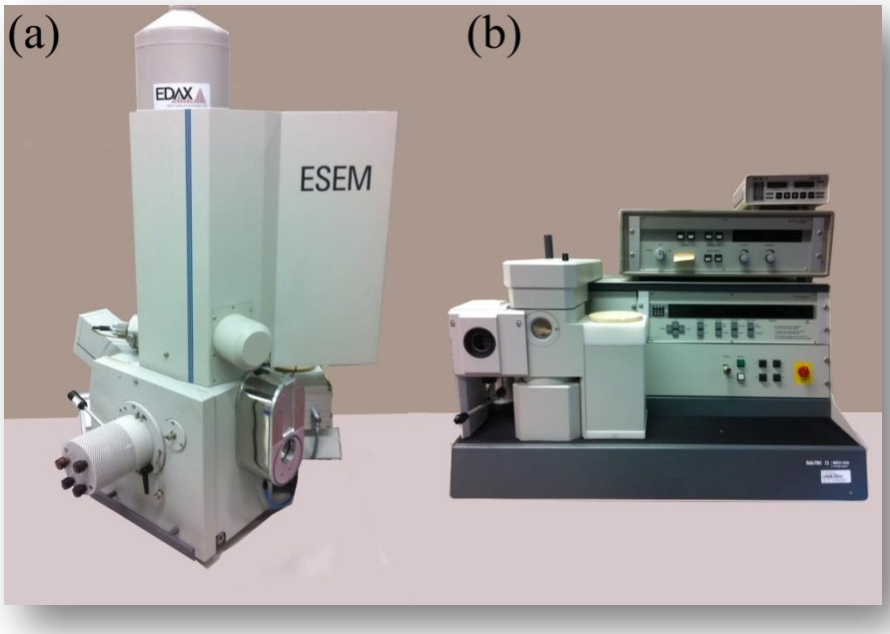

Figure 18: Real image of a) Scanning Electron Microscopy, and b) coating system that have been used in this study.

Elemental analysis has been performed using the energy dispersive X-ray fluorescence spectroscopic unit (EDX) from EDAX with a liquid nitrogen cooled Sapphire Si(Li) detector. For the spectra collection the microscope was operated with a 100 µm aperture.

5.2.2. 3D scanning laser microscopy

For further morphological assessments, color 3D laser scanning microscope (VK-9710, Keyence, Germany) has been used (Figure 19) to screen the remaining barnacle cements after removing the organisms. This investigation is necessary before the start of the measurements, in order to make sure that there are solely cements attached to surfaces. The 3D laser microscope has also provided us with the dimensional information of the remaining barnacle cements, which was not clear before.

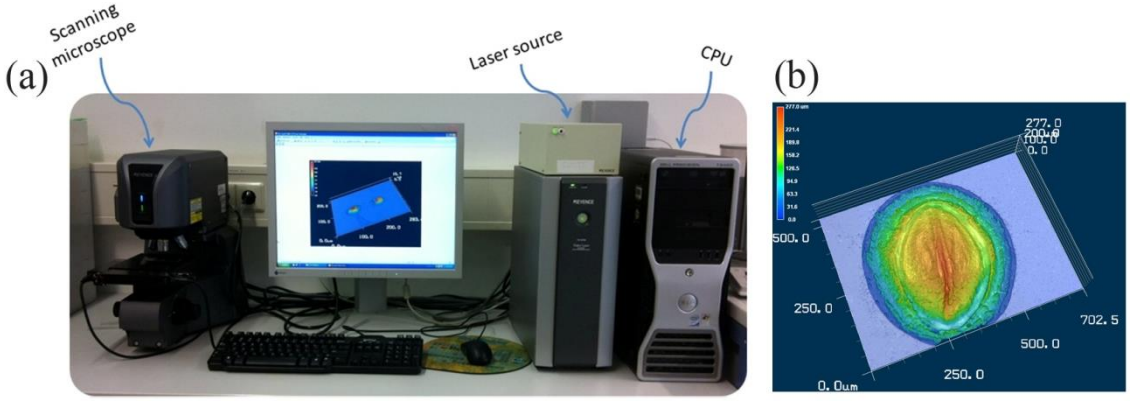

Figure 19: a) Real image of 3D laser scanning microscope (VK-9710, Keyence, Germany), that has been used in this study, and b) example of 3D image taken by 3D laser microscope for 2 days old juvenile barnacle (*B. amphitrite*)

5.3. Strategies of sample preparation

Barnacle larvae of both species (*B. amphitrite* and *B. improvisus*), being stored at 6°C, have been transported from Newcastle University (School of Marine Science and Technology, Newcastle University, UK) to Karlsruhe Institute of Technology (KIT, Germany) for experiments. Ten vital cyprids have been selected using a pipette and set free in 1 cm^3 of artificial seawater (ASW, Instant Ocean, in distilled water; salinity ~ 32 ppt for *B. amphitrite* and ~15 ppt for *B. improvisus*) to settle on both CaF_2 disks and kapton® foils. Both of calcium fluoride disks and kapton® foils have been placed in a dark and humid environment (65±5%) at room temperature (22–25°C) for different time periods depending on the developmental stage to be studied (5 hours for footprint and from one-day to fourteen-days-old for juvenile barnacles). Subsequently, the substrata with the attached organisms were turned upside-down and mounted into the wet cell filled with ASW and transferred into the measurement devices for measurement (Figure 20). In order to prepare samples for *ex-situ* studies, juvenile barnacles settled on both substrata (CaF_2 disks and kapton® foils), have been rinsed with milli-Q water (Millipore Corp., Billerica, Ma, USA), and carefully removed (Figure 21). The remaining cement specimen on the surfaces have been washed gently with distil water to avoid any contamination of the remaining organs/parts of the organism as well as any other impurities from the ambient water. Directly after washing ready for studying cement samples have been transferred into fresh artificial seawater.

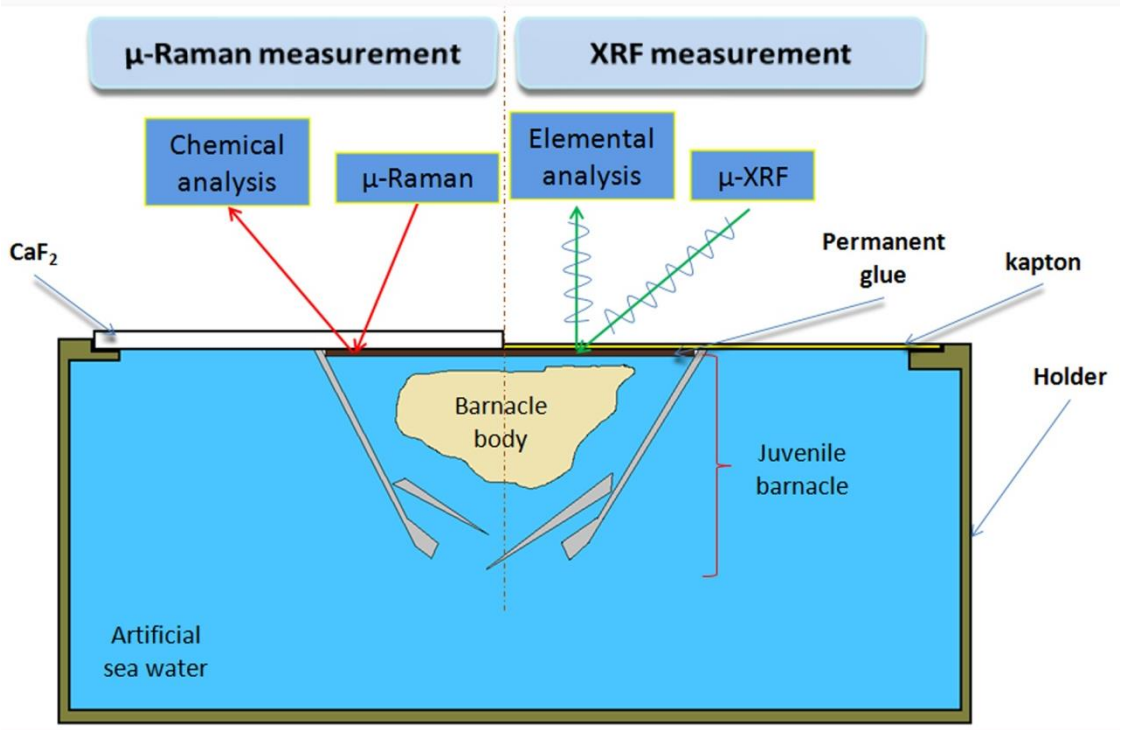

Figure 20: General setup of *in-situ* X-ray microfluorescence and µ-Raman analysis

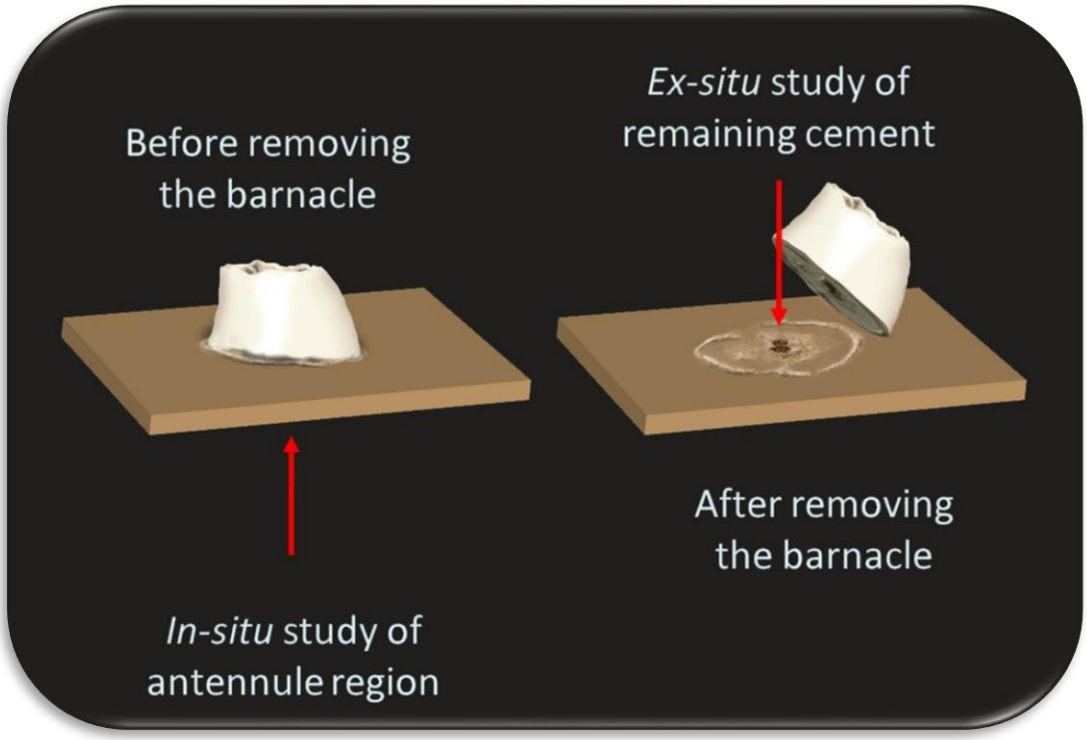

Figure 21: Orientation of the samples in regards to the incident beam.

***Tetraselmis* algae:** Green algae (*Tetraselmis*) sent by Newcastle University have been used to feed the settled juvenile barnacles. The green algae were maintained in the lab for several days at a temperature of 20°C, light source (bright lighting 24L:0D), and an oxygen supply. Juvenile barnacles were given the same amount of food at each time point equalling to 1 ml of green algae suspension per 30 ml artificial seawater.

5.4. Reference substances

Insulin (Insulin, human, Sigma-Aldrich, Louis, Germany), pepsin (Pepsin, from porcine gastric mucousa, Sigma-Aldrich, Louis, Germany) and amyloid (Amyloid β-protein fragment 1–42, Empirical Formula (Hill Notation): $C_{203}H_{311}N_{55}O_{60}S$, Molecular Weight: 4514.04, Sigma-Aldrich, Louis, Germany) were purchased to be used as a sample reference for different protein secondary structures. Standard β-carotene (Type II, synthetic, ≥ 95% (HPLC), crystalline Sigma-Aldrich, Louis, Germany ($C_{40}H_{56}$)), has been exploited as a reference sample for C=C str. bands identification.

6. Results and discussion

This chapter summarizes the key findings of the thesis and is divided into three major subsections. First, the *in-situ* and *ex-situ* results of µ-Raman spectroscopy of cyprid and juvenile barnacle cements are presented and discussed. The results of *in-situ* and *ex-situ* µ-X-ray fluorescence (µ-XRF) of cyprid and juvenile barnacle cements are included into the second subsection. Additionally, a comparison of two different species (*B. amphitrite* and *B. improvisus*) using µ-Raman and µ-XRF techniques is presented in subsection 6.3. Finally, the major results of both aforementioned techniques are summarized in the last subchapter.

6.1. Raman spectroscopy results

6.1.1. *In-situ* results of µ-Raman spectroscopy

The *in-situ* experiments are intended to study barnacle cements without removing the organism from the original adhesion position, while at the same time it stays in an environment similar to its natural habitat in terms of temperature, salinity, lighting etc.

In spite of several advantages of *ex-situ* analysis of adhesive proteins, it is necessary to evaluate the extent to which the information obtained from such studies reflects the chemistry in the intact interface. An advantage of vibrational spectroscopy techniques for under water bio adhesion studies is its capability to characterize buried adhesive interfaces of live organisms.

In this subsection all *in-situ* results of µ-Raman spectroscopy will be presented and discussed in detail.

6.1.1.1. Chemical variations across the juvenile barnacle baseplate

To visualize the distribution of molecular composition in the barnacle baseplate, 4 days old barnacles have been grown on calcium fluoride disks and imaged by µ-Raman spectromicroscopy. The measurements were done in a conventional (nonconfocal) mode and are sensitive to the interface area up to a depth of > 20 µm. An optical micrograph of the adherent barnacle is shown in Figure 22(a). Figure 22(b) shows the sum of 400 individual Raman spectra recorded at different positions within the barnacle baseplate. It is obvious that the chemistry at the interface is composed of a variety of chemical groups and components, including calcite (277 cm^{-1} and 1085 cm^{-1}) [176], amides (e.g. amide-I bands at 1640 cm^{-1}, υ(C=O)), conjugated, unsaturated components (υ($C=C_{conj}$) modes (1518 cm^{-1}), a pronounced C–H stretching region (2880–2980 cm^{-1}) [10, 177], a broad band of amine contributions at ≈3250 cm^{-1}, and a broad OH band at ≈3400 cm^{-1} [10, 177, 178]. The assignment of the different vibrational modes according to literature references is compiled in Table 2. In order to visualize the spatial distribution of the different Raman bands within the baseplate, the intensity of selected bands (indicated by the colored bars in Figure 22(b)) at the different scan positions was evaluated and represented as color images (Figure 22(c–h)). The subfigures in

Figure 22 show the spatial distribution of amide-I contributions (panel c, υ(C=O), 1600–1700 cm^{-1}), calcite (panel d, $\upsilon_1(CO_3^{2-})$, 1000–1100 cm^{-1}), the distribution of unsaturated, conjugated C=C double bonds (panel e, υ_1(C=C str.), 1480–1540 cm^{-1}), C–H stretching of different vibration modes between 2880–2980 cm^{-1} (panel f), hydroxyl stretching modes at 3300–3500 cm^{-1} (panel g), and amine modes (panel h, 3200–3300 cm^{-1}).

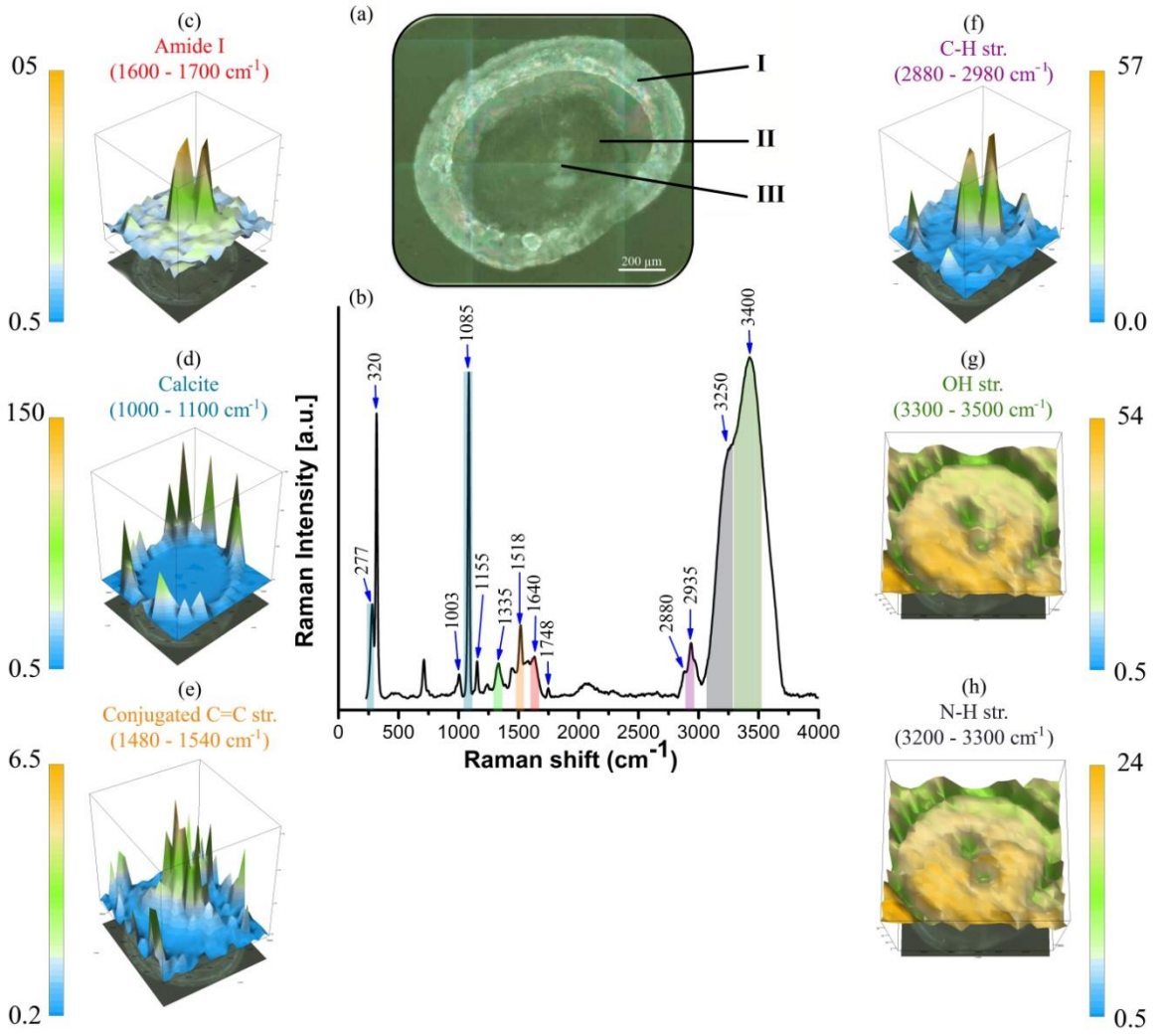

Figure 22: (a) Light microscopy image (20 X) of four-days-old juvenile barnacle *B. amphitrite* settled on CaF_2 disk, (b) Sum of all (400) Raman spectra measured across the whole baseplate, (c) micro Raman map integrating the Raman signal at 1600 – 1700 cm^{-1} for amide I, (d) 1000 – 1100 cm^{-1} for calcite, (e) 1480 – 1540 cm^{-1} for the conjugated C=C stretching, (f) C–H stretching modes between 2900 – 2980 cm^{-1} (g) 3300 – 3500 cm^{-1} for OH modes, and (h) 3200 – 3300 for N–H stretching vibrations.

From the Raman-maps in Figure 22, three prominent regions of different chemistry were distinguished (labeled I–III in Figure 22a): (I) calcite rich regions (Figure 22d) close to the

exterior part of the barnacle (shell region). Beside the strong calcium carbonate modes, significant conjugated C=C contributions were found (Figure 23e). The baseplate region (II) is characterized by a homogeneous appearance in the optical micrograph and a low and even distribution of amide-I (Figure 22c), N–H (Figure 22h), and –OH (Figure 22g) vibrational modes. However, within this baseplate area, two distinct spots became obvious in the optical micrograph, which we assigned to region III. In the amide-I distribution in 22(c) and the CH-stretching region 22(f), a significantly different signal was observed compared to the rest of the baseplate. A morphological comparison with the optical micrographs revealed a relation of the Raman bands to the attachment position of the antennules, which established the first contact of the cyprids with the surface. Obviously, the cyprid cement area gave a significantly different Raman signal compared to the rest of the baseplate area.

TABLE 2: Assignments of the vibrational modes found in the µ-Raman spectromicroscopy data of barnacles.

Assignment	Band position [cm^{-1}]	Corresponding References
Calcite ($CaCO_3$)	277 & 1085	[176]
CaF_2	320	[179]
υ(C–CH_2)	1003	[10, 177, 180]
υ_2(C–C)	1155	[10, 177, 180]
δ(O–H)	1335	[181]
υ_1(conjugated C=C)	1518	[10, 182]
Amide-II	1580	[177, 183]
Amide-I	1640	[10, 177, 183]
υ(C=O)	1748	[177, 178]
$\upsilon_{1+}\upsilon_2$(C=C)	2673	[10, 182]
$\upsilon_{s,as}$(C–H)	2880 –2980	[10, 177, 180]
2 υ_1(C=C)	3036	[10, 182]
υ(N–H)	≈ 3250	[10]
υ(O–H)	≈ 3400	[10, 177, 178]

Spectra of the three distinct regions and their development at different time points after metamorphosis are shown in Figure 23. All spectra were normalized to the CaF_2 peak to account for intensity variations that might occur during long-term measurements. The normalized spectra in the calcareous region (I) (Figure 23 (c)) show the expected two main peaks of the calcite group at ≈277 cm^{-1} (Lattice mode), and ≈1085 cm^{-1}($\upsilon_1(CO_3^{2-})$ str. mode) [176]. These peaks are only prominent in the exterior region and intensity strongly decreases towards the interior of the barnacle (Figure 23 (a and b)). It is noticeable that the calcareous region shows weak peaks for amide-I, amide-II, amide-III and amide IV at 1636 cm^{-1}, 1565 cm^{-1}, 1265 cm^{-1} and 747 cm^{-1}, respectively (Table 2) [10, 180, 183], indicating the presence of small amounts of organic, amide rich material even in the mineralized part of the juvenile barnacle. The baseplate area surrounding the antennules (II), and the antennule region (III) reveal much higher intensities of the amide bands, presumably due to larger amounts of

proteinaceous material. Considering the penetration depth of the µ-Raman experiment of > 20 µm, it is possible that besides the cement also soft tissue inside the organism contributed to the amide signal.

Despite the fact that water is a relatively weak Raman scatterer, a broad peak for –OH str. of water at ≈3420 cm^{-1} is observed outside of the barnacle (Figure 22h) [10, 177,178]. In the shell region, this signal is strongly decreased, pointing to a much lower presence of water and hydroxyl groups in the mineralized area. Interestingly, the signal is surprisingly high in the baseplate region (II). The presence of hydroxyl-rich material could indicate a high amount of hydrated, hydroxylated functional groups. The intensity of –OH modes is depleted in the antennule region. It could be speculated that the highly crosslinked cyprid cement, is less hydrated and its composition contains less hydroxyl groups.

The main peaks of different CH vibration modes (symmetric CH_3, symmetric CH_2 and asymmetric CH_2 at 2880, 2935 and 2973 cm^{-1} respectively) [180] appear in all spectra (Figure 23). As shown in the Raman map (Figure 22f), the intensity of these band ranges from 2880 to 2980 cm^{-1} is located in the antennule region. These CH bands have been found in each *in-situ* spectra of antennule region of *B. amphitrite* juvenile barnacles from one up to fourteen days old with rather high intensity and therefore has drawn attention (Figure 23). This result may indicate that juvenile barnacle cement is an hydrophobic material in agreement with the work of Kei Kamino [140], who stated that barnacle cement is a proteinaceous material that consists of hydrophobic amino acids.

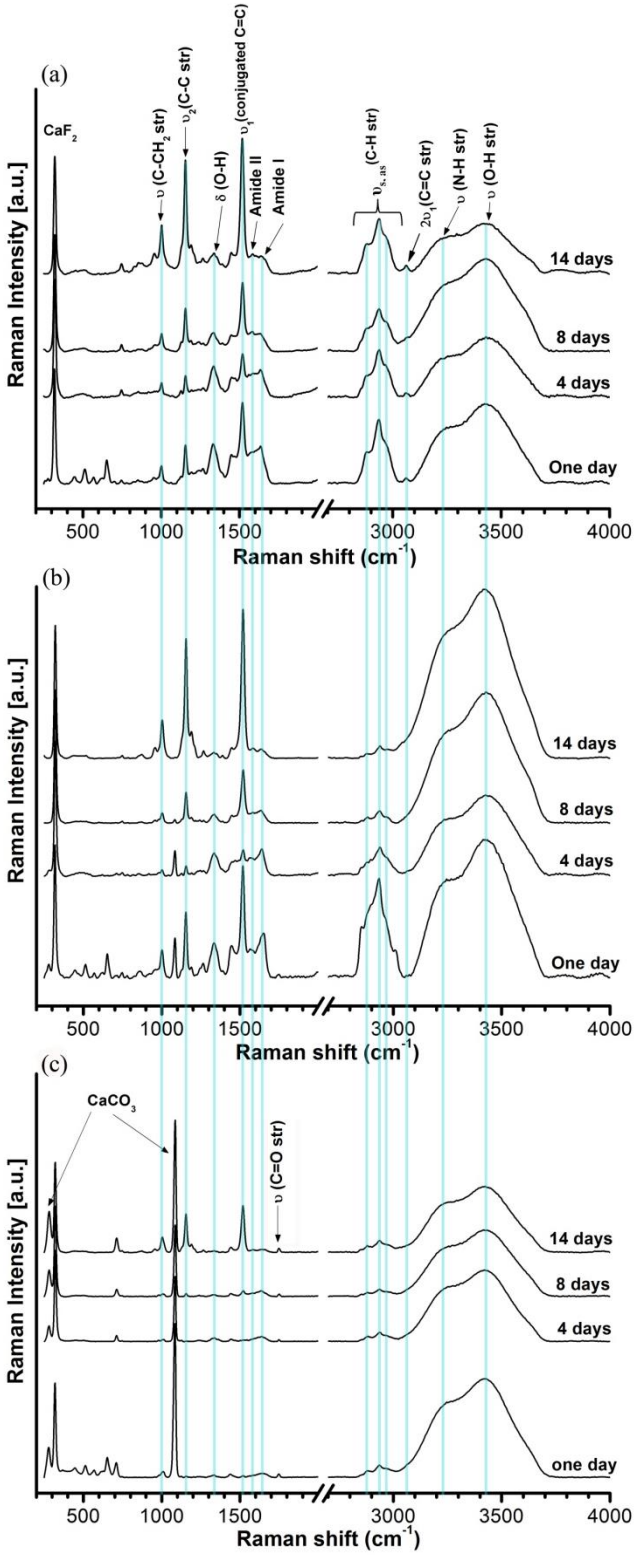

Figure 23: Raman spectra of juvenile barnacles at different time points after settlement (one day up to 14 days). a) Antennule region (III), b) baseplate region surrounding the antennule (II) and c) calcareous region (I).

At early time points after settlement (one-day to four-days), the main peaks of C–CH_2 stretching mode at 1003 cm^{-1}, υ_2(C–C) at 1155 cm^{-1} [10, 177, 179, 180] and the conjugated C=C str. (υ_1(C=C)) at 1550 cm^{-1} in the calcareous region (I) were very weak. At later time points, these peaks have significantly increased. Especially the strong presence of unsaturated compounds (C=C vibration modes) has been surprising and recent measurements of Schmidt *et al* [10] assigned them to carotenoids. Additionally, in the antennule region (III) and the area surrounding the antennule (II), the C–C str. and the C=C str. modes were very prominent and their intensities changed with time. At all time points, a weak band of C=O str. at 1750 cm^{-1} [177–178] was observed in the calcareous region (I), while it was lacking in all other areas (antennule region and/or baseplate area around the antennule). This C=O str. band might be related to the chemical composition of the *mantle epidermis*, which is the primary substrate for calcareous shell formation [184].

6.1.1.2. Reproducibility of spectra

An important question stated at the beginning of the study has been the repeatability of spectra taken at apparently similar positions in different barnacles or even for different footprints. As illustrated in Figure 24, the five different individual Raman spectra have been recorded within the region where footprints are expected after one-day of surface exploration on a CaF_2 disk (Figure 24(c)). Furthermore, three spectra (Figure 24 (b)) have been recorded for the remaining cement of two-days-old juvenile barnacle after removal of the organism from the surface. Additionally, spectra of four different, four-days-old settlement juvenile barnacles (*B. amphitrite*), recorded at the antennule region are shown in Figure 24 (a). Most importantly, it has been found that all the spectra from similar regions, but different individuals, look alike, that is have similar shape and peak intensities. This shows that reproducible data can be generated from several different individual barnacles for the different characteristic regions.

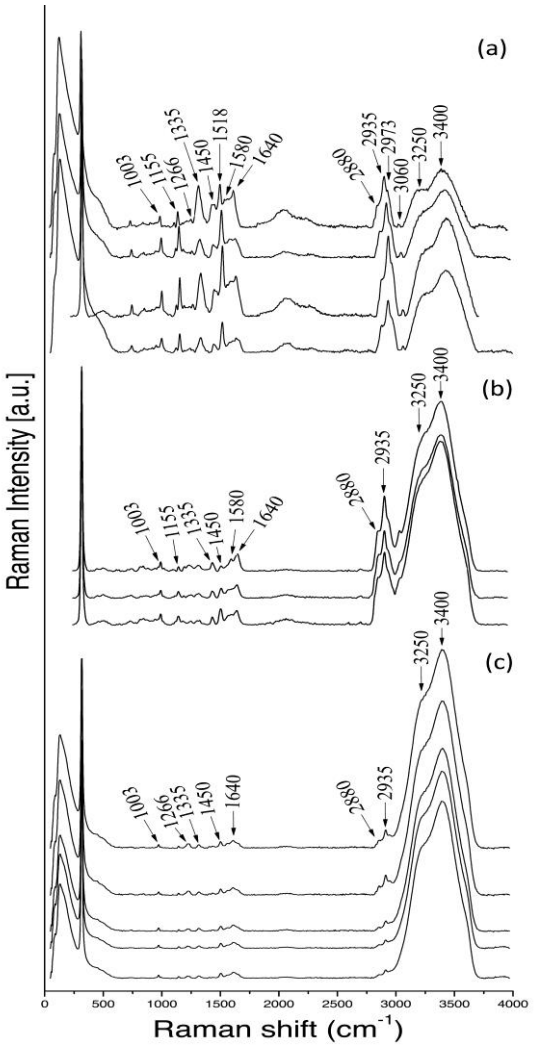

Figure 24: a) Four spectra recorded in the antennule region of different four-days-old juvenile barnacles (*B. amphitrite*), b) three spectra recorded in the remaining barnacle cement (after juvenile barnacle removal) and c). Five Raman spectra recorded within the region where footprints are expected after one day of surface exploration (CaF_2 disk).

6.1.1.3. Comparison of cyprid footprints and juvenile barnacle cement

As described in subsection 2.2.1, the cypris larva explores surfaces in order to find the optimum place for adhesion. In this process, it uses a pair of antennules to secrete an appropriate amount of protein temporary adhesive that is left on surfaces and defined as footprint (Figure 7 (B)). When the larva finds the right place for adhesion, it secretes another type of sticky permanent adhesive known as cyprid cement as shown in (Figure 7(C)).

Figure 25 (b) shows the average spectra of five individual Raman spectra recorded within the region where footprints are expected after one-day of cyprids' exploration of CaF_2 disks. In addition, average of 4 Raman spectra recorded within the antennule region of recently attached cypris larva (after permanent settlement and before metamorphosis) is shown in Figure 25 (a). It can immediately be seen that the intensity of footprints showed much lower overall signal intensities compared to the *in-situ* data of the juvenile barnacles due to the

lower total amount of material probed and the fact that in case of *in-situ* study the high penetration depth (>20 µm) can capture not only the interface area between the surface and the baseplate but also part of juvenile barnacle bodies. The noteworthy regions are the amide bands and the C=C stretching region. Footprint spectra show the absence of amide-IV at 747 $cm^{-1}$and relatively weak peaks of C–CH_2 str., C–C str., and C=C str. at 1003 cm^{-1}, 1155 cm^{-1} and 1550 cm^{-1}, respectively. Interestingly, the C=C str. vibrations were much weaker in the footprints compared to the cyprid cement. Thus, the carotenoid seems to be rather located in the interior of the barnacle than in the cement.

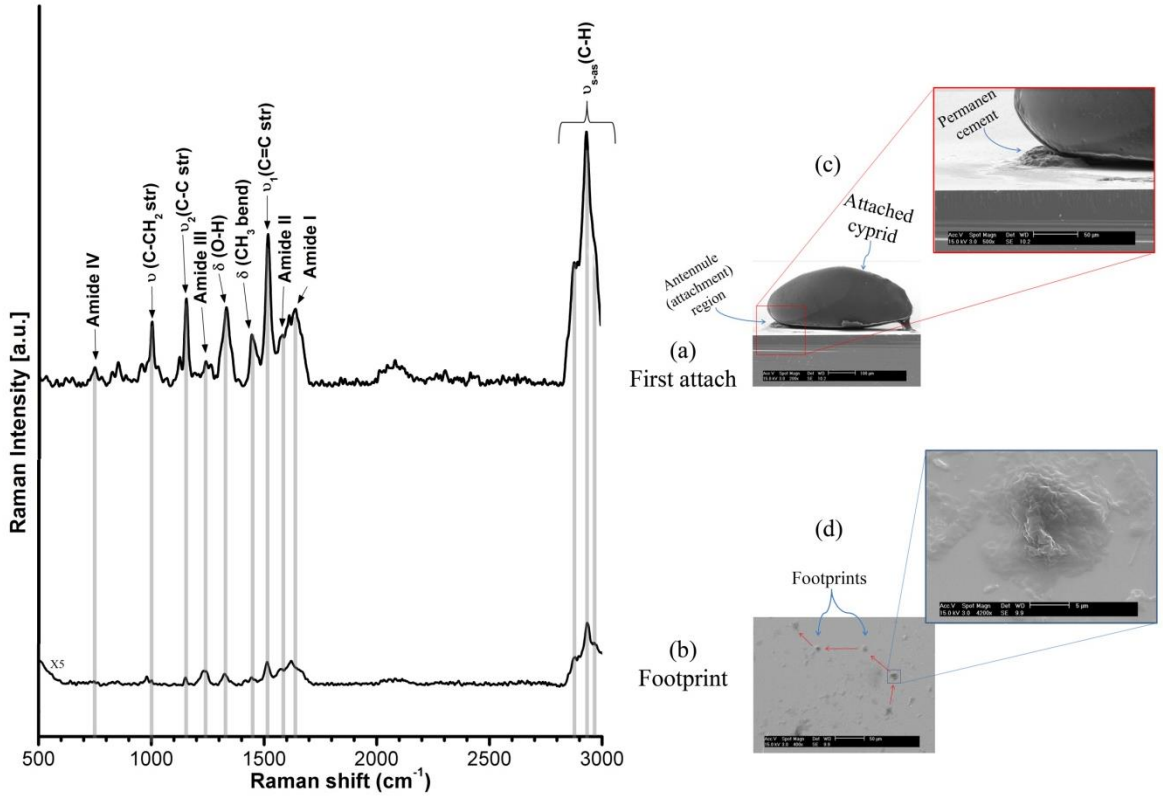

Figure 25:a) Average of 5 Raman spectra (magnified "X5") recorded within the region where footprints are expected after one-day of surface exploration (CaF_2 disk), compared with b) average of 4 Raman spectra recorded within the antennule region of *B. amphitrite* settled on CaF_2 disk (first attach). c and d) SEM images of attached cyprid and footprint blobs respectively.

6.1.1.4. Protein secondary structure of cyprid cements at different time points

It is well known that protein secondary structure is a main characteristic of protein biomolecular structure. Protein is a polymer made up from various residues of L-α-amino acids. Driven by a number of non-covalent interactions, e.g. ionic interactions, Van der Waals forces, hydrogen bonding, hydrophobic, packing, proteins fold into specific spatial conformation, one or several at a time, in order to perform their biological functions. Proteins can form four different levels of structure: primary, secondary, tertiary and quaternary

(Figure 26 (A). Principal protein secondary structures are α-helix, β-sheet, β-turn and unordered structure (Figure 26 (B)).The determination of protein three-dimensional structure and its type should be performed in order to understand protein functions at a molecular level [185].

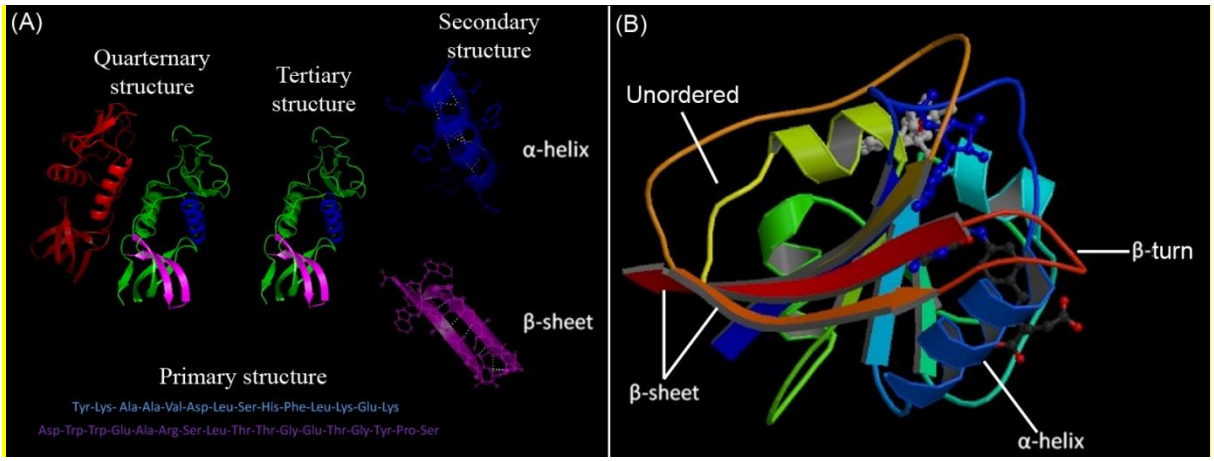

Figure 26: A) Levels of protein structure [186], and B) main types of protein secondary structures [187].

Especially the amide-I band at 1600–1700 cm^{-1} provides information on the secondary structure of proteins [188]. As relative peak intensities might change compared to IR spectroscopy, insulin and pepsin were included as reference materials in the study (Figure 27.1 and 27.2). Insulin is a model compound for α-helix and shows, in agreement with both IR and Raman measurements [189– 190], a main peak at 1654 cm^{-1}. Pepsin in turn is rich in parallel β-strands and shows a main band at 1669 cm^{-1}, also in good agreement with the peak positions found in IR spectroscopy [191]. The vertical lines in the spectra indicate the typical positions of the amide-I vibrations of the different secondary structures. In addition to α-helix (1654 cm^{-1}) and parallel β-strands (1665 cm^{-1}), some further wavenumbers are marked: β-turn at 1693 cm^{-1} [9], unordered at 1645 cm^{-1} [9, 189], antiparallel β-sheet at 1637 cm^{-1} [9]. At lower wavenumbers, two typical ring modes of the phenolic compounds phenylalanine and tyrosine, at 1615 cm^{-1} and 1604 cm^{-1} are indicated [192]. At 1622 cm^{-1}, phenolic compounds or β-motifs of amyloid fibers [13] are likely to contribute. The latter have recently been identified in ATIR measurements and assigned to vibrational modes of amyloid structures [13]. In order to verify this statement, amyloid reference sample of (Amyloid β-protein fragment 1–42, Sigma-Aldrich, Louis, Germany) have been examined and compared with the amide-I bands of variously aged cyprid cement specimens. Both amyloid and phenolic compound bands will be discussed in detail below.

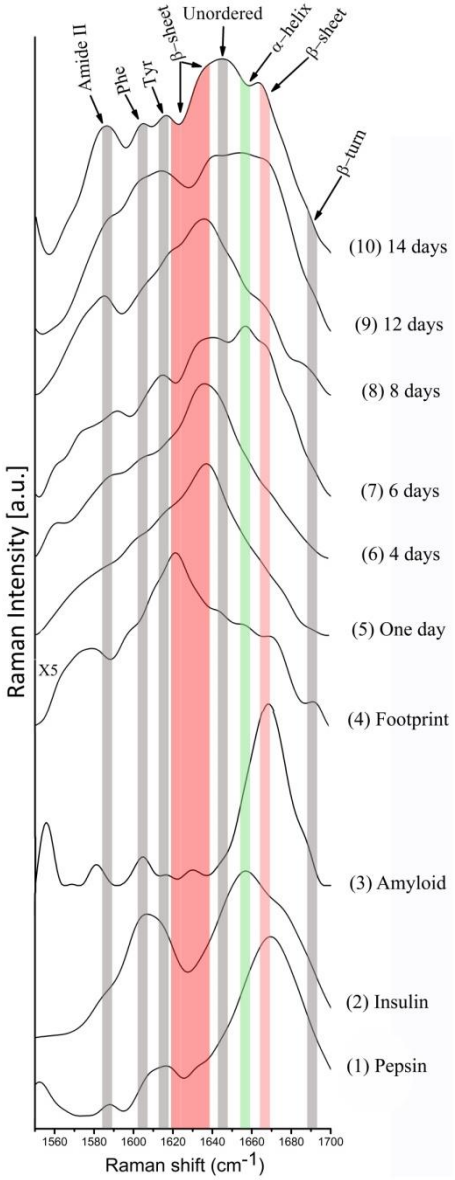

Figure 27: Raman spectra of the amide-I region. Comparison of cyprid cements with reference spectra ((1) pepsin (β-sheet), (2) insulin (α-helix), (3) amyloid β-protein), (4) footprint spectra (intensity five times magnified), and (5–10) spectra recorded at the antennule regions of the juvenile barnacles settled on CaF_2 disks at different time points (from one-day to fourteen-days-old).

The spectra in Figure 27, compare the reference compounds (27.1 and 27.2) with the cyprid footprints (Figure 27.3), and the amide-I spectra recorded at the antennule region of the juvenile barnacles settled on CaF_2 disks at different time points (Figure 27.4 – 27.9). It is to be kept in mind that the spectra in the *in-situ* analysis of the antennule region by conventional Raman microscopy are different as probing is not only sensitive to the surface, but also to the bulk of the young barnacle (>20 µm penetration depth). In the footprint spectra (Figure 27.3), the major amide-I band is located at 1622 cm^{-1}. This band is associated with cross-βmotifs that were previously identified as a major structural feature in deconvoluted

spectra of adult barnacle adhesive [13]. From the first glance, it can be easily seen that spectra of permanent cyprid cement are markedly different from the footprint spectrum, indicating a different protein secondary structure. *In-situ* data of the antennule region of the juvenile barnacle (one-day up to fourteen-days after settlement (Figure 27.4 – 27.9)) show a high variability and the shape of the spectra changes over time. Two dominant peak shapes become visible. At the 1, 4 and 8 days time points, major bands at 1637 cm^{-1} and two shoulders at lower wavenumbers at 1604 cm^{-1} and 1615 cm^{-1} and another shoulder at high wavenumbers at 1665 cm^{-1} is measured. The first and most intense peak is at 1637 cm^{-1} and the shoulder at higher wavenumber at 1665 cm^{-1} point towards strong β-sheet contributions. Two bands at low wavenumbers were previously assigned in Raman spectroscopy to aromatic residues, the band around 1604 cm^{-1} to phenylalanine and the band at 1615 cm^{-1} to tyrosine [192]. The majority of the spectra shown in Figure 27 contain contributions at these lower wavenumbers, indicating a potential presence of the two amino acids. Indeed it is reported that phenolic compounds are essential in cross-linking and adhesion of barnacle cement.

In turn after 6 and 12 days, a strong α-helix band at 1654 cm^{-1} is observed. It is also interesting to note that the intensity of the two bands at 1602 cm^{-1} and 1615 cm^{-1} seems to be correlated with the intensity of the α-helix band at 1654 cm^{-1}. As mentioned above, these Raman signals were previously assigned to aromatic phenylalanine and tyrosine [192] and they could be involved in cross-linking of the adhesive. All the above mentioned results are described in detail in subsection 6.2.3.

6.1.1.5. Calcification process

The calcareous barnacle shell and the baseplate are formed by the deposition of seawater elements such as K, Sr, Sn, and mainly Ca on the outer membranes (*Mantle epithelium*) of the organism. The specific structure of mantle epithelium cells allows lime transportation through the mantle from the ambient seawater [193].

Raman spectroscopy was used *in-situ* to follow the initial calcification process of a barnacle (*B. amphitrite*). Barnacle specimens were investigated by Raman from the cyprids' first attachment on the calcium fluoride (CaF_2) surface up to several days after juvenile barnacles were completely formed and the changes in calcite bands intensity with time was quantified.

During the experiment, artificial seawater inside the sample holder container with barnacles was exchanged two times per day in order to maintain the same concentration (concentration values) of elements in the barnacle ambient media, because the growth of the calcareous shell and baseplate requires continuous availability of calcium from the surrounding seawater [193].

The results of this study have shown that four-days-old cyprids start to settle on the CaF_2 surface after about 18 hours from the beginning of exploratory process. Within 3–4 hours after settlement cyprids go through metamorphosis and become juvenile barnacles within

several hours. The characteristic bands of calcite ($CaCO_3$) can be observed at 275±5cm^{-1} and 1088±5 cm^{-1} [176]. It takes around 3–4 hours for the settled barnacle to start metamorphosis that will last for around 5 hours and end by disposal of the a cyprid protective biomembrane carapace. Right after the protective carapace is disposed, the calcite peaks start to appear (Figure 28 (a)), thus the shell calcification process starts around 8–9 hours after permanent attachment. Within the first 8 hours of the calcification process, the intensity of calcite bands exhibits a steep growth of about 0.204 a.u./hr as is shown in Figure 28 (b), and decreases about 10 times to the rate of 0.022 a.u./hr afterwards. The results obtained correspond to the research work of Bourget and Crisp [194], who stated that barnacle shell plates are growing rapidly during the first several hours after metamorphosis. The fast growth within first few hours is related to high accumulation of the calcium from the ambient water in the epidermis layer that is present directly under the shell and is known as mantle epithelium. Scheme of barnacle transformations at its early life stages are represented in Figure 29.

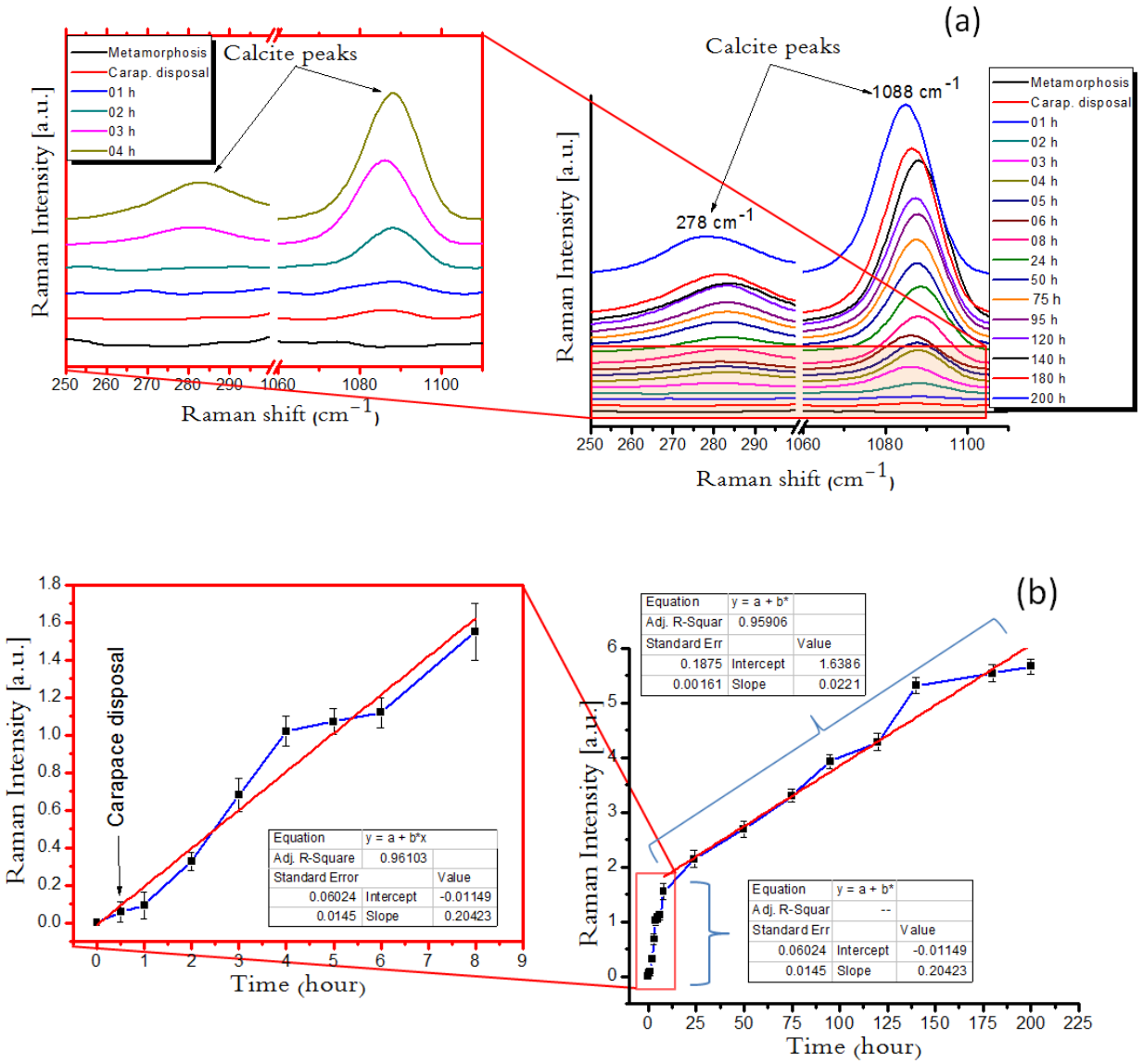

Figure 28: a) Calcite bands spectra of juvenile barnacle (*B. amphitrite*) at different time points from metamorphosis to 200 hr, and b) calcite bands intensity peak values at the same time points, error bars according to Student's t-distribution.

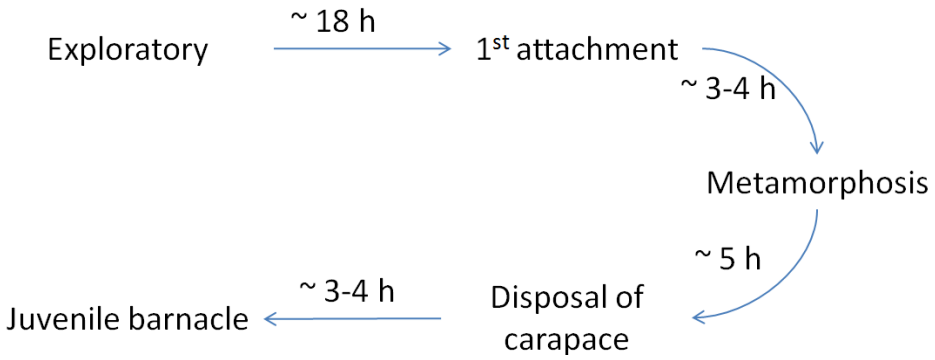

Figure 29: Time scheme of barnacle transformations at early life stages

6.1.2. *Ex-situ* Raman spectroscopy results

Due to the relatively large penetration depth of Raman spectroscopy (>20 µm), it cannot be excluded that besides the adhesive also inner tissues of the organisms contributed to the signal. To further enhance surface sensitivity, barnacles have been removed and the remaining cements have been studied. As described in section 5.3, barnacle cement samples have been obtained through careful removal of settled barnacles, followed by gentle rinsing of the baseplate region with distilled water to remove salts and debris. Both light microscopy and 3D laser microscopy have been used to select samples which show solely residues from the baseplate free from any other remaining parts of the barnacle. It has been observed that the majority of remaining cement is localized in the antennule region after barnacle removal. Furthermore, it is noteworthy that the diameter of the remaining cement plaque increases with time (≈50µm for metamorphosis, ≈80 µm for one-day-old, ≈100µm for two-days-old and ≈140 µm for six-days-old barnacles) as shown in Figure 30 (B). The increasing diameter of the cement plaque can be explained by the fact that juvenile barnacles continue to secrete additional cement portions in order to increase the strength of adhesion to the surface.

Figure 38 (A) shows the average spectra of four individual Raman spectra recorded at the antennule region of *B. amphitrite* settled on CaF_2 disks at different time points (metamorphosis, one-day, two-days, six-days-old) after barnacle removal ("remaining cements").

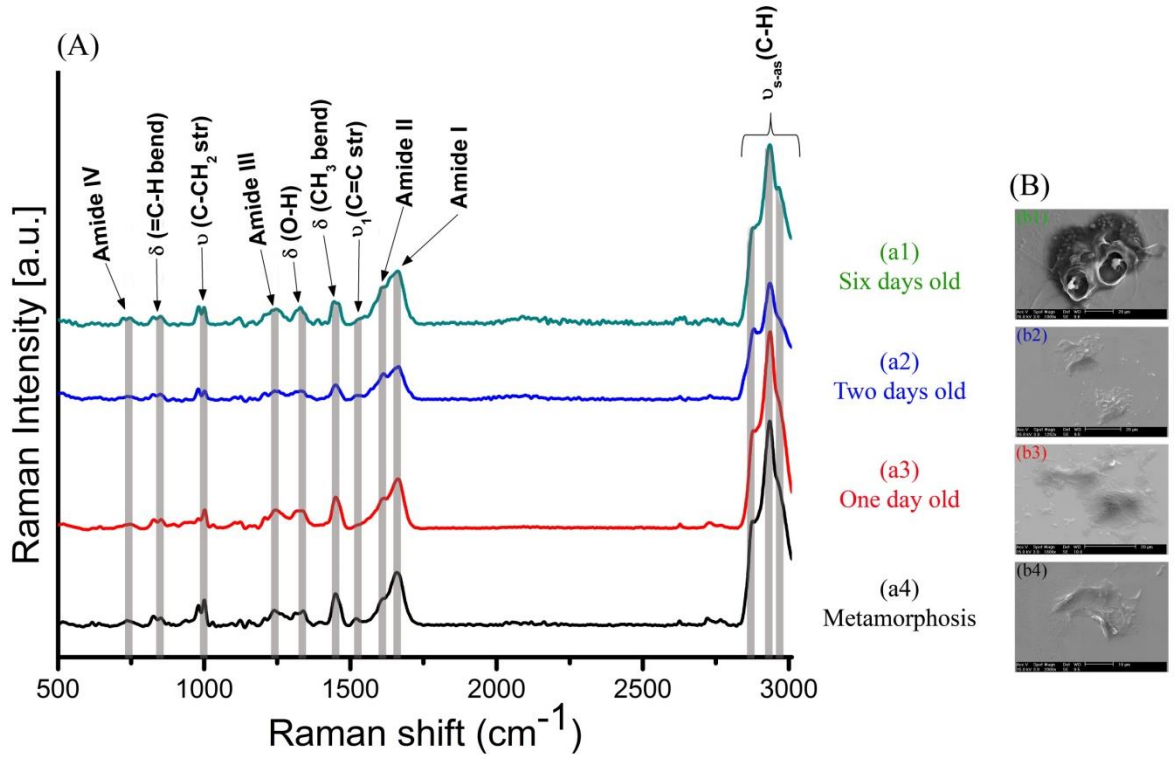

Figure 30: A) Average of four Raman spectra recorded at antennule region of *B. amphitrite* settled on CaF_2 disks at different time points (a1 – a4) after barnacle removal. B) SEM of the remaining cements at the same ages (b1– b4).

Interestingly, all Raman spectra that have been recorded at different time points are very similar in contrast to the *in-situ* data. This similarity may be explained as termination of the crosslinking process of the cement after removal of the organism. Raman spectra of the remaining barnacle cements has shown that the original interface consists of proteinaceous material, since amide-I and II bands near 1636 and 1565 cm^{-1} [10, 177, 183], respectively, are the most dominant peaks. Also, both of amide-III and amide-IV bands were also present, as indicated by the small peak at 1265 and 747 cm^{-1}, respectively [177, 180–183].

All remaining cement spectra that have been recorded at different time points (Figure 30 (A)) shows an intense bands of CH stretching of different vibration modes at range of 2880–2980 cm^{-1} [9, 17, 20], which earlier has been detected in the *in-situ* spectra, specially, in the antennule regions of the juvenile barnacles. This result enhances the hypothesis that juvenile barnacle cement is a hydrophobic material [140].

Furthermore, all spectra of the remaining cements show a weak peaks of amide-IV at 747 cm^{-1} and a very weak bands related to carotenoid (C=C and C–CH_2 str. vibrations at 1550 cm^{-1} and 1003 cm^{-1} respectively) [10, 177, 178, 180]. Similarly to footprint spectrum (Figure 25 (a)), the carotenoid seems to be more likely located in the interior of the barnacle rather than in the adhesive.

As in *in-situ* study, amide-I bands of all remaining cement spectra (Figure 31) are examined carefully in order to study the protein secondary structure of the remaining cyprid

cements and to determine if there are any differences in the secondary structure at these different time points or not (Metamorphosis, one-day, two-days and six-days-old).

Spectra of amide-I in Figure 31, compare the reference (insulin, pepsin and amyloid β-protein) compounds (Figure 31 (1–3)) with the spectra recorded at the antennule regions after removal of the barnacles "remaining cements" at different time points (Figure 31 (5–8)). The vertical lines in the spectra indicate the typical positions of the amide-I vibration. As described before both of insulin and pepsin showed the expected main secondary structure which is in agreement with IR measurements [189–191]. While, Amide-I spectrum of the amyloid sample showed main band at 1667 cm^{-1} with a small identification band at 1625 cm^{-1} [195].

Many of the previous studies [9, 11, 37, 137–139] focused on the protein secondary structure of the adult barnacle cements by using Fourier Self-Deconvolution (FSD) and peak fitting of the amide-I bands of the IR spectra. The results of these studies showed that adult barnacle cement has primarily a amyloid-β-sheet secondary structure (~40% of the overall peak area) appear at 1620–1630 cm^{-1}, in addition to other secondary structures with a low percentage of α-helix, β-turn and disordered, which appear at 1655, 1680 and 1640 cm^{-1}respectivily. Amyloid-β-sheet is suggested to be the final form of the secondary structure of the adult barnacle cement after completing cross-linking (curing) [14]. In the current, study the spectra recorded in the antennule region, after removal of the barnacles (Figure 31 (4–7)), show mainly β-sheet structures at 1665 cm^{-1} with a broad contribution at lower wavenumbers. Over the course of one week, the general shape of the amide bands remain similar and only subtle changes are observed. This observation correlates with the slow growth of the plaque of cyprid cement in the antennule region and indicates that no major chemical changes occur in the cement over time.

The reference sample of amyloid β-protein also shows a main peak at 1667 cm^{-1} (Figure 31 (3)) [52]. However, it is well known that the band at 1665–1670 cm^{-1} is the principle band for a number of proteins, main secondary structure of which is β-sheet. Additionally, ATIR measurements have been conducted for the amyloid reference sample that gave typical spectrum for amyloid main band at 1628 cm^{-1} (Figure 32) [52]. Concluding the result of these experiments it can be stated that Raman spectroscopy can distinguish between α-helix and β-sheet protein secondary structure, but, is however, not sensitive enough to distinguish between different types of β-sheet structure, that can also be confirmed by the fact that insulin (Figure 31 (2) and Figure 32 (c)) and amyloid structure (Figure 31 (3) and Figure 32(b)) are indistinguishable. Thus, this band at 1665 cm^{-1} of the spectra of the remaining juvenile barnacle cement could be related to amyloid protein structure.

In addition to the band at 1665 cm^{-1} of β-sheet, spectra of remaining barnacle cements show two bands at low wavenumbers that were previously assigned in Raman spectroscopy to aromatic residues, the band around 1604 cm^{-1} to phenylalanine and the band at 1615 cm^{-1} to tyrosine [192]. As described before, these bands of phenolic compounds are essential in cross-linking and adherence of barnacle cementing bioadhesive [13, 25].

This similarity of the protein secondary structure of the cyprid cements remaining on the CaF_2 surfaces at different time points emphasizes the advantage of the *in-situ* studies, which

enables the follow-up of chemical and physiological changes that happen with time, at variance with the *ex-situ* studies which show only the final form of the protein cement.

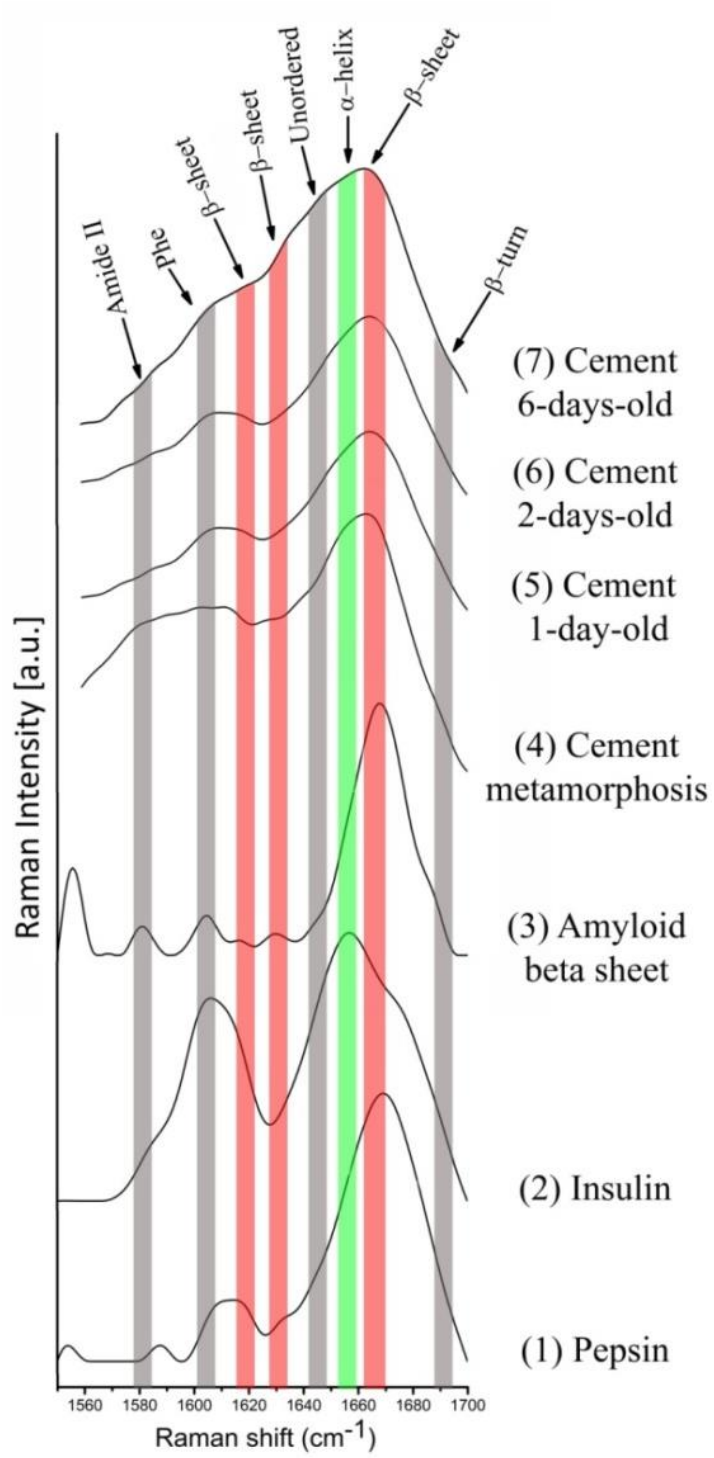

Figure 31: Raman spectra of the amide region. Comparison of cyprid cements with reference spectra ((1) pepsin (β-sheet), (2) insulin (α-helix), (3) amyloid β-protein), and (4–7) spectra recorded of cements remaining on CaF_2 disks after removal the organisms at different time points (metamorphosis, one-day, two-days and six-days-old).

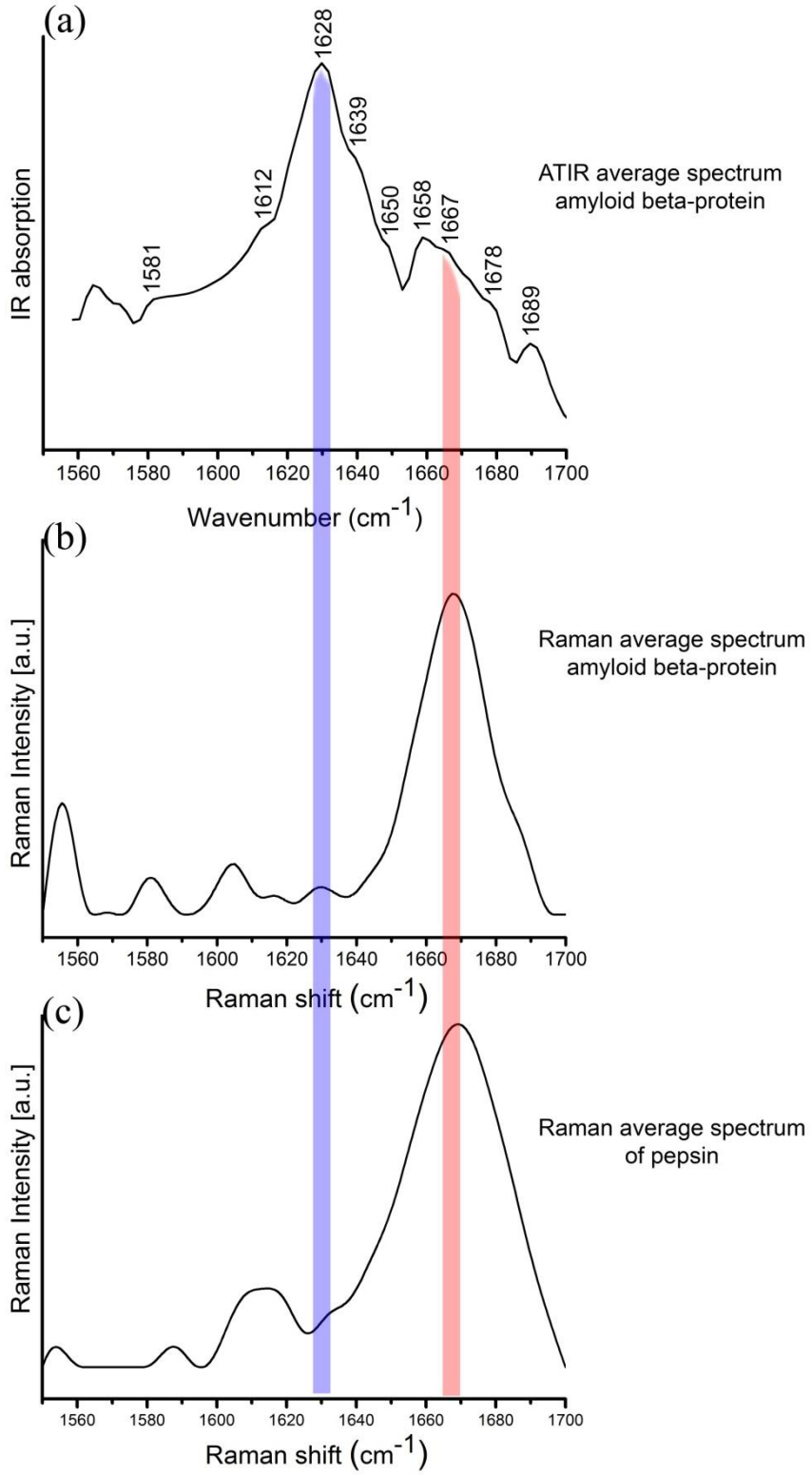

Figure 32: Comparison between a) amide-I ATIR average spectrum, b) amide-I Raman average spectrum of amyloid and c) pepsin as a reference samples of β-sheet secondary structure.

6.1.3. Discussion of *in-situ* and *ex-situ Raman results*

In this section, results of both *in-situ* and *ex-situ* Raman spectroscopy are discussed. As has been mentioned before Raman spectroscopy has a relatively large penetration depth (>20 µm), therefore, the comparison between *in-situ* and *ex-situ* results is a good opportunity to check if there is any effect of the penetration depth on the *in-situ* results.

6.1.3.1. Comparison of spectra recorded at antennule region (in-situ), remaining cement (ex-situ), and cyprid footprints

Figure 33 shows the average spectra of five individual Raman spectra recorded within the region where footprints are expected after one-day of cyprids' exploration of CaF_2 disks. In addition, average of 4 Raman spectra recorded within the antennule region of one-day-old juvenile barnacle (*B. amphitrite*) settled on CaF_2 disk before (*in-situ*) and after removing (*ex-situ*) the organisms. The intensity of footprints and remaining barnacle cement showed much lower overall signal intensities compared to the *in-situ* data of the juvenile barnacles due to the lower total amount of material probed and the fact that in the case of *in-situ* study the high penetration depth (>20 µm) captured not only the interface area between the surface and the baseplate but also part of juvenile barnacles' bodies. Generally, both spectra recorded at the antennule region (*in-situ*), and at remaining cement (*ex-situ*) showed similarity in most bands, while, the noteworthy regions are the amide bands and the carotenoid region. The footprint spectra show the absence of amide-IV at 747 cm^{-1}, while either of amide-I, II and III, at 1640, 1580 and 1266 cm^{-1} respectively spectra have shown shifting, what in case of amide-I and amide-III indicate difference in the protein secondary structures. Therefore, amide-I bands of all spectra have been taken and plotted separately in order to clarify these differences in the protein secondary structures. The differences in the protein secondary structures between *in-situ* (spectra recorded at the antennule region), *ex-situ* (remaining cyprid cement) recorded at the same time point, and the temporary adhesive (footprint) are discussed in details in following subsection 6.1.3.1.1. Another important observation in this comparison is that *in-situ* spectrum (recorded at the antennule region) showed quite intense bands of all carotenoid peaks (C–CH_2 str., C–C str., and C=C str. at 1003 cm^{-1}, 1155 cm^{-1} and 1550 cm^{-1},respectively) [10, 177, 178, 180], while, these bands are much weaker in the footprints and approximately vanish in the cement remaining after removal of the barnacle compared to the *in-situ* spectrum. This result supports the previously mentioned hypothesis that carotenoid seems to be rather located in the interior of the barnacle than in the adhesive. The hypothesis of carotenoid origin is discussed in detail in the following subsection 6.1.3.1.2.

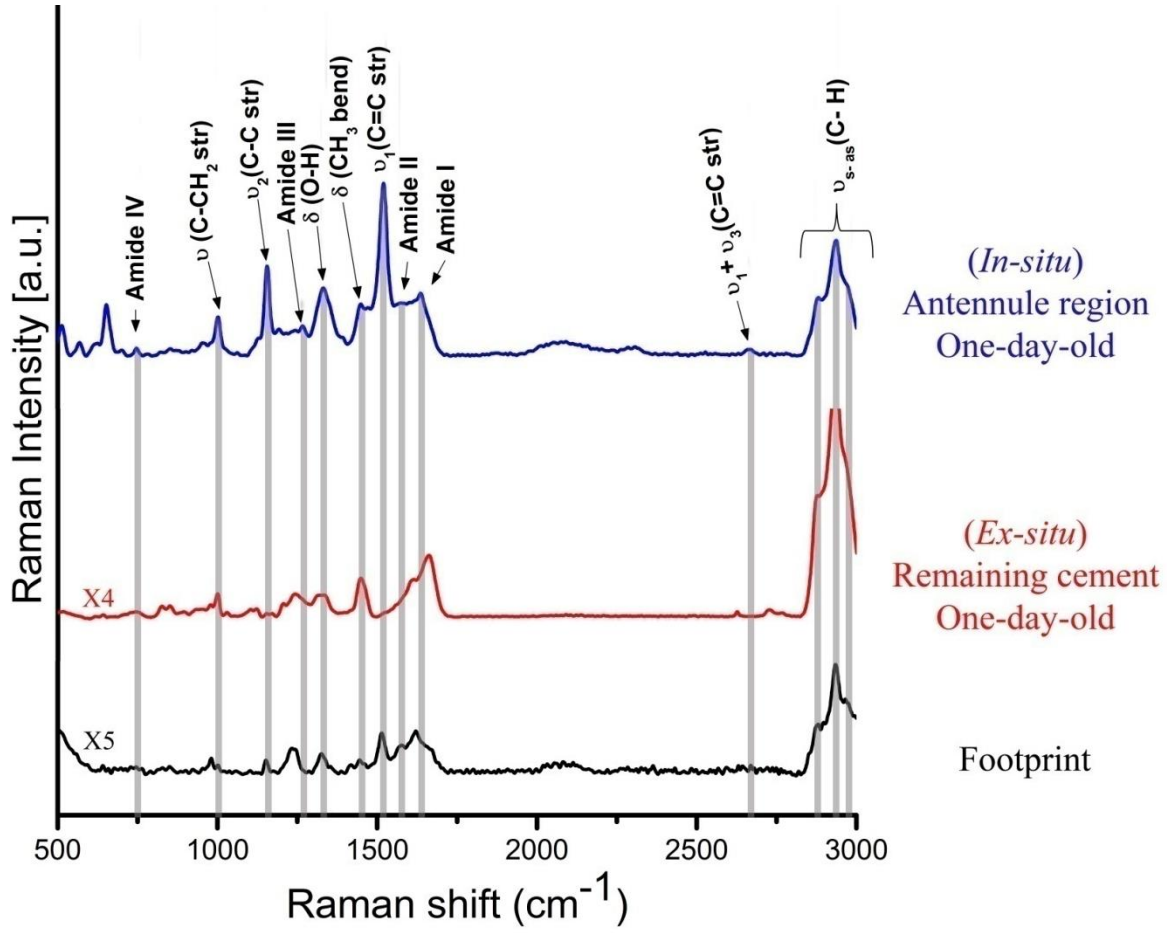

Figure 33: Comparison of Raman spectra recorded within the region where footprints are expected after one-day of surface exploration (CaF_2 disk), with Raman spectra obtained from the same one-day-old juvenile *B. amphitrite* individual settled on CaF_2 disk within the antennule region, before and after removing the organism. Each spectrum is an average of 5, 4 and 4 repetitions, respectively.

6.1.3.1.1. Protein secondary structure in *in-situ* and *ex-situ* study

In-situ and *ex-situ* spectra from Figures 27 and 31, which are discussed in 6.1.1.3. and 6.1.2. subsections, are plotted together in Figure 34 for comparison. As in previous Raman spectra images, the vertical lines reflect the typical peak positions for different protein conformations and compositions.

General observations that can be made from this image are: 1) the spectra recorded at the antennule regions are markedly different from the footprints spectra, 2) *ex-situ*: all the main protein secondary structures in remaining cement stay the same at different time points, 3) *in-situ*: data of the antennule region show high variability, shape of the spectra changes with time.

The fact that all the main protein secondary structures in remaining cement stay the same at different time points means that what is left on the surface is completely cured cement and no more crosslinking occurs.

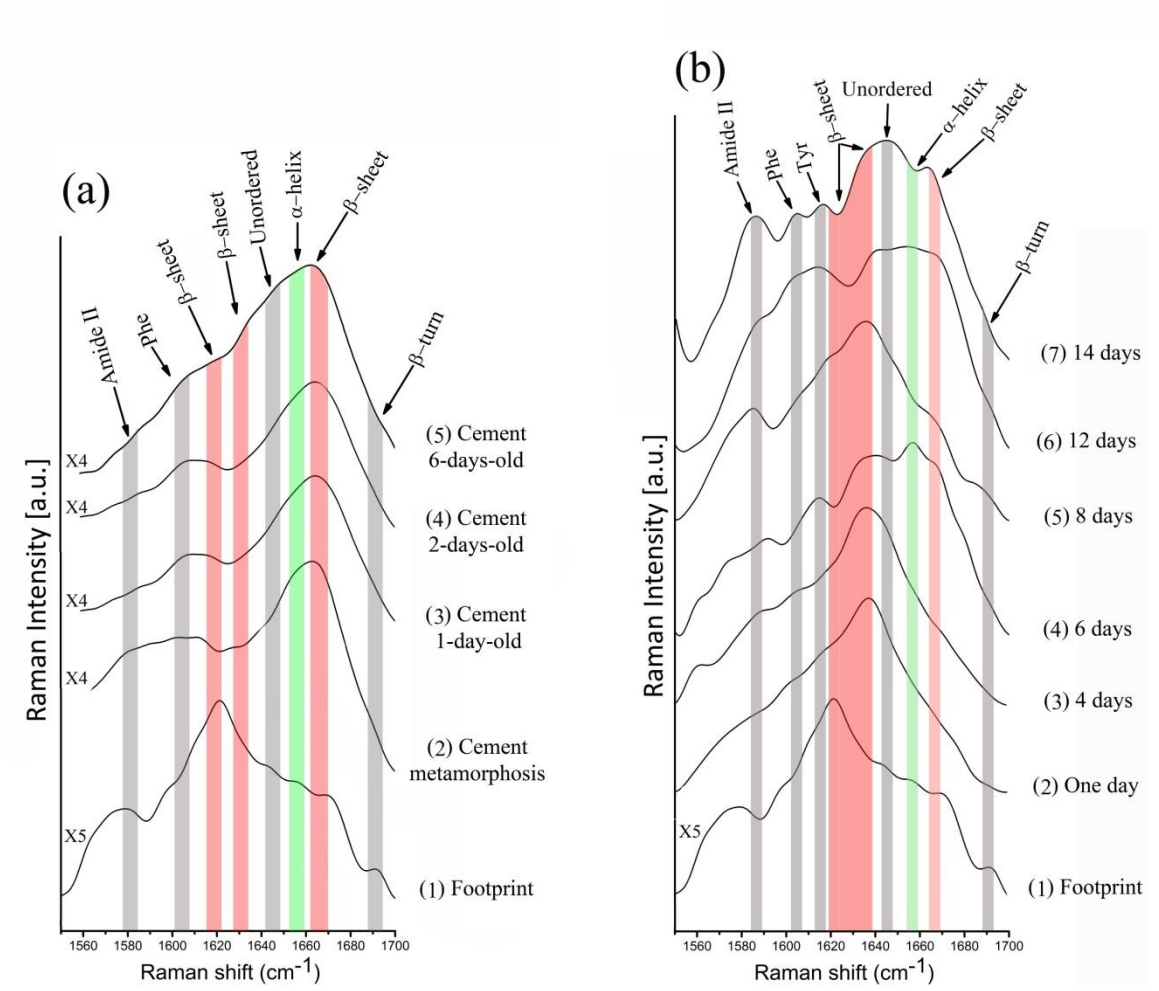

Figure 34: Raman spectra of the amide region. (a) Comparison of remaining cement region with (a1) footprint spectra (intensity five times magnified), and (a2–a5) spectra recorded of cements remaining on CaF_2 disks after removal the organisms at different time points (metamorphosis, one-day, two-days and six-days-old). (b) Comparison of (b1) footprint spectra (intensity five times magnified) and (b2–b7) spectra recorded at the antennule region of juvenile barnacles settled on CaF_2 disks at different time points.

The drastic variations in the amide-I band of *in-situ* results at different time points after settlement could be attributed to various reasons. First of all, spectra in the *in-situ* analysis of the antennule region by conventional Raman microscopy may differ as probing is not only sensitive to the surface, but also may acquire information from the bulk of the young barnacle (≈20 μm penetration depth), so that possibly not only the interface is probed, but also part of the interior of the barnacle. Thus, Raman data could be sensitive to physiological processes inside the barnacle in addition to cement secretion. However, one could also speculate that such fluctuations could also happen due to different secretory activity of the barnacles. However, one could also speculate that such fluctuations could also happen due to the difference in barnacle secretory activity. Transformation processes between β-sheet and α-helical structure was for example observed by FTIR during the conversion of native insulin

from the helical form to the fibrillar β-conformation [196]. Elhaddaoui *et al*. [196] observed that α-helix shifting from 1657 cm^{-1} to 1632 cm^{-1} can be indicative for a conversion to β-sheet, and a shoulder at 1660 cm^{-1} can be assigned to the vibrations of the non-transformed α-structure incorporated into the β-fibres.

The differences in *in-situ* spectra might be caused by either the physiology inside the barnacle or the secretory activity of the barnacles. The latter hypothesis that this variability is related to the resuming secretion of another amount of the cement in order to increase the adhesive strength with the surface [13, 25] seems more appealing due to several reasons. First, 3D laser microscope images have shown that the thickness of the remaining cyprid cements are between 10–20 μm (Figure 35), which means that main information is more probably related to the cyprid cement rather than to any other physiological parts of the organism. Secondly, this variability does not occur randomly, but there is an organised process happening with time, i.e. increasing of α-helix band at 1654 cm^{-1} is accompanied by an increasing of the phenolic bands at 1615 and 1604 cm^{-1} (Figure 34 (b4 and b6)) and decreasing of the phenolic bands intensities occur with the shifting of the α-helix band at 1654 cm^{-1} to disorder at 1645 cm^{-1} (Figure 34 (b5 and b7)). The absorption of the α-helix is shifting from 1654 cm^{-1} to 1640 cm^{-1} during the conversion to β-sheet, i.e. from liquid to solid phase [196]. Finally, it is well known that the phenolic compounds are consumed during curing process of barnacle cement [13, 25]. Therefore, the changes in secondary structure could be correlated to the cement curing process.

The result of this comparison between *in-situ* and *ex-situ* results have shown the advantage of the *in-situ* studies because *in-situ* studies allow us to follow the dynamics of the changes in real times, depending time step chosen. In order to verify this hypothesis further research is needed with use of a different technique or modification of the existing experimental methods.

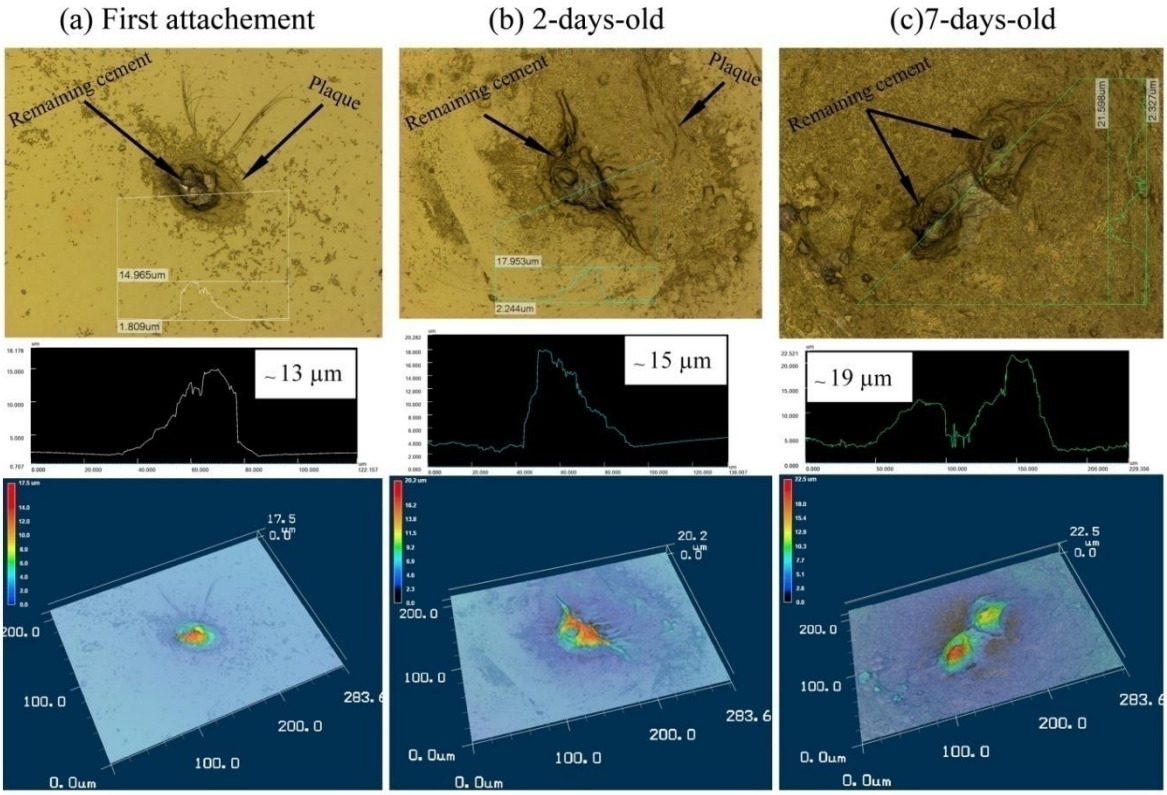

Figure 35: 3D laser microscope images of the cyprid cement remaining on the Kapton® surfaces at a) first attachment, b) 2-days-old and c) 7-days-old after removing juvenile

6.1.3.1.2. Origin of carotenoid bands

In agreement with previously published data [10] a high intensity of unsaturated C=C str. vibrations at 1518 cm^{-1} has been observed. These signals have been assigned to carotenoid components, which are mostly terpenoids that contain polyene hydrocarbon chains. Carotenoids are well known for their essential role in colored pigments and light harvesting complexes [197]. As shown in Figure 23, these components can be found across the whole barnacle and are present in both, the baseplate and the shell region. Interestingly, their concentration is very low in the antennule region in the early attachment phase (Figure 23 (a)). Thus, they have only a weak contribution to the cyprid cement. After barnacle removal the C=C str. modes are absent in the remaining cement, but in the footprints spectrum it is observed with very low intensity which means that footprints seem to contain some of these unsaturated components (Figure 33). This again supports the notion that footprints and the cyprid cement use a different chemistry. Especially at later time points of the experiments, strongly varying carotenoid content has been observed in the sample (e.g. increase towards 14 days in Figure 24 (a)). This raised the question about the origin of these compounds. Since β-carotenoid is specifically required for the formation of oligomeric forms of the light harvesting complex in the green algae [197], it is possible that the detection of carotenoid bands in all juvenile barnacle spectra are related to the green algae (*Tetraselmis*), which were

used for feeding. In Figure 36, spectrum of the antennule region (a) of 14 days old juvenile barnacle is compared to Raman spectra of *Tetraselmis* algae (b) and commercially β-carotene (c). All three spectra show intense str. vibrations at 1518 cm^{-1} which are related to υ_1(C=C str.). The υ_2(C–C) str. and C–CH_2 str. vibrations, at 1155 $cm^{-1}$and at 1003 cm^{-1}, respectively, are visible at similar wavenumbers and slightly vary in intensity with respect to the C=C band. In all three cases, the overtones of the C=C vibration become additionally visible. The similarity of the spectra suggests that one source of carotenoids could indeed be the algae used for feeding.

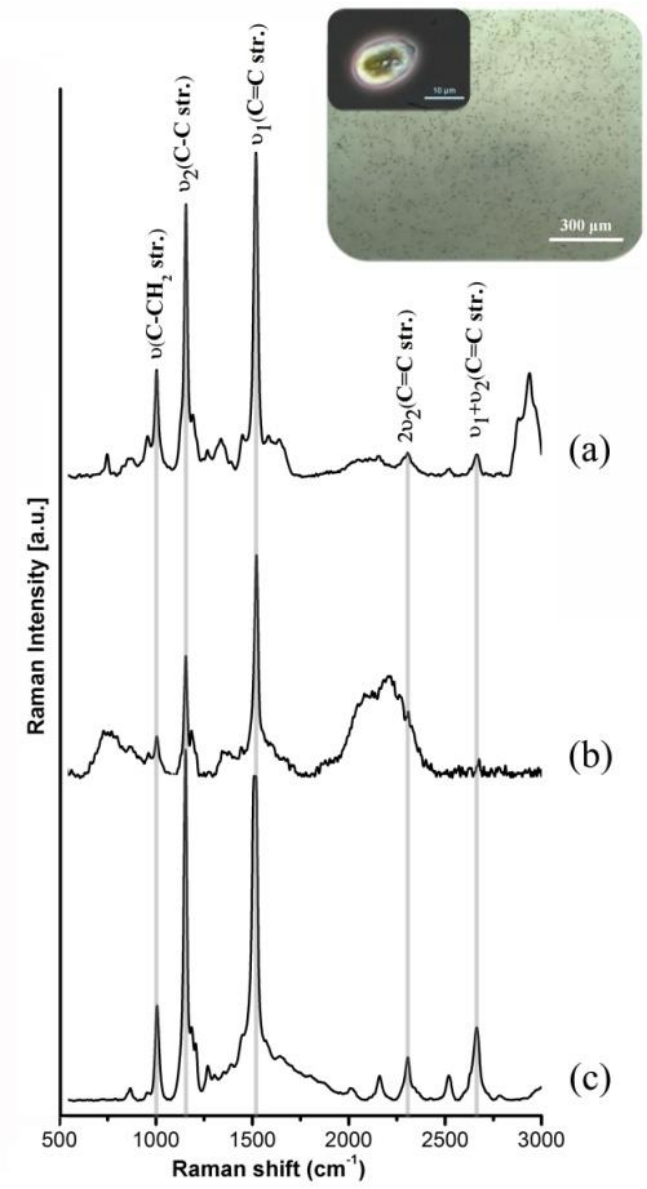

Figure 36: Agreement of carotenoid bands in Raman spectra of a) antennule region of 14-days-old juvenile barnacle (*B. amphitrite*) settled on a CaF_2 disk, b) green algae (*Tetraselmis*) used to feed the barnacles, and c) standard β-carotene.

To further understand this phenomenon, *in-situ* Raman measurements were conducted within the antennule region of juvenile barnacles one hour before and after feeding the organisms with algae. The experiments were conducted with juvenile barnacles between ten to thirteen-days after settlement. The results in Figure 37 show that the overall carotenoid band intensity decreases over time. This phenomenon could be attributed to the bleaching of the photosensitive pigment by the laser beam after a long illumination period, which commonly occurs in natural systems with carotenoid pigments [112]. After feeding the carotenoid signal is in all cases enhanced compared to the signal before feeding, clearly indicating that the algae are the source of unsaturated components visible in Raman.

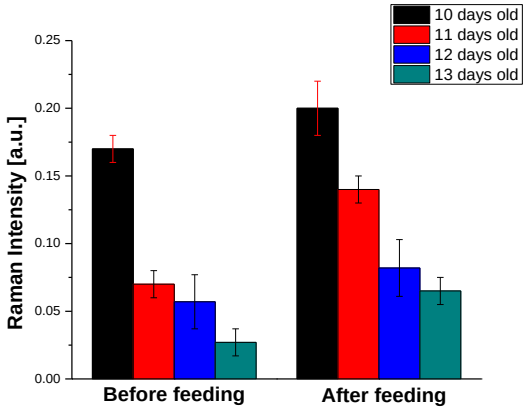

Figure 37: Young barnacles between 10 and 13 days after settlement were observed. Bars represent the mean of Raman intensity of the carotenoid bands one hour before and one h after feeding, error bars are related to the student's t-distribution.

The difference between this result and the results shown before (Figure 23 (a)), occurs since barnacle feeding times have not been mentioned in the earlier studies. Therefore, peaks intensities of carotenoids in Figures 23 vary greatly at different time points. This fluctuation of carotenoid bands intensity in the spectra recorded at different time points (Figure 23 (a)) may be related to the amount of food juvenile barnacles were fed.

6.1.3.2. Confocal Raman spectroscopy maps

Application of confocal mode in Raman spectroscopy allows to restrict the thickness of the probed volume and thus to make the measurements more interface sensitive. This technique has been used to investigate the chemical distribution of the: 1) juvenile barnacle baseplates (*B. amphitrite*) settled on CaF_2 disks at different time points (*in-situ* study), and 2) cyprid cements remaining on the CaF_2 disks after juvenile barnacle removal (*ex-situ* study). In course of the *in-situ* study, firstly some difficulties arose during the initial attempts to get explicit mapping due to the numerous movements of organism during measurement since after permanent attachment barnacle rotates itself to find the best orientation of cirri depending on the currents and other conditions to reassure the easiest flow of food.

Therefore, only older juvenile barnacle individuals (over 5 days old) have been chosen for the experiment to avoid this problem.

In order to visualize the spatial distribution of elements, 2D distribution maps have been generated by integrating the intensity of 400 scan points of the selected bands over the entire baseplate and antennule region and represented as color images in Figure 38 (a and b), respectively. The chemical bands included in Figure 38 are calcite $\upsilon_1(CO_3^{2-})$ vibration (1000–1100 cm^{-1}); amide-I contributions (υ(C=O) str. (1600–1700 cm^{-1}); a combination band of CH str. (2880–2980 cm^{-1}); the broad –OH str. signal (3300–3500 cm^{-1}); and unsaturated C=C double bond υ_1(C=C str.) vibrations (1480–1565 cm^{-1})).

The *in-situ* results (Figure 38 (a)) have shown that calcite is located at the rim of the juvenile barnacle baseplate at the calcareous shell region, whereas in the *ex-situ* distribution map calcite is absent, which means that there is not any calcite present in the composition of the cyprid cement. Interestingly, the intensity of the calcite located at the boundary of the calcareous rim is not the same in the *in-situ* maps (Figure 38 (a)), i.e. the intensity distribution is not continuous and is separated into discrete peaks. This phenomenon could occur due to one or combination of the following reasons. First, presence of the cement ducts at specific parts of the rim [13] may lead to the lower thickness at these duct areas than in others, and therefore lower intensities at these duct areas can occur. Second, distances between the selected measurement points could have resulted in discrete peaks after integration. Finally, the calcareous shell could form unevenly and that may have resulted in different intensities along the rim.

Except for calcite, both of *in-situ* and *ex-situ* maps showed similarities. Both amide-I and CH are localized at the antennule region, where the adhesive is secreted (in case of *in-situ*), and in the remaining cyprid cement (in case of *ex-situ*). This result supports the previous assumption that cyprid adhesive is a proteinaceous material which has hydrophobic properties. In the *in-situ* maps, both amide-I and CH groups appear as two steep "mounts" located exactly at the antennule region, which supports the previously mentioned assumption that juvenile barnacle cement is localized only at the antennule region in these earlier time points.

Most of the OH str. has been detected in the area surrounding the antennules and surrounding the organism itself (Figure 38 (a)). It can be assumed that in comparison to the shell and the antennule region, a greater amount of water is present in this region. The depletion of OH str. in the antennule region could arise from the highly crosslinked cyprid cement, which is less hydrated in comparison to the surrounding baseplate since regions around the antennule and around the organism are filled with artificial seawater.

Confocal results provide further proof that carotenoid signal (υ_1(C=C str.) vibrations) is most probably not related to the cyprid cement, since it is present randomly with different intensities in entire baseplate region in the *in-situ* maps (Figure 38 (a)), while it vanishes in the *ex-situ* maps of the remaining cement (Figure 38 (b)).

Finally, the confocal Raman data is consistent with previous non-confocal Raman microspectroscopy results and in both cases the different three regions (calcareous region, area surrounding the antennule region and the antennule region) can be distinguished.

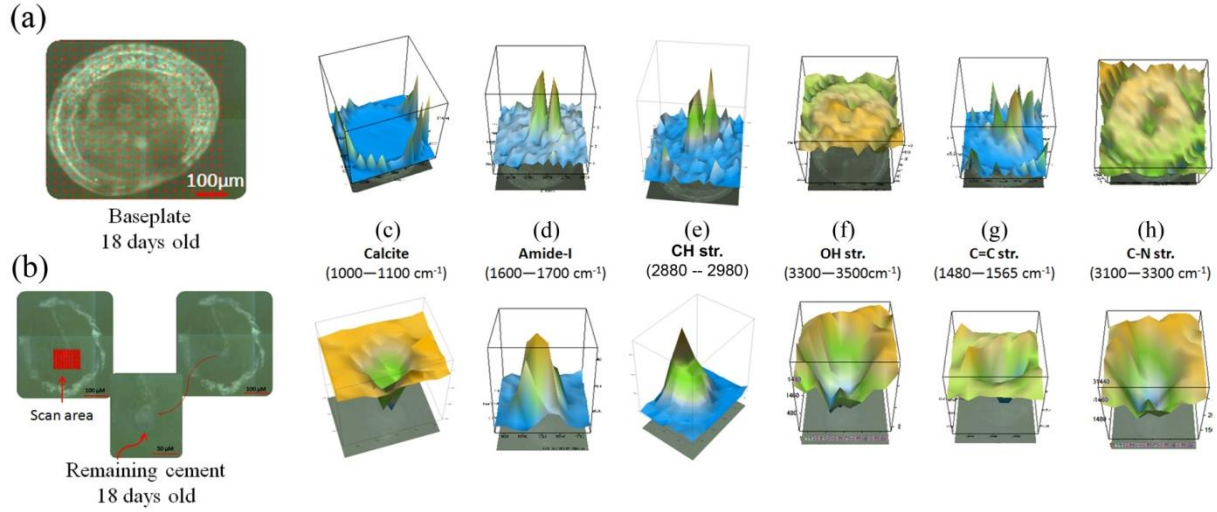

Figure 38: 3D distribution maps of selected Raman bands intensities: calcite $\upsilon_1(CO_3^{2-})$ vibration (1000–1100 cm^{-1}); amide-I contributions (υ(C=O) str. (1600–1700 cm^{-1}); a combination band of cyanogen bromide type ($\upsilon_3+2\upsilon_2$(Br–C≡N) str. (2900–2980 cm^{-1}); the broad –OH str. signal (3300–3500 cm^{-1}); and unsaturated C=C double bond υ_1(C=C str.) vibrations(1480–1565cm^{-1}))

6.2. µ-X-ray microprobe fluorescence results

The results presented in the following chapter were obtained through collaborative work of several people. The samples with juvenile barnacles of specific ages were prepared personally by me. Experiments were conducted by Mr. T. Senkbeil and me under attentive guidance of Dr. Rolf Simon and Dr. David Batchelor. The raw data was processed by Mr. T. Senkbeil. Finally, I performed the data processing and results are being discussed below.

6.2.1. *In-situ* results of µ-X-ray microprobe fluorescence

The advantage of X-ray microprobe fluorescence technique over electron microscopy is its greater penetration depth compared to electron microscopy, i.e. ~100 µm compared to only a few nanometers in electron microscopy and ~20 µm in case of Raman spectroscopy. *In-situ* *µ*-X-ray fluorescence (µ-XRF) has been used in order to provide a 'distribution map' of the constituent elements of the baseplate of the juvenile barnacle settled on the Kapton® foil (8 µm thickness and 64 mm in diameter) in artificial seawater at different time points (from cyprid to seven-days-old) *in-situ*. As described in subsection 5.1.2, kapton® is necessary as the substrate needs to be X-rays transmissive. The boundary ages, studied in this experiment, metamorphosis and 7 days old, were chosen for a better demonstration of the change in the chemical elemental distribution with age and are presented in Figure 39 and discussed below.

Calcareous shell: Figure 39 shows that at baseplate rims of the juvenile barnacle settled at different time points (metamorphosis and 7-days-old), calcium (Ca) is co-localized with high concentrations of other elements such as potassium (K), strontium (Sr) and manganese (Mn).

Indeed, Sr and Mn are known to be built into the calcareous shell plates [198]. To build a strong calcareous shell these elements were deposited during calcification process on the outer membranes (*Mantle epithelium*) of the organism most likely from artificial seawater components. The specific structure of mantle epithelium cells allows lime transportation through the mantle from the ambient seawater [193]. µ-XRF maps of metamorphosis showed that there are no Ca, K, Sr or Mn at the rim, which means that the calcification process has not started yet. This result is supported by the Raman result for calcareous process commencement (section 6.1.2), which has shown that the calcification process starts during the final stage of metamorphosis along with the disposal of the carapace.

A general observation of stronger signal on one side of the rim has been made for all recorded datasets. Most probably this artifact has occurred due to the geometry of the non-confocal setup and not due to an asymmetry of the elemental concentrations. Since penetration depth for each of the afore mentioned elements is greater than 100 µm, the concentrations of each element are seemingly projected into the plane of the Kapton® foil under a 45° angle. The signal is intensified on one side and is unaffected on another side of the rim, if the orientation of a shell plate coincides with the direction of the X-ray beam, as it is the case for the side with high intensity of the rim.

Center of baseplates: µ-XRF maps of juvenile barnacles have also shown that other elements such as iron (Fe), copper (Cu), zinc (Zn), arsenic (As), and bromine (Br) are observed near the center of baseplates. It could be possible that both of Fe and Cu are related to the blood vessel of the organism [50]. However, to date there is no evidence in presence of Zn and Br in barnacle blood or blood vessels. These results of XRF are in agreement with results of conventional and confocal Raman, which showed that different regions of juvenile baseplate have different chemical structure, exactly what was observed in the XRF results. Raman and confocal Raman results showed that calcite is localized at the rim of the baseplate, which supports the XRF result for occurrence of Ca also at the rim. Furthermore, the distribution of these elements (Fe, Cu, Zn , Br and As) at the center point of the baseplate may be related to the specific protein confermation expected in the cement at the antennule region. This hypothesis can be supported by the proteinaceous nature of the cement at the antennule region what is supported by Raman and confocal Raman spectroscopy results described in subsection 6.1.

The maps recorded for the metamorphosis show that Fe, Cu, Zn, As and Br are located in the middle of the baseplate, which is also truef or juvenile barnacles. However, in the case of metamorphosis, other elements (Ni, Mn, Sr) are also located in the middle, but with a low concentration.

Interestingly, in all maps Cu, Fe and Zn are located at the central part of cyprid, while Br is only localized as two points in the antennule region. The shift observed in XRF maps between Br position and Fu, Cu, Zn and As could be related to the inner organs of the juvenile barnacle related to the high penetration depth. Therefore, these signals might come from the abdomen that is why it was necessary to study the food of the juvenile barnacle, green algae. Indeed, these elements have been found in the green algae, in addition to high signal for Br. The fact that all Br signal is located at the antennule region and no Br signal was observed at the abdomen area could have occurred since juvenile barnacle had consumed

this element because it plays a role in protein curing process. However in order to avoid the penetration depth problem the *ex-situ* studies were conducted.

A comparison with control spectra of green algae (Figure 40) has shown similarities and thus a potential correlation of feeding with the occurrence of these elements. The presence of these elements (Fe, Cu, Zn, As and Br) will be discussed in detail in the subsection 6.2.3.

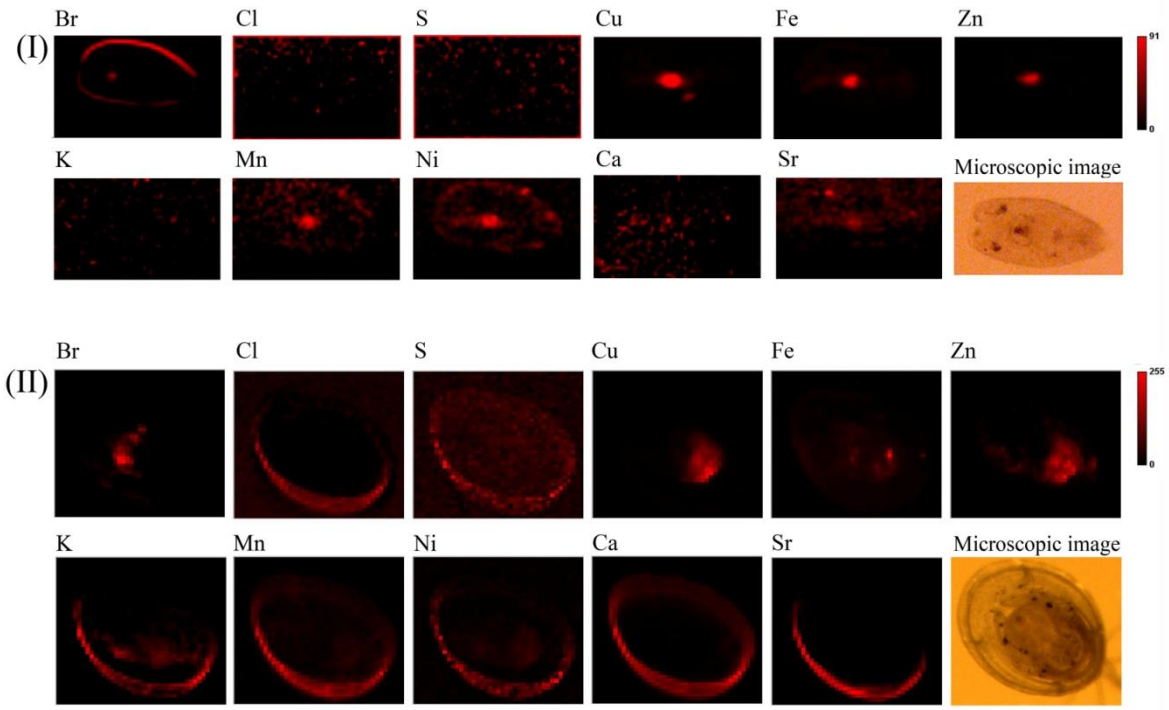

Figure 39: *In-situ* X-ray fluorescence maps of juvenile barnacle baseplates (*B. amphitrite*) settled on Kapton® foils at: (I) Metamorphosis, and (II) 7 days old. Optical micrographs of the scanned barnacles are presented below the XRF maps.

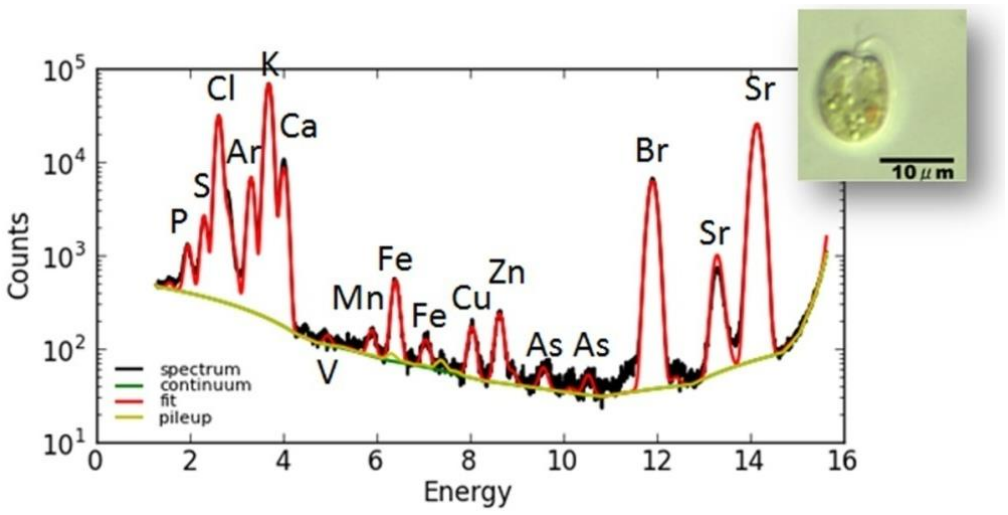

Figure 40: *In-situ* X-ray fluorescence spectrum of green algae (*Tetraselmis*). (Provided by T. Senkbeil)

6.2.2. *Ex-situ* µ-X-ray fluorescence mapping of cyprid cement

Ex-situ µ-X-ray fluorescence experiments of remaining cyprid cements left on Kapton® foil organisms at different time points have been conducted at the FLUO beamline. The samples were carefully prepared as described in section 5.3. to avoid any contamination.

Figure 41 shows the elemental distribution maps of the remaining cyprid cements that had been left on the Kapton® foils after organisms' were carefully removed at different time points (1st permanent attachment (Figure 41.1), one-day-old (Figure 41.2), two-days-old (Figure 41.3) and 7-days-old (Figure 41.4), which have been recorded *ex-situ* by using µ-XRF spectroscopy. By looking at the elemental mapping of the remaining cements (Figure 41.1–4) one can easily see the similarity of the elemental distributions on the samples at different time points, although each sample exhibits different distributional patterns. The distribution of these elements is mainly localized in one smeared spot (Figure 41.3–4), whereas in the other two samples they appear as two close adjoining spots (Figure 41.1–2). Both single and double spots situated approximately in the center of the juvenile barnacle manifest the initial place of the cyprid larvae permanent attachment site. After comparison of the spot areas where these elements are observed with the 3D images that have been obtained using the 3D laser microscope (Figure 41) it became clear that these high intensity spots are located exactly at the antennule region where the cement adhesive is expected at these earlier time-points. This deviation in distance between spots occurs due to the fact that a cyprid is able to start permanent settlement with different distances between its antennules, so that sometimes antennules adhere rather close to each other and attachment place merges in one smeared spot.

µ-XRF maps for all *ex-situ* samples have shown that bromine (Br), chlorine (Cl), sulfur (S), copper (Cu), zinc (Zn), selenium (Se) and scandium (Sc) are mainly concentrated in the remaining cements. However, iron (Fe), nickel (Ni), calcium (Ca) and strontium (Sr) are found in the cyprid cements as well, but they have shown low concentrations in comparison to the other elements. In the two-days-old maps (Figure 41.3), Fe spot shifted to upper left corner and is intensely pronounced. This spot rich with Fe could be attributed to contamination, so that µ-XRF measurement device could not detect the Fe in all other area of the map due to the significant difference in intensity. In addition to location of Cu, Fe, Ca and Sr in the spots of the remaining cement they are also concentrated in a ring-like pattern bounding the base of the barnacle, and this pattern correlates to the distribution pattern of adult cement adhering baseplate yet to be calcified to the substratum. This observation is difficult to see at first (Figure 41.1), since at this time point remaining cyprid cement of the initial attachment has not any contact yet between the cyprid and the surface but only the pair of antennules.

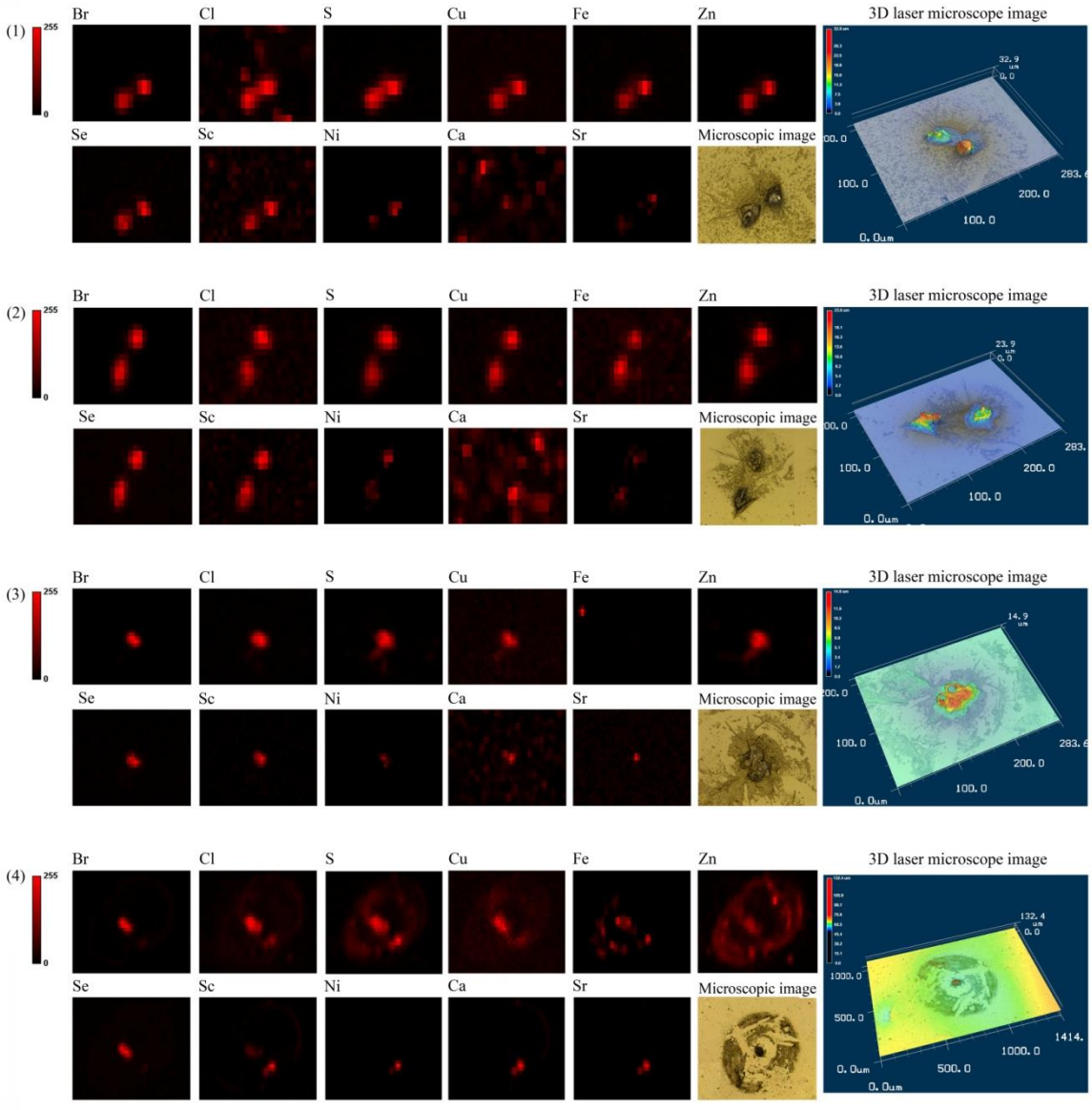

Figure 41: Elemental mappings of the cement deposits of four barnacles (*B. amphitrite*) adherent to Kapton foil. The organisms were removed from the Kapton substrate directly after (1) the permanent attachment, (2) one day, (3) two days and (4) seven days after settlement and the remains have been analyzed using a non-confocal setup.

Interestingly, the remaining cyprid cement of old organism (seven days old) show a quite high concentrations of each of Cl, S, Cu, Fe and Zn in the baseplate ring (Figure 41.4), which could be attributed to remains of a fine biological membrane forming the baseplate area as at earlier life stages before forming the calcareous baseplate. Furthermore, the same sample has shown that all Ni, Ca and Sr are found colocalized in a small spot on the outer rim of the barnacle baseplate, and is most likely to be the remains of a shell plate. The previous *in-situ* measurements have already confirmed the presence of these three elements in the shell plates.

However, the role that the majority of these elements, like Br, Se, Sc, play in the marine bioadhesives still remains vague. In the following subsection 6.2.3., some possible

explanations of the role of the elements detected during *in-situ* and *ex-situ* µ-XRF will be discussed in detail.

6.2.3. Discussion of *In-situ* and *Ex-situ* µ-XRF mapping

This section is meant to draw the comparison between µ-XRF maps of baseplates of 7-days-old juvenile barnacles (*B. amphitrite*) settled on Kapton® foil that have been obtained *in-situ* and *ex-situ,* i.e. for the remaining cyprid cement left on the Kapton® foil after organisms removal. This section is divided into two subsections: the first one contains short summary of both *in-situ* and *ex-situ* mapping results and the comparison between them, while the second subsection produce possible explanations of role of the elements detected in the antennule region and remaining cyprid cement as an adhesive constituents.

6.2.3.1. The comparison between in-situ and ex-situ results

As shown in Figure 42.1, all calcium (Ca), strontium (Sr), manganese (Mn), sulfur (S) potassium (K), nickel (Ni) and chlorine (Cl) are concentrated in the outer rim of barnacles and as described before this indicates the bio-mineralization process. Ca, Sr, and Ni appear also in the *ex-situ* maps, but with low concentration and being localized in a small spot on the rim that delimits the baseplate of the removed barnacle (Figure 42.2), while high concentrations of Cl and S appear in the spot area of the remaining cement.

As described above, *in-situ* maps have shown that each of bromine (Br), copper (Cu), iron (Fe) and zinc (Zn) are localized approximately in the middle of the barnacle baseplate (Figure 42.1), but only Br is localized in the two spots closely placed to each other at the antennule region, while all other elements (Cu, Fe and Zn) are shifted closer to the gut region of the organism. At the beginning this result has been thought to be related to the high penetration depth of the X-ray beam, but, interestingly, the *ex-situ* maps have shown that all of these elements in addition to Br are found at the region of the remaining cyprid cement, which means that these elements could be a part of the chemical composition of the cyprid cement. Each of these elements has been found in the XRF spectrum of the green algae that were used for feeding the juvenile barnacles. Therefore, it is possible that barnacles consume these elements from the food and employ them in cement formation.

In the *ex-situ* maps selenium (Se) and scandium (Sc) are localized in the remaining cyprid cement, while these elements are absent in the *in-situ* maps, which means that in *in-situ* measurement their intensities have been lower than the overall noise signal and therefore they have not been included into mapping. Despite the advantages of *in-situ* experiments, *ex-situ* measurements allow to focus on the cement interface and to avoid signals from the inner organs of the organism due to large penetration depth.

6.2.3.2. Possible explanations of the role of the detected elements

As described before, the role of most of these elements (Br, Cu, Fe and Zn) in the marine bioadhesives still remains vague. In this subchapter, some ideas that may provide assistance to understand the role of these elements are explained.

Firstly, **Bromine (Br)**: as described above Br has shown a different distribution pattern in comparison to all other elements, detected in the middle of barnacle in this study. Although it is still not clear which function Br has in barnacles, but perhaps it can be linked to substantial amounts of chitin found in barnacle cyprids and juvenile barnacles [199–200]. Since the location where Br has been found corresponds to the place of permanent attachment of cypris larvae, further experiments have been conducted in order to investigate whether the presence of bromine could be linked to the cyprid cement or not.

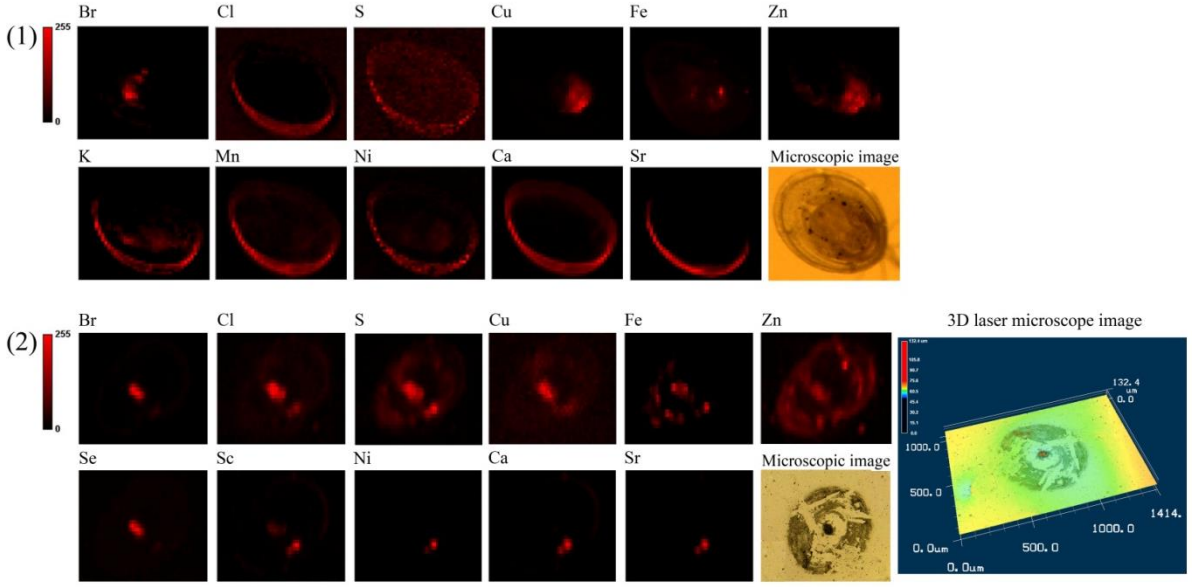

Figure 42: µ-X-ray fluorescence maps of 1) 7-days-old juvenile barnacle baseplates (*B. amphitrite*) settled on kapton (*In-situ* study) and 2) adherent deposits of 7-days-old juvenile barnacle (*B. amphitrite*) left on a Kapton foil after barnacle removal (*ex-situ* study).

Secondly, **copper (Cu) and zinc (Zn)**: the presence of these elements may contribute to the understanding of the role of Cu and Zn in the cyprid cement. At the early stage of cyprid settlement, proteinaceous material is secreted from the tip of each of cyprid's two antennules and at this stage, cyprids must find or be provided with new interface suitable for amyloid fibril like protein formation. This interface of β-sheet, consisting of strands parallel to each other, may lead to complexation with some metal ions like Cu and Zn to enhance the tendency for β-sheet formation. Interestingly, it was found in recent studies that some metal ions such as Cu^{2+} and Zn^{2+} might play an essential role for denaturation of proteins and their transformation into amyloid fibers [201]. These two transition metal ions Cu^{2+} and Zn^{2+} are related to Alzheimer's disease and cause protein denaturation and formation of amyloid fiber. At the interface, Cu^{2+} and Zn^{2+} are found to be relevant to the transformation of α-helix to β-

sheet leading to protein aggregation [201], which is in agreement with the variability of protein secondary structures of the juvenile barnacle cement at different time points that was observed in the *in-situ* amide-I Raman spectra, described in subsection 6.1.1.4. Due to this relation between the metal ions complexation with the initial protein used for the settlement, in this study it has been possible to detect these ions under the cyprid antennules by using μ-XRF technique. As the ability of peptide sequence to chelate with zinc ions is not possible in the α-helix state and crosslinked β-sheet, new configuration of non-crosslinked antiparallel β-sheet at the interface is necessary to form metal-peptide complexation accelerating the aggregate formation [201]. Therefore, these elements observed could be involved in the cement curing process.

Finally, **iron (Fe)**: As described before in subsection 6.2.1, both Fe and Cu could be related to the blood vessel of the organism [50]. However, this suggestion is quite controversial because Fe has been found not only in the *in-situ* maps, but also in the *ex-situ* maps in the remaining cyprid cement. However, metal elements such as Cu and Fe have been previously found in bioadhesives of marine organisms, e.g. mussel foot protein [128]. It is suggested in [128] that cohesive strength that is based on the same chemical mechanisms as adhesive interactions, are governed by the formation of Hydrogen bonds and complexes between DOPA (3, 4-dihydroxyphenylalanine), common mussels' protein constituent, and metal ions. The studies by Taylor et al., [202, 203] and Fant [204] showed respectively that Fe^{3+} and Cu^{2+} ions are able to increase the rigidity of the cementing material. Sever et al., proposed in [205] that protein cross-linking during mussel adhesive synthesis occurs mainly due to the presence of transition metals, especially iron, because this trivalent ion was suggested to serve as a center for cross-linking of three DOPA residues. Therefore, a number of authors proposed involvement of metal-protein interaction in formation, synthesis and curing of marine bioadhesives, including barnacle cement [128]. Although the chemical composition, sequence and sticking mechanisms of barnacle adhesive differs from those of mussels [128], therefore, it could be possible that elements Br, Cu, Fe and Zn detected in both *in-situ* and *ex-situ* experiments play similar role in the crosslinking of barnacle cement proteins as in mussel adhesive.

6.3. Similarity of juvenile cement of different barnacle species (*B. amphitrite* and *B. improvisus*)

The same *in-situ* and *ex-situ* experimental techniques, employed in experiments with *B. amphitrite*, have been also applied to another barnacle species known as *Balanus improvisus*. As has been described in subsection 2.2.2, both species are exposed slightly different environmental factors such as temperature, salinity etc. Therefore, the aim of studying another species has been to see if these differences in the environmental conditions could affect the adhesive chemical composition or not. All results (*in-situ* and *ex-situ*) obtained for *B. improvisus* have shown similarity with the results for with *B. amphitrite*, which supports the hypothesis that both species use chemically similar adhesives.

Following are some of *in-situ* and *ex-situ* results obtained for *B. improvisus* juvenile barnacles in comparison with the previous results for *B. amphitrite*.

6.3.1. Raman spectroscopy

Raman spectra of the three distinct regions (Calcareous region, area surrounding the antennule and the antennule region) for both species (*B. amphitrite* and *B. improvisus*), and their dynamics at different time points after metamorphosis are shown in Figure 43. The only difference we can observe between both species is the intensity of the C=C str. band at 1518 cm^{-1} related to carotenoid. As has been described in subsection 6.3.1.2, this band is most probably related to the green algae and is not related to the barnacle adhesive. Therefore, it should not be accounted as a difference criterion for both species.

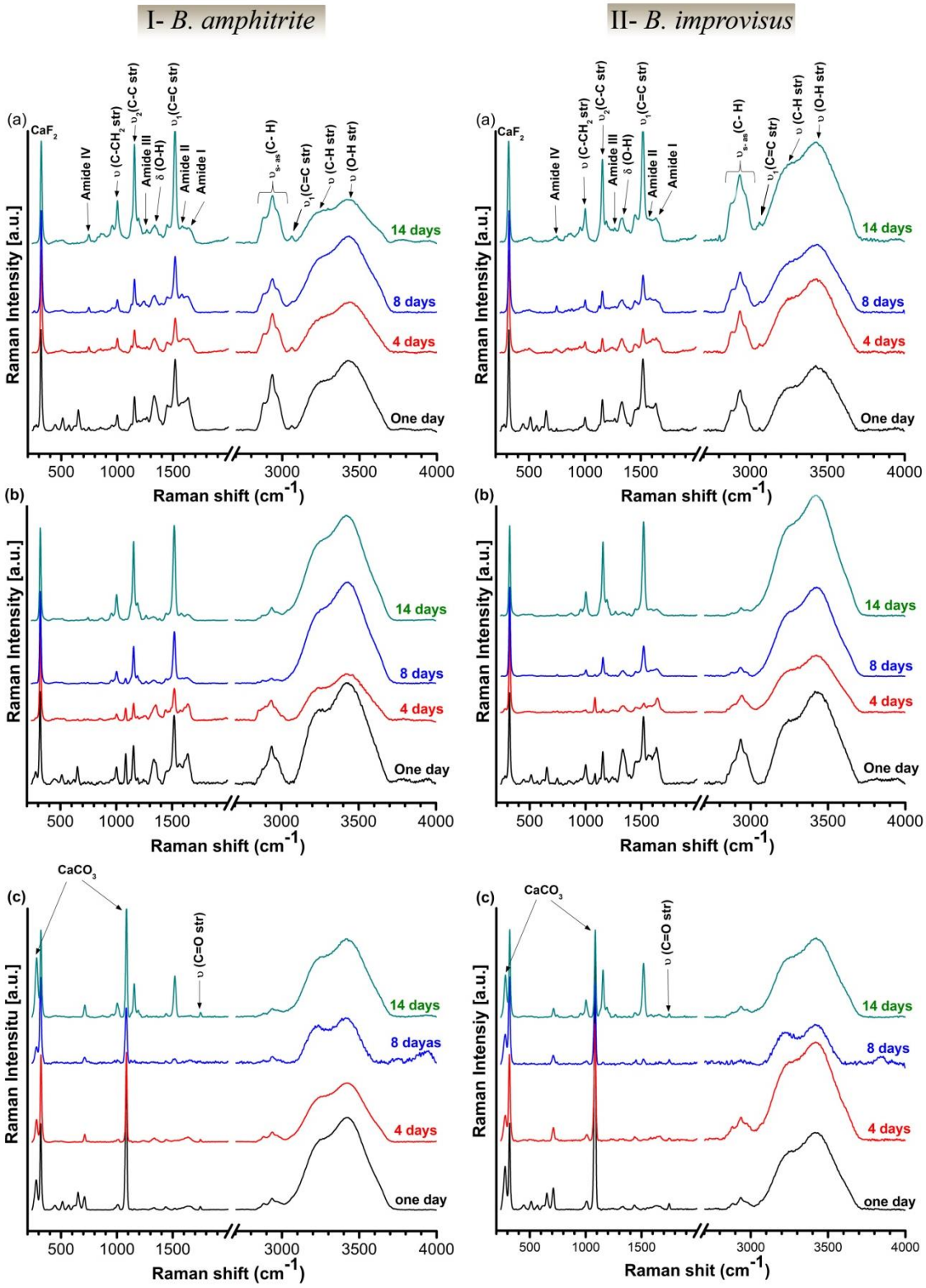

Figure 43: Raman spectra of juvenile barnacles I) *B. amphitrite* and II) *B. improvisus*at different time points after settlement (one day up to 14 days). (a) Antennule region,(b) baseplate region surrounding the antennule and (c) calcareous region.

6.3.2. Confocal μ-Raman spectroscopy

As shown in Figure 44 and 45 the *in-situ* and *ex-situ* confocal Raman spectroscopy results of both species have shown the same chemical distribution through the juvenile barnacle baseplate (in case of *in-situ*) and the remaining cyprid cement specimens after barnacle removal (in case of *ex-situ*).

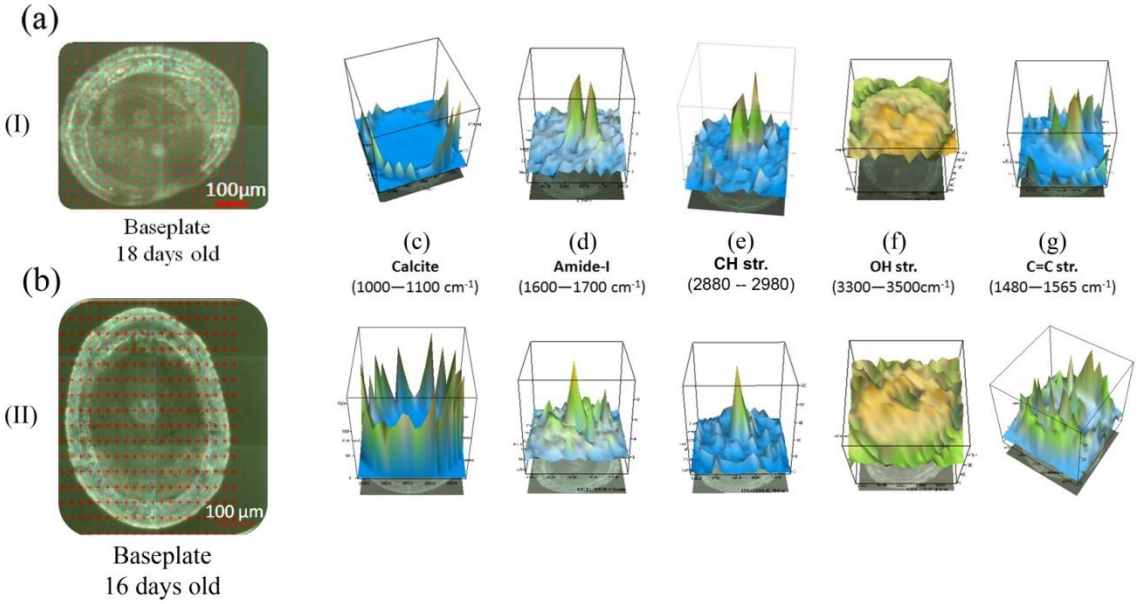

Figure 44: Mapping of confocal Raman spectroscopy for both species I) *B. amphitrite* and II) *B. improvisus*. (a) and (b) – the microscopic images with the measurement points for both species, (c–g) – 2D distribution maps of selected Raman bands intensities: (c) – calcite $\upsilon_1(CO_3^{2-})$ vibration (1000–1100 cm^{-1}); (d)–amide-I contributions (υ(C=O) str. (1600–1700 cm^{-1}); (e) –a combination band of C–H str. (2880–2980 cm^{-1}); (f) –the broad –OH str. signal (3300–3500 cm^{-1}); and (g)–unsaturated C=C double bond υ_1(C=C str.) vibrations(1480–1565cm^{-1}).

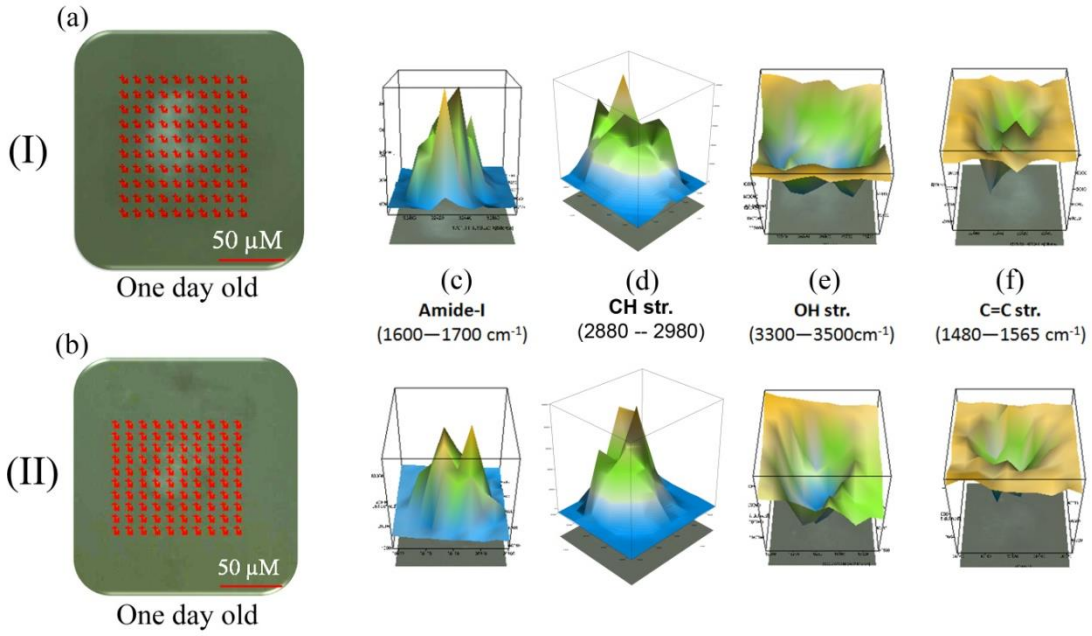

Figure 45: Mapping of confocal Raman spectroscopy of the remaining cyprid cements for both species I) *B. amphitrite* and II) *B. improvises*. (a) and (b) – the microscopic images with the measurement points for both species, (c–f) – 2D distribution maps of selected Raman bands intensities: (c)–amide-I contributions (υ(C=O) str. (1600–1700 cm^{-1}); (d) –a combination band of C–H str. (2880–2980 cm^{-1}); (e) –the broad –OH str. signal (3300–3500 cm^{-1}); and (f)–unsaturated C=C double bond υ_1(C=C str.) vibrations(1480–1565cm^{-1}).

6.3.3. Calcification process

Figure 46 shows the similarity in starting of calcification process of both species (*B. amphitrite* and *B. improvisus*). Interestingly, both species show the same behavior: within the first 8 hours of the calcification process, the intensity of calcite bands exhibits a steep growth, and decreases about 10 times afterwards.

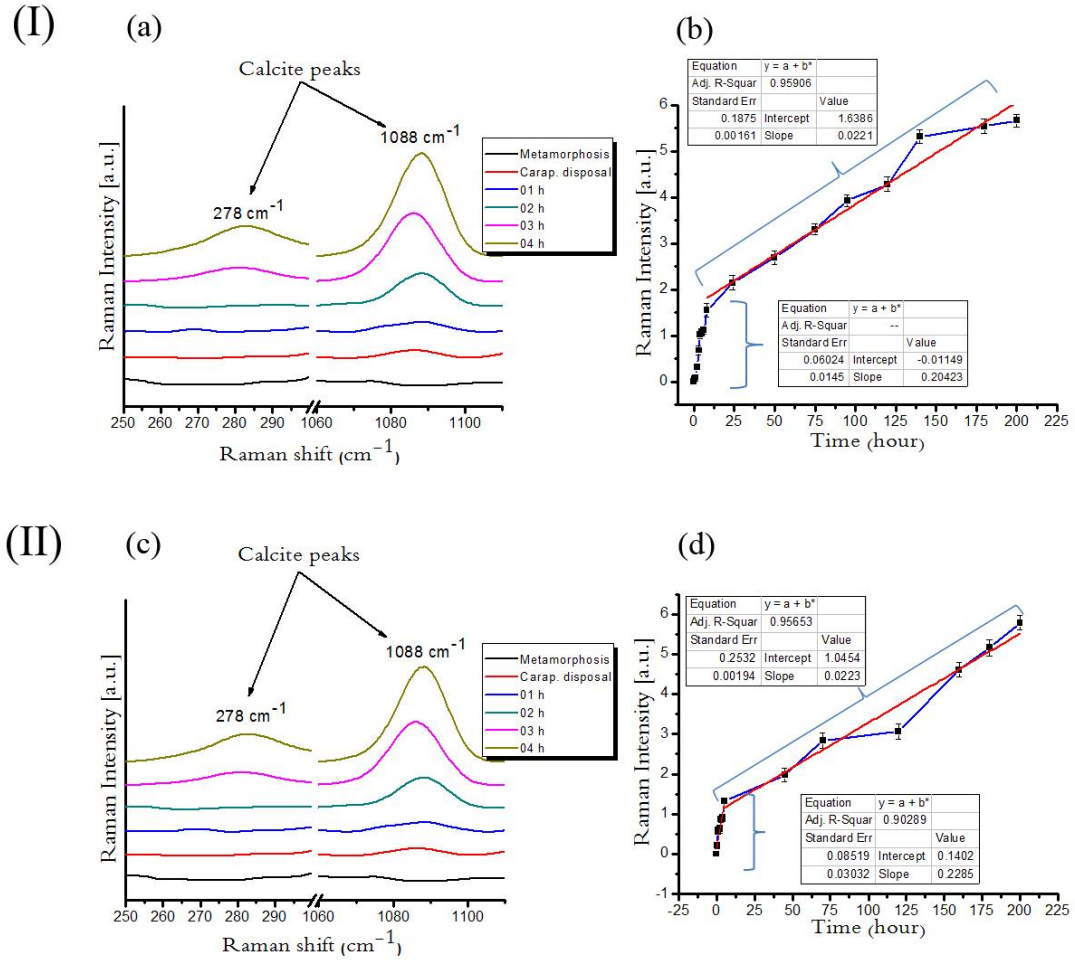

Figure 46: Starting of calcification process of I) B. amphitrite and II) B. improvisus. (a) and (c)– Calcite bands spectra of both juvenile barnacle species at different time points from metamorphosis to 4 hours after metamorphosis, and (b) and (d) –calcite bands intensity peak values at the same time points, error bars according to Student's t-distribution.

6.3.4. μ-X-ray microprobe fluorescence

μ-XRF maps of elemental distribution in juvenile barnacle baseplate (in case of *in-situ*, Figure 47) and in the remaining barnacle cement (in case of *ex-situ*, Figure 48) have shown similar results for both species.

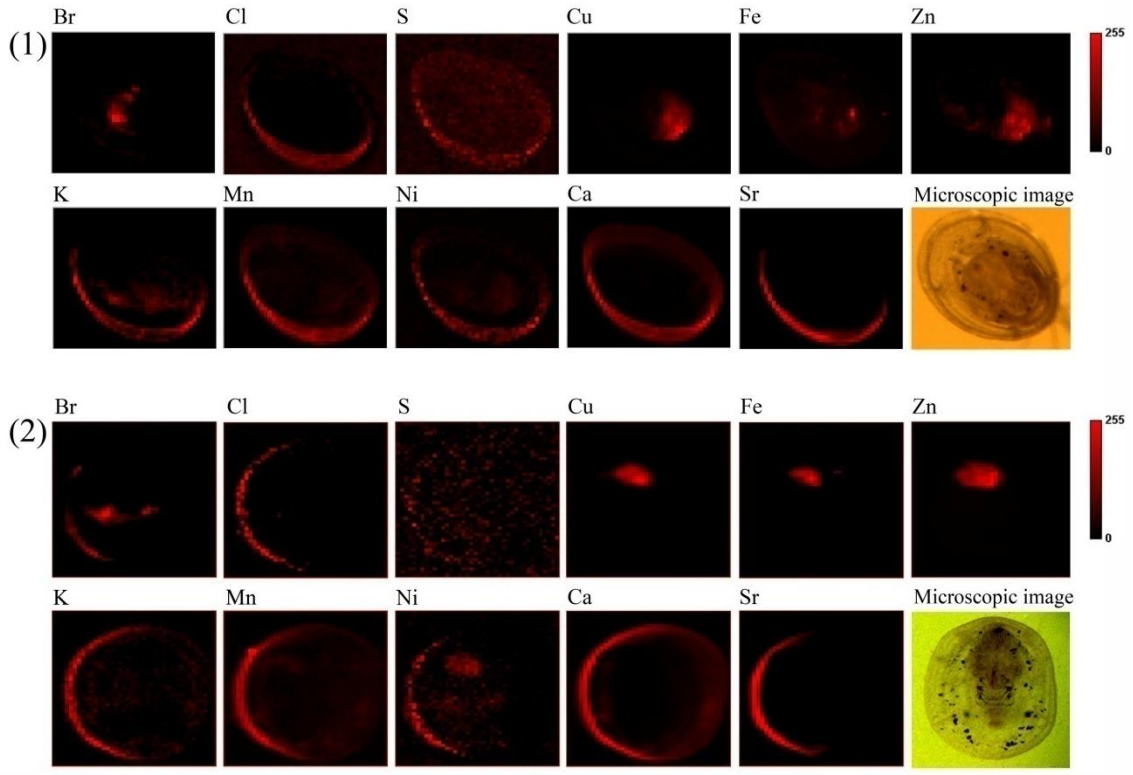

Figure 47: *In-situ*μ-X-ray fluorescence maps of juvenile barnacle baseplates: 1) *B. amphitrite* and 2) *B. improvisus* settled on Kapton® foils at 7 days old. Optical micrographs of the scanned barnacles are presented in the figure.

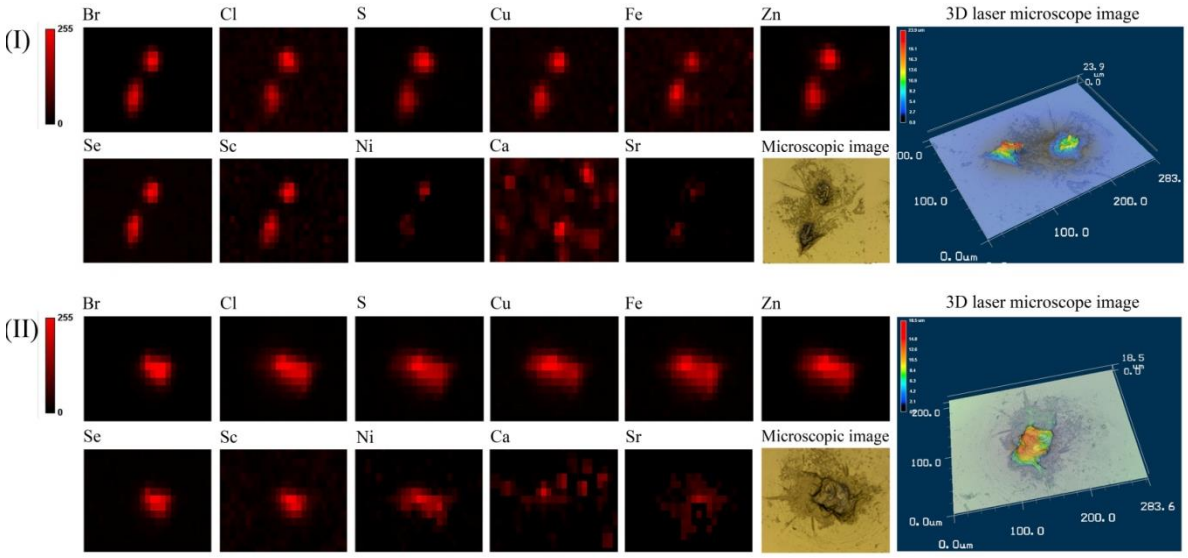

Figure 48: Elemental mappings of the cement deposits of juvenile barnacles 1) *B. amphitrite* and 2) *B. improvisus* adherent to Kapton foil. The organisms were removed from the Kapton® substrate directly after one day after settlement and the remains have been analyzed using a non-confocal setup.

6.4. Conclusion

Early adhesion of barnacle cyprids has been studied by Raman microspectroscopy and µ-X-ray microprobe fluorescence (µ-XRF). The settled juvenile barnacles have been investigated *in-situ* using two different substrata (CaF_2 disks for Raman studies and Kapton® foils for µ-XRF studies). All spectra obtained from the cement of living organisms were compared to the cement remaining after removal of barnacles (*ex-situ* results) and to footprints (temporary adhesive) of cyprids.

Firstly, the major Raman spectroscopy results are to be concluded. Raman spectra of footprints as well as antennule regions of different individuals look alike, which means that Raman spectroscopy results are reproducible measurements for any individual barnacles. Raman microspectroscopy measurements recorded at different *B. amphitrite* and *B. improvisus* juvenile barnacles have shown that the baseplate is divided into three major regions (calcareous region, antennule region and the area surround the antennule), which have various chemical composition. Additionally, confocal Raman spectroscopy has been used to investigate the chemical distribution in juvenile barnacle baseplates (*in-situ*) and the remaining cyprid cement (*ex-situ*). Firstly, results of confocal Raman spectroscopy have shown that calcite is localized only at the rim of the baseplate under the shell ring, and vanishes in the remaining cement. These results are in agreement with both *in-situ* and *ex-situ* µ-XRF maps that have shown that different regions of juvenile barnacle baseplate show different elemental distribution. Moreover, Ca has been found in the same region where calcite is localized, while it vanishes in the µ-XRF of remaining cement.

Both *in-situ* and *ex-situ* Raman results have shown that the antennule region as well as the remaining cement are rich of amide-I and show different vibrational modes of CH than the other regions (calcareous region and the area around the antennule). This result supports the fact that juvenile barnacle cement is a proteinaceous material that has hydrophobic properties.

Raman spectra recorded at the same region at different time points look alike. Additionally, *ex-situ* Raman spectra that have been recorded at the remaining juvenile barnacle cement at different time points look the same. Moreover, all spectra obtained during *in-situ* (in the antennule region) and *ex-situ* (remaining cement) Raman experiments generally look the same. The only differences between *in-situ* and *ex-situ* results are observed in two main types of region: amide-I and carotenoid. Therefore, amide-I bands have been studied more carefully *in-situ* and *ex-situ* in order to investigate the differences in the protein secondary structures. Generally, amide-I spectra of footprint have different protein secondary structure than the spectra of permanent cement. This examination revealed that *ex-situ* spectra of amide-I of all remaining cyprid cement over the course of one week of barnacle lifetime show similar shapes and mainly β-sheet structures at 1665 cm^{-1}. Therefore, this observation indicates that all material left on surface is cured cement and there are not any major chemical changes occurring in it over time. However, *in-situ* amide-I band of the spectra recorded at the antennule region have shown strong changes over time, which could be attributed to continuous juvenile barnacle cement secretion and the cement curing process.

The carotenoid bands have been detected only in the *in-situ* Raman spectra, while they vanish in the *ex-situ* spectra recorded for the remaining cement. Comparison of the *in-situ* spectra with reference material and green algae, the main nutrient for the young barnacles, has revealed that feeding is the major source of the carotenoids.

The calcification process of the barnacle calcareous shell has been studied *in-situ* also using Raman spectroscopy. The result of this study has shown that commencement of the calcification process coincides with carapace disposal about 8–9 hours after the organism's permanent attachment. The rate of the calcification process within initial 10 hours for both species is 10 times greater, than afterwards.

Secondly, the major µ-XRF results are to be concluded. µ-XRF has proved to be a powerful and useful tool for investigation of marine bioadhesives, since it can be used *in-situ* on biofouling organisms.

Results of µ-XRF experiments of the juvenile barnacle baseplate have shown that at the rim, calcium is colocalized with K, Sr and Mn while in the center part Fe is occurring along with Cu, Zn, Br and As. The presence of elements that have been detected at the rim region could be attributed to the calcareous shell formation. Interestingly, *in-situ* µ-XRF maps have shown that only the Br signal is localized at the antennule region while all of Fe, Cu, Zn and As are shifted closely to the center point of the juvenile barnacle baseplate which is expected to correspond to the abdomen position of the organism. In order to clarify this phenomenon, *Tetraselmis* green algae have been studied separately by µ-XRF. µ-XRF spectrum of the green algae has shown presence of each of these elements that have been shifted from the Br region. This could be related to the high penetration depth of X-ray beam (≈100 µm) and these elements might be detected from the abdomen. However, *ex-situ* µ-XRF maps of the remaining cements show presence of all these elements in addition to Br. Therefore, it could

be concluded that barnacles consume these elements from food or take them up from the seawater in order to use them in adhesive formation or its curing process.

Nevertheless, the role of these elements in the biofouling adhesives is still to be found.

All Raman and μ-XRF experiments have been conducted for both *B. amphitrite* and *B. improvisus* and results have shown the similarity in the chemical composition and elemental distribution of the juvenile barnacle baseplate regions and remaining cement studied at different time points.

7. Summary and outlook

Biofouling is an undesired agglomeration of maritime organisms, including animals, plants and protozoa, on the surfaces immerged into marine environment, and in long term it usually constitutes a menace to the durability and functionality of man-made underwater surfaces and constructions. These marine dwellers employ different adhering mechanisms in order to securely attach themselves to the surfaces and endure violent ambient media, e.g. currents and varying water temperatures. For instance, macro-fouling crustaceans that are so detrimental for ships and industrial and nuclear plants cooling systems predominately attach to the surfaces using permanent or temporary adhesives. Each year billions of dollars are spent to repay or at least partially refund damage caused by biofouling. Therefore, nowadays approach to find effective solutions to the problem of biofouling has become a complex matter of research. Scientific groups throughout the world investigate the conditions required for successful biofouler's attachment, develop antifouling release coatings, and the physicochemical mechanisms of marine bioadhesion.

Barnacles are abundant marine biofouling crustaceans and their adult cement has been extensively studied for years. However, current knowledge about footprint temporary adhesive and juvenile barnacle permanent cement is yet quite poor. A number of questions are still to be answered: if there is any difference between the temporary (footprint) and the permanent adhesives; if the juvenile barnacle cement is proteinaceous as the adult cement or has other components and if it has the same type of protein as the adult cement; if different species have the same adhesive composition; if the cement adhesive keep the same chemical composition throughout its life cycle (i.e first attachment, metamorphosis, juvenile barnacle), or changes with time; and finally, when the calcification process starts.

Therefore, the chemistry behind adhesive mechanisms of barnacles at early life stages, abundant marine biofouling crustaceans, has been chosen as the principle subject of current PhD thesis. This study aims to understand and compare spatial chemical distribution of the adhesive secreted by two different species (*Balanus amphitrite* and *Balanus improvisus*) of cyprid larvae and juvenile barnacles for settlement. Additionally, it has been inspiring to investigate the protein secondary structure content of adhesive cement at early life stages, from temporary adhesive secretion during surface exploratory process up to 14 days lifetime on the surface after permanent settlement.

To fulfill this task, both *in-situ* and *ex-situ* approaches have been applied. More attention has been paid to *in-situ* experiments since just a few works have studied juvenile barnacle adhesives in real time conditions, this method gives an advantage of following the dynamical changes occurring in the sample with time in conditions reproduced close to real life without its severe alteration. 3D laser microscope images have shown that thickness of the remaining cyprid cement left on the kapton® foil after organism's removal lies in range of 10 µm to 20 µm, which means that the main information that has been obtained during *in-situ* studies are related mainly to the cyprid cement. Nevertheless, *ex-situ* study of the remaining cyprid cement have also been conducted in order to eliminate the signal that could come from the physiological parts of the organisms, that might be detected during *in-situ* study due to the

penetration depth of laser beam in Raman spectroscopy (>20 µm) and synchrotron radiation in µ-XRF technique (≈100 µm) that sometimes, or usually for µ-XRF, can be greater than the thickness of the adhesive plaque.

In both cases principle techniques used have been Raman spectromicroscopy and synchrotron based µ-XRF, Raman also applied in confocal mode, with additional experiments in 3D laser microscopy, light microscopy and SEM. As a result, chemical distribution of elements throughout the baseplate of barnacle, as well as presence of certain functional groups and changes in protein secondary structure has been described for permanent juvenile barnacle cement from one day old to the age of fourteen days old. Additionally, functional groups detected in footprints (temporary cyprid adhesive) are presented.

Raman spectra taken from different individuals' specimens have shown similarity in shape and band intensity correlation, which proves the reproducibility of the Raman spectromicroscopy results in case of barnacle study. On the first place it was required to know how cement is distributed in the space between juvenile barnacle that undergone the metamorphosis and the substratum. Confocal Raman spectromicroscopy has revealed the chemical heterogeneity of the barnacle baseplate and allowed to distinguish three regions of various chemical compositions: calcareous rim, baseplate region surrounding the antennule and antennule region. The latter, where presence of cement is expected, has been chosen the focus of this study and has been studied in detail for cyprids from metamorphosis to age of fourteen days. Although both antennule and baseplate region surround the antennule have shown protein signal, but *ex-situ* study has proved that protein signal in baseplate region surround the antennule comes from or its inner organs or biological membrane underneath the barnacle, a stage which precedes the formation of calcareous baseplate, because at early life stages after removal of the organism the cement is observed merely in the antennule region.

One of the additional focuses of this research work has also been the calcareous shell of juvenile barnacles. The calcification of the barnacle outer shell has been studied for juvenile barnacles up to the age of 9 days old in order to determine the time-point when the calcareous rim starts to be formed and to follow the tendency in its formation rate. It has been shown that calcification process starts after ≈ 8–9 hours after permanent attachment, coinciding with the carapace removal. Moreover, it has been observed that for both species first 10 hours of calcification occurs in a rather intensive rate, which drops 10 times after that time and keeps the same tendency of growth up to the 9 days age. Results of confocal Raman spectroscopy have shown that calcite is localized only at the rim of the baseplate under the shell ring, and vanishes in the remaining cement. In agreement to these results, it has been observed during both *in-situ* and *ex-situ* µ-XRF study of the elemental distribution of the rim that calcium is co-localized there with elements that form the calcareous shell – K, Sr, Cl, Ni and Mn–while these elements vanish in the antennule region and remaining cement in juvenile barnacles (*B. amphitrite*).

Being in agreement with Raman and confocal Raman results, *in-situ* µ-XRF study of the elemental distribution has shown the localization of high intensity of calcium at the rim, while other elements have been found at the center part of the juvenile barnacle baseplate (*in-*

situ maps) and in the remaining cement (*ex-situ* maps), which is in agreement with presence of some functional groups such as amides and CH vibration modes in both Raman and confocal Raman results.

Ex-situ experiments helped to conclude if any changes occur in the already cured cement, left on the surface after barnacle removal. In case of *ex-situ* study a careful attention must be paid to the sample preparation, since parts of the organism may stay after organism's removal. Therefore, SEM and 3D laser microscope have been used to select the clean samples. In addition, SEM images have shown that the diameter of the remaining cement plaque increases with time, confirming continuous resuming of adhesive secretion by barnacles.

Comparison between *in-situ* and *ex-situ* results have shown that *in-situ* Raman spectra recorded at the antennule region showed peaks similar to the *ex-situ* spectra that have been recorded for the remaining cyprid cement. Additionally, both *in-situ* and *ex-situ* μ-XRF distribution maps have shown that amide-I and different vibration modes of CH stretching are located at the antennule region and the remaining cement, which supports the fact that juvenile barnacle cement is proteinaceous material that consist of different hydrophobic amino acids. Therefore, amide-I bands have been studied more carefully with Raman spectroscopy *in-situ* and *ex-situ* in order to investigate the differences in the protein secondary structures. This examination revealed that footprints have shown secondary structures different from the permanent cement. Additionally, *ex-situ* amide-I bands spectra of remaining cyprid cement over the course of one week of barnacle life-time have shown similar shapes and mainly β-sheet structures at 1665 cm^{-1}, indicating that after removal of the organism crosslinking is could be terminated. However, *in-situ* amide-I band of the spectra recorded at the antennule region have shown strong fluctuations observed over time, which could be attributed to continuous juvenile barnacle cement secretion, or, perhaps, to cement curing process.

The main corresponding with each other results of *in-situ* and *ex-situ* μ-XRF maps of the cyprid cements in antennule region at different time points have shown localization of Br, Cu, Fe, and Zn in this region, that can be consumed from the food, *Tetraselmis* green algae, that has shown the presence of these elements. By analogy to other biofouling organisms' adhesives, these elements might play an important role in the crosslinking of the protein and thus curing process of barnacle cement. Further research can unshed their influence on bioadhesive chemistry.

Finally, *in-situ* maps have shown a random distribution of the carotenoid C=C str. band, while it completely vanishes in the remaining cement *ex-situ* maps, which means that carotenoid signal seems to be originated from the interior of the barnacle rather than from the adhesive. Comparison of the cement *in-situ* spectra with spectra of green algae specimens, the main nutrient for the young barnacles, has revealed similarities in the carotenoid bands, which supports the hypothesis that carotenoid signal is related to the green algae that has been used to feed the juvenile barnacles.

To conclude, it has been proven that *in-situ* approach is very powerful for investigation of marine biofouling adhesives at early life stages. The results of this study provide initial information about the chemical composition and elemental distribution in both juvenile

barnacle baseplate and remaining cement of both barnacle species (*B. amphitrite* and *B. improvisus*) at different life stages. The obtained results are quite promising and offer an interesting path for further investigations. Furthermore, the derived chemical understanding of the adhesive composition is supposed to lead to new, environmentally benign antifouling solutions, like specially designed antifouling release coatings, aiming on the termination of curing process of juvenile barnacles and thus influencing the successful permanent settlement. Moreover, the detailed understanding of these bioadhesive may lead to great benefits for biomedical industry.

List of abbreviations and shortenings

AFM	Atomic Force Microscopy
AFTIR	Attenuated Fourier transform Infrared
ANKA	Angstromquelle Karlsrue
ASW	Artificial seawater
ATR-FTIR	Attenuated Total Reflectance-Fourier Transform Infrared
B. amphitrite	*Balanus amphitrite*
B. improvisus	*Balanus improvisus*
BCS1	First Barnacle Cement Secretion
BCS2	Second Barnacle Cement Secretion
CBB	Coomassie Brilliant Blue
CLSM	Confocal 3D Laser Scanning Microscopy
DOPA	3, 4-dihydroxyphenylalanine
EDX	Energy Dispersive X-ray Spectroscopy
ESEM	Environmental Scanning Electron Microscopy
FSD	Fourier Self-Deconvolution
PDMS	Polydimethylsiloxane
FTIR	Fourier Transform Infrared
PMMA	Poly(methyl methacrylate)
PTFE	polytetrafluoroethylene
SEM	Scanning Electron Microscopy
SiMCD	Silicon Multi-cathode Detector
SR	Synchrotron Radiation
Str.	Stretching
TBT	Tributyltin
XRF	X-ray Fluorescence

List of publications

Articles in preparation

- T. Mohamed, S. Heissler, A. Di Fino, A. S. Clare, M. Grunze, A. Rosenhahn "*In-situ* Raman spectromicroscopy of the early attachment phase of *Balanus amphitrite*".

- T. Senkbeil, T. Mohamed, R. Simon, D. Batchelor, A. Di Fino, A. S. Clare, A. Rosenhahn "Elemental mapping of barnacle larvae and juvenile barnacles using *in-vivo* and *in-situ* synchrotron µ-XRF ".

- T. Mohamed, T. Senkbeil, S. Heissler, R. Simon, D. Batchelor, A. Di Fino, A. S. Clare, M. Grunze, A. Rosenhahn "*In-situ* and *ex-situ* study of juvenile barnacle (*Balanus amphitrite* and *Balanus improvisus*) cements using µ-Raman spectroscopy and X-ray microprobe fluorescence techniques.

List of conferences

- 2nd International Workshop on "Advanced Atomic Force Microscopy Techniques" Karlsruhe Institute of Technology (KIT), Germany, 28th February - 1st March, 2011.

- Regular Seminars at KIT as well as at the University of Heidelberg from December 2010 until December 2013. (***Lecturer***)

- Regular SEACOAT meetings (every six months) from December 2010 until December 2013. (***Lecturer***)

- Retreat meeting 2011 - BioInterfaces International Graduate School, 31st August – 2nd September 2011, Bad Herrenalb, Germany. (***Poster***)

- Workshop with the US Office of Naval Research, entitled "International Workshop on Marine Biofouling" Planet Hollywood hotel, Las Vegas, USA, December 4th - 6th, 2011. (***Winner Poster***)

- 1st International Conference of "Biological and Biomimetic Adhesives" Lisbon University, Portugal, May 9th – 11th, 2012.

- 16th International Congress on "Marine Corrosion and Fouling" Seattle, Washington, USA, June 24th – 28th, 2012. (***Poster***)

- Webcast On Ethics In Scientific Article Submission &Publishing, In proud partnership with Trinty College Dublin, 11th of July 2012, Dublin.

- Retreat meeting 2012 - BioInterfaces International Graduate School, September 3rd - 5th, 2012, Herrenbad, Germany. (***Lecturer***)

- 2nd International Conference (30th Annual) on Corrosion Mitigation and Surface Protection Technologies, Hurghada, Egypt, December 10th – 13th, 2012. (***Lecturer***)

- 3rd International Workshop on "Advanced Atomic Force Microscopy Techniques" Karlsruhe Institute of Technology (KIT), Germany, *March 5-6, 2012*

Bibliography

[1] **J. A. Callow and M. E. Callow.** Trends in the development of environmentally friendly fouling-resistant marine coatings. *Nature Communication*, 2: 244, **2011**.

[2] **R. Sangeetha, R. Kumar, R. Venkatesan, M. Doble, L. Vedaprakash, Kruparatnam, K. Lakshmi and Dineshram.** Understanding the structure of the adhesive plaque of Amphibalanus reticulatus. *Materials Science and Engineering* C, 30: 112–119, **2010**.

[3] **D. M. Yebra, S. Kiil and K. D. Johansen.** Antifouling technology—past, present and future steps towards efficient and environmentally friendly antifouling coatings. Progress in Organic Coatings, 50: 75–104, **2004**.

[4] **L. Fitzsimons**. Sensing technologies for monitoring the marine environment. MaroTech conference, **2011**.

[5] ***M. Killalea.*** Biofouling is tip of green iceberg. available online at http://www.drillingcontractor.org/biofouling-is-tip-of-green-iceberg-1995. Created on line **2009**.

[6] **Buck Albert.** Smithsonian Marine Station at Fort Pierce. available online at http://www.sms.si.edu/irlspec/Perna_viridis.htm. Modified October **2007.**

[7] **A. Boetius**. Microfauna–Macrofauna Interaction in the Seafloor: Lessons from the Tubeworm. *PLoS Biology.* 3: e102, **2005**.

[8] **S. Travisak.** Barnacles: Wild Life World. available online at http://wild-life-world.blogspot.de/2014/02/barnacles.html. Modified in **2013**.

[9] **D. E. Barlow, G. H. Dickinson, B. Orihuela, J. L. Kulp, D. Rittschof and J.Kathryn.** Characterization of the adhesive plaque of the barnacle *Balanus amphitrite*: amyloid-like nanofibils are a major component. *Langmuir*. *American Chemical Society*, 26: 6549–6556, **2010**.

[10] **M. Schmidt, A. Cavaco, N. Gierlinger, N. Aldred, P. Fratzl, M. Grunze, and A. S. Clare.** *In Situ* Imaging of Barnacle (*Balanus amphitrite*) Cyprid Cement Using Confocal Raman Microscopy. *Journal of Adhesion*, 85: 139–151, **2009**.

[11] **K. Kamino.** Underwater adhesive of marine organisms as the vital link between biological science and material science. *Marine Biotechnolog*, 10: 111–121, **2008**.

[12] **N. Aldred and A. S. Clare.** The adhesive strategies of cyprids and development of barnacle-resistant marine coatings. *Biofouling*, 24(5): 351–363, **2008**.

[13] **D. K. Burden, D. E. Barlow, C. M. Spillmann, B. Orihuela, D. Rittschof, R. K. Everett and K. J. Wahl.** Barnacle *Balanus amphitrite* Adheres by a Stepwise Cementing Process. *American Chemical Society, Langmuir*, 28: 13364–13372, **2012**.

[14] **D. E. Barlow and K. J. Wahl.** Optical spectroscopy of marine bioadhesive interfaces. *Annual review of analytical chemistry*. 5: 229–251, **2012**.

[15] **A. M. Smith, J. A. Callow.** Biological adhesives. Berlin: *Springer*, *Chapter 8*, **2006**.

[16] **M. E. Callow and J. E. Callow.** Marine biofouling: a sticky problem. *Biologist*, 49: 1–5, **2002**.

[17] ***K. Pollock***. Barnacles. The Islander available online **April, 2014** at http://theislandermagazine.com/?p=1184.

[18] **A. Soos**. The Undersides of Boats and Control of the Barnacles and Bacteria Growth available online at http://www.enn.com/top_stories/article/43489. Created on October, **2011**.

[19] **K. K Satpathy, A. K. Mohanty, G. Sahu, S. Biswas, M. V. R. Prasad and M. Slvanayagam.** Biofouling and its control in seawater cooled power plant cooling water system - a review. *Nuclear Power*, Pavel Tsvetkov (Ed.), ISBN: 978-953-307-110-7, In Technology, **2010**.

[20] **D. M. Yebra, S. Kiil and K. Dam-Johansen.** Antifouling technology—past, present and future steps towards efficient and environmentally friendly antifouling coatings. Progress in Organic Coatings, 50: 75–104, **2004**.

[21] **C. D. Anderson and J.E. Hunter.** Whither antifoulings after TBT? NAV2000 Conference Proceedings, Venice, September, **2000**.

[22] **W. G. Characklis.** Microbial fouling and microbial biofouling control, Biofilms, Ed. W. G. Characklis et K.C. Marshall, *New York, John Wiley and sons*, 523–634, **1990**.

[23] **R. E. Baier.** Proceedings of the Third International Congress on Marine Corrosion and Fouling, *National Bureau of Standards, Gaithersburg*, MD, 633–639, **1972**.

[24] **C. Compère, M. N. Bellon-Fontaine, P. Bertrand , D. Costa, P. Marcus, C. Poleunis , C. M. Pradier, B. Rondot, and M. G.Walls.** Kinetics of conditioning layer formation on stainless steel immersed in seawater. *Biofouling*, 17(2): 129–145, **2001**.

[25] **J. A. Callow and M. E. Callow.** Trends in the development of environmentally friendly fouling-resistant marine coatings. *Nature communications*, 2: 244–254, **2011**.

[26] **L. D. Chambers, K. R. Stokes, F. C. Walsh, R. J. K. Wood.** Modern approaches to marine antifouling coatings**.** *Surface & Coatings Technology*, 201: 3642–3652, **2006**.

[27] Woods Hole Oceanographic Institution, Marine Fouling and Its Prevention, Navy Dept. Bureau of Ships, United States Naval Institute, available online at /http://hdl.handle.net/1912/191 , **1952**.

[28] **R. Sangeetha, R. Kumar, M. Doble, and R. Venkatesan**. Barnacle cement: An etchant for stainless steel 316L?. *Colloids and surfaces. B, Biointerfaces*, 79(2): 524–530, **2010**.

[29] **M. P. Schultz, C. J. Kavanagh, G. W. Swain.** Hydrodynamic forces on barnacles: inplications on detachment from fouling-releae surfaces. *Biofouling*, 13: 323–335, **1999**.

[30] **R. L. Townsin.** The ship hull fouling penalty. *Biofouling*, 19: 9–15, **2003**.

[31] **M. Schultz.** Effects of coating roughness and biofouling on ship resistance and powering. *Biofouling*, 23: 331–341, **2007**.

[32] **M. A. Champ.** A review of organotin regulatory strategies, pending actions, related costs and benefits. *The Science of the Total Environment*, 258: 21–71, **2000**.

[33] **A. Abbott, P. D. Abel, D. W. Arnold and A. Milne.** Cost-benefit analysis of the use of TBT: the case for a treatment approach. *The Science of the Total Environment*, 258: 5–19, **2000**.

[34] **M. S. Brancato.** OCEANS'99 MTS/IEEE, Riding the Crest into the 21st Century, 2 (2): 548–1080, **1999**.

[35] **K. Reise, S. Gollasch and W.J. Wolff.** Introduced marine species of the North Sea coasts. *Helgoländer Meeresunters*, 52: 219–234, **1999**.

[36] **I. Y. Phang, K. C. Chaw, S. S. Hui Choo, R. K. C. Kang, S. S. C. Lee, W. R. Birch, S. L. M. Teo and G. M. Vancso.** Marine biofouling field tests, settlement assay and footprint micromorphology of cyprid larvae of *Balanus amphitrite* on model surfaces. *Biofouling*, 25 (2): 139–147, **2009**.

[37] **R. M. A. Sullan, N. Gunari, A. E. Tanur, Y. Chan, G. H. Dickinson, B. Orihuela, D. Rittschof, G.C. Walker.** Nanoscale structures and mechanics of barnacle cement. *Biofouling*, 25 (3): 263–275, **2009**.

[38] **N. Aldred, I. Y. Phang, S. L. Conlan, A. S. Clare and G. J. Vancso.** The effects of a serine protease, Alcalase®, on the adhesives of barnacle cyprids (*Balanus amphitrite*). Biofouling, 24 (2): 97–107, **2008**.

[39] **C. D. McQuaid and K. Miller.** Larval Supply and Dispersal. *Biofouling*, *Chapter 2* Wiley-Blackwell, Oxford, UK. **2010**.

[40] **C. Zimmer.** Parasite Rex: Inside the Bizarre World of Nature's Most Dangerous Creatures, available on line at http://www.amazon.com/Parasite-Rex-Bizarre-Dangerous-Creatures, **2000**.

[41] **M. Walters and J. Johnson.** The World of Animals. Available online at http://www.amazon.com/World-Animals-Martin-Walters/dp/0890516170, **2007**.

[42] **P. Rawes.** Relational Architectural Ecologies: Architecture, Nature and Subjectivity" 1st Eddition, Routledge, available online at http://www.amazon.com/Relational-Architectural-Ecologies-Architecture-Subjectivity/dp/0415508584, **2013**.

[43] **B. A. Foster and J. S. Buckeridge.** Barnacle paleontology, 41–63. Available online at http://en.wikipedia.org/wiki/Barnacle,**1987**.

[44] **P. Doyle, A. E. Mather, M. R. Bennett and A. Bussell.** Miocene barnacle assemblages from southern Spain and their palaeoenvironmental significance. *Lethaia*, 29 (3): 267–274, **1997**.

[45] **G. Hoyle and T. Smyth Jr.** Giant muscle fibers in a barnacle, *Balanus nubilus* Darwin. *Science*, 139(3549): 49–50, **1963**.

[46] **D. T. Anderson.** Barnacles: structure, function, development and evolution. *Springer*, **1994**.

[47] **T. C. Lacalli.** Serial EM analysis of a copepod larval nervous system. *Arthropod Structure & Development*, 38 (5): 361–75, **2009**.

[48] **W. A. Newman.** Cirripedia. In Sol Felty Light & James T. Carlton. The Light and Smith Manual: Intertidal Invertebrates from Central California to Oregon (4th ed.). *University of California Press*. 475–484, **2007**.

[49] **P. Jiang. Barnacle. *Snowbio*.** Available online at http://snowbio.wikispaces.com/Barnacle+(crustacean).

[50] **C. Dreanno, R. R. Kirby and A. S. Clare.** Locating the barnacle settlement phermone: spatial and ontogenetic expression of the settlement-inducting protein complex of *Balanus amphitrite*. *Proceedings of the royal society B*, 273: 2721–2728, **2006**.

[51] **H. M. Leslie, E. N. Breck, F. Chan, J. Lubchenco and B. A. Menge.** Barnacle reproductive hotspots linked to nearshore ocean conditions. *Proc. Natl Acad. Sci. USA*, 102: 10 534–539, **2005**.

[52] **Z.-F. Chen, H. Wang, K. Matsumura, P.-Y. Qian**. Expression of Calmodulin and Myosin Light Chain Kinase during Larval Settlement of the Barnacle *Balanus amphitrite*. *PLoS ONE*, 7: 1–9, **2012**.

[53] **H. Barnes and M. Barnes**. Studies on the reproduction of cirripedes. I. Introduction: Copulation, release of oocytes and formation of the egg lamellae. *Journal of Experimental Marine Biology and Ecology*, 27: 195–218, **1977**.

[54] **C. Hellio, C. Simon-Colin, A. S. Clare, E. Deslandes**. Isethionic acid and floridoside isolated from the red alga, *Grateloupia turuturu*, inhibit settlement of *Balanus amphitrite* cyprid larvae. *Biofouling*, 20: 139–145, **2004**.

[55] **D. J. Crisp, G. Walker, G. A. Young and A. B. Yule**. Adhesion and Substrate Choice in Mussels and Barnacles. *Journal of Colloid Interface Science*. 104, 40–50, **1985**.

[56] **I. Y. Phang, N. Aldred, X. Y. Ling, N. Tomczak, J. Huskens, A. S. Clare and G. J. Vancso.** Chemistry-specific interfacial forces between barnacle (*Semibalanus balanoides*) cyprid footprint proteins and chemically functionalized AFM tips. *Journal of Adhesion*, 85: 616–630, **2009**.

[57] **E. C. Fischer, V. J. Castelli, S. D. Rodgers and H. R. Bleile.** in: J. D. Gostlow, R. C. Tipper (Eds.). Marine Biodeterioration: An Interdisciplinary Study, Naval Institute Press, MD, USA, **1984**.

[58] **J. E. Eckman, W. B. Savidge and T. F. Gross.** Relationship between duration of cyprid attachment and drag forces associated with detachment of *Balanus amphitrite* cyprids. *Marine Biology*, 107: 111–118, **1990**.

[59] **M. R. Koehl.** Mini review: hydrodynamics of larval settlement into fouling communities. *Biofouling*, 23(5-6):357–368, **2007**.

[60] **A. B. Yule and D. J. Crisp.** Adhesion of cypris larvae of the barnacle, *Balanus balanoides*, to clean and arthropod in treated surfaces. *Journal of Marine Biology Assoc UK*, 63: 261–271, **1983**.

[61] **A. B. Yule and G. Walker.** The temporary adhesion of barnacle cyprids: effects of some differing surface characteristics. *Journal of Marine Biology Assoc UK*, 64:429–439, **1984**.

[62] **A. S. Clare.** Signal transduction in barnacle settlement: Calcium re-visited. *Biofouling*, 10: 141–159, **1996**.

[63] **K. Kamino.** Barnacle underwater attachment. *Biological Adhesives*, 145–166, **2006**.

[64] **G. Walker.** Swimming speeds of the larval stages of the parasitic barnacle, *Heterosaccuslunatus* (Crustacea: Cirripedia: Rhizocephala). *Journal of Biological. Association, UK*, 84: 737–742, **2004**.

[65] **D. J. Crisp.** The behaviour of barnacle cyprids in relation to water movement over a surface. *Journal of Experimental Biology*, 32: 569–590, **1955**.

[66] **A. B. Yule.** The application of new techniques to the study of planktonic organisms. PhD thesis, University of Wales, Bangor, **1982**.

[67] **N. C. Lagersson.** The ultrastructure of two types of muscle fibre cells in the cyprid of *Balanus amphitrite* (Crustacea: Cirripedia). *Journal of the Marine Biological Association, UK*, 82: 573–578, **2002**.

[68] **A. S. Clare and J. A. Nott.** Scanning electron microscopy of the fourth antennular segment of *Balanus amphitrite*. *Journal of the Marine Biological Association, UK*, 74: 967–970, **1994**.

[69] **J. A. Nott and B. A. Foster.** On structure of antennular attachment organ of cypris larva of *Balanus balanoides* (L). *Philosophical Transactions of the Royal Society London B*, 256: 115–134, **1969**.

[70] **K. Matsumura, M. Nagano and N. Fusetani.** Purification of a larval settlement-inducing protein complex (SIPC) of the barnacle, *Balanus amphitrite*. *Journal of Experimental Zoology*, 281:12–20, **1998**.

[71] **K. Matsumura, M. Nagano, Y. Kato-Yoshinaga, M. Yamazaki, A. S. Clare and N. Fusetani.** Immunological studies on the settlement-inducing protein complex (SIPC) of the barnacle *Balanus amphitrite* and its possible involvement in larva-larva interactions. *Proceedings of the Royal Society of London B. Biological Science*, 265: 1825–1830, **1998**.

[72] **A. B. Yule and G. Walker.** Settlement of *Balanus balanoides*: the effect of cyprid antennular secretion. *Journal of the Marine Biological Association, UK*, 65: 707–712, **1985**.

[73] **C. Dreanno, R. R. Kirby and A. S. Clare.** Smelly feet are not always a bad thing: the relationship between cyprid footprint protein and the barnacle settlement pheromone. *Biological Letter*, 2: 423–425, **2006**.

[74] **K. Okano, K. Shimizu, C. G. Satuito and N. Fusetani.** Visualization of cement exocytosis in the cypris cement gland of the barnacle *Megabalanus rosa*. *The Journal of Experimental Biology*, 199: 2131–2137, **1996**.

[75] **M. E. Pettitt, S. L. Henry, M. E. Callow, J. A. Callow and A. S. Clare.** Activity of commercial enzymes on settlement and adhesion of cypris larvae of the barnacle *Balanus amphitrite*, spores of the green alga *Ulvalinza*, and the diatom *Navicula perminuta*. *Biofouling*, 20: 299–311, **2004**.

[76] **F. J. Bernard and C. E. Lane.** Early settlement and metamorphosis of the barnacle *Balanus amphitrite* niveus. *Journal of Morphology*, 110: 19–39, **1962**.

[77] **G. Walker.** The adhesion of barnacles. *The Journal of Adhesion*, 12: 51–58, **1981**.

[78] **A. B. Yule, G. Walker.** Adhesion in barnacles. In: *Southward AJ (ed) Barnacle biology*, 389–402, **1987**.

[79] **E. Bourget.** Barnacle shells: Composition, structure, and growth. In Crustacean Issues: *Southward AJ (ed) Barnacle biology*; A. A. Balkema: Rotterdam, 5: 267−285, **1987**.

[80] **N. J. O'Connor and D. L. Richardson.** Attachment of barnacle (*Balanus amphitrite* Darwin) larvae: responses to bacterial films and extracellular materials. *Journal of Experimental Marine Biology and Ecology*, 226: 115−129, **1998**.

[81] **J. F. Dineen and A. H. Hines.** Interactive effects of salinity and adult extract upon settlement of the estuarine barnacle *Balanus improvisus* (Darwin, 1854). *Journal of Experimental Marine Biology and Ecology*, 156: 239−252, **1992**.

[82] **K. F. Vasa**. Immigrants among the animals of the delta-area of the SW. Netherlands. *Hydrological Bulletin*, 9: 114−119, **1978**.

[83] **A. Zaiko**. Balanus improvisus. In: Baltic Sea Alien Species Database. S. Olenin, E. Leppakoski and D. Daunys (eds.). available at http://www.corpi.ku.lt/nemo/balanus.html. Created online 2005.

[84] **A. Nasrolahi, F. Farahani and S. J. Saifabadi.** Effect of salinity on larval development and survival of the caspian sea barnacle, *Balanus improvisus* Darwin (1854). *Journal of Biological sciences*, 6(6) : 1103−1107, **2006**.

[85] **A. N. Cohen.** Guide to the Exotic Species of San Francisco Bay. San Francisco Estuary Institute, Oakland, CA. **2005**.

[86] **D. V. Desai, A. C. Anil and K. Venkat.** Reproduction in *Balanus amphitrite* Darwin (Cirripedia: Thoracica): influence of temperature and food concentration. *Marine Biology*, 149: 1431−1441, **2006**.

[87] **E.L. Charnov.** Sexuality and Hermaphroditism in barnacles: a natural selection approach. Crustacean Issues 5. *Barnacle Biology*. AA Balkema, Rotterdam, 89−104, **1987**.

[88] **E. R. Furman and A. V. Yule.** Self-fertilization in *Balanus improvisus* Darwin. *Journal of Experimental Marine Biology and Ecology*, 144: 235−239, **1990**.

[89] **M. M. El-Komi and T. Kajihara.** Breeding and moulting of barnacles under rearing conditions. *Journal of marine biology*, 108: 83−89, **1991**.

[90] **G. Walker and A. B. Yule.** Temporary adhesion of the barnacle cyprid: the existence of an antennular adhesive secration. *Journal of marine biology*, 64: 679−686, **1984**.

[91] **R. Saroyan, E. Lindner and C. A. Dooley.** Repair and reattachment in the balanidae as related to their cementing mechanism, *The Biological Bulletin*, 139: 333−350, **1970**.

[92] **N. Aldred and A. S. Clare.** Mechanisms and principles underlying temporary adhesion, surface exploration and settlement site selection by barnacle cyprids: a short review. In: Gorb S, editor. *Functional surfaces in biology*. New York: Springer-Verlag, **2009**.

[93] **E. Lindner.** The attachment of macrofouling invertebrates. In: Cost low JD, Tipper RC, editors. *Marine biodeterioration*: an interdisciplinary study. Annapolis: Naval Institute Press, 183–201, **1984**.

[94] **H. Barnes.** A review of some factors affecting settlement and adhesion of some common barnacles. In: Manly RS, editor. *Adhesion in biological systems*. New York, London: Academic Press, 89–111, **1970**.

[95] **N. C. Lagersson and J. T. Høeg.** Settlement behavior and antennulary biomechanics in cypris larvae of *Balanus amphitrite* (Crustacea: Thecostraca: Cirripedia). *Journal of marine biology*, 141, 513–526, **2002**.

[96] **I. Y. Phang, N. Aldred, A. S. Clare, J. A. Callow and G. J. Vancso.** Towards a nanomechanical basis for temporary adhesion in barnacle cyprids (*Semibalanus balanoides*). *Journal of Royal Society Interface*, 5: 397–401, **2008**.

[97] **G. Huber, H. Mantz, R. Spolenak, K. Mecke, K. Jacobs, S. N. Gorb and E. Arzt.** Evidence for capillarity contributions to gecko adhesion from single spatula nanomechanical measurements. *Proceedings of the National Academy of Science, USA*, 102: 16293–16295, **2005**.

[98] **G. Walker.** Marine organisms and their adhesion. In Synthetic adhesives and sealants (ed. W. C. Wake), *Chichester, UK*: Wiley, 112–135, **1987**.

[99] **G. Walker.** Cirripedia. In: Harrison FW, Humes AG, eds. Microscopic anatomy of the invertebrates: *Crustacea. New York*: Wiley, 9: 249–311, **1992**.

[100] **D. J. Crisp.** Settlement responses in marine organisms. In Adaptation to the environment: essays on the physiology of marine animals (ed. R. C. Newell), London, UK: Butterworth, 83–124, **1976**.

[101] **C. Dreanno, R. R. Kirby, and A. S. Clare.** Locating the barnacle settlement pheromone: spatial and ontogenetic expression of the settlement-inducing protein complex of *Balanus amphitrite*. *Proceedings of the Royal Society B:* 273: 2721–2728, **2006b**

[102] **C. Dreanno, K. Matsumura, N. Dohmae, K. Takio, H. Hirota, R. R. Kirby, A. S. Clare.** A novel alpha 2-macroglobulin-like protein is the cue to gregarious settlement of the barnacle, *Balanus amphitrite*. *Proceedings of the National Academy of Science, USA*. 103:14396–14401, **2006c**.

[103] **A. S. Clare, and K. Matsumura**. Nature and perception of barnacle settlement pheromones. *Biofouling*, 15: 57–71, **2000**.

[104] **G. Walker**. A Study of the cement apparatus of the cypris larva of the barnacle *Balanus balanoides*. *Journal of Marine Biology*. 9: 205–212, **1971**.

[105] **K. Odling, C. Albertsson, J. T. Russell, L. G. E. Martensson**. An in vivo study of exocytosis of cement proteins from barnacle *Balanus improvisus* cyprid larvae. *Journal of Experimental Biology*. 209:956–964, **2006**.

[106] **I. Y. Phang, N. Aldred, A. S. Clare, J. A. Callow, G. J. Vancso**. An *in situ* study of the nanomechanical properties of barnacle (*Balanus amphitrite*) cyprid cement using atomic force microscopy (AFM). *Biofouling*. 22:245–250, **2006**.

[107] **K. Kamino, Y. Shizuri**. Structure and function of barnacle cement proteins. In New developments in marine biotechnology, eds LeGal Y., Halvorson H. O., editors. New York: Plenum Press. 77–80, **1998**.

[108] **Y. J. Sun, S. L. Guo, G. C. Walker, C. J. Kavanagh, G. W. Swain**. Surface elastic modulus of barnacle adhesive and release characteristics from silicone surfaces. *Biofouling*. 20:279–289, **2004**.

[109] **M. Nakano, J. R. Shen, K. Kamino**. Self-assembling peptide inspired by a barnacle underwater adhesive protein. *Biomacromolecules*. 8:1830–1835, **2007**.

[110] **M. Berglin, P. Gatenholm**. The barnacle adhesive plaque: morphological and chemical differences as a response to substrate properties. *Colloids and Surfaces B: Biointerfaces*, 28: 107–117, **2003**.

[111] **IY Phang, N Aldred, AS Clare, GJ Vancso**. Develop- ment of effective marine antifouling coatings: studying barnacle cyprid adhesion with atomic force microscopy. *Nano Science.* 1: 35–39, **2007**.

[112] **M. Pezolet, M. Pigeon-gosselin, J. Nadeau, J. P. Caille**. Laser Raman Scattering. A molecular probe of the contractile state of intact single muscle fibers. *Biophysical Journal*. 31: 1–8, **1980**.

[113] **W. Ghidalia**, in: The Biology of Crustacea: Integument, Pigments and Hormonal Processes, D. E. Bliss and L. H. Mantel (Eds.) (Academic Press, London), 301–394, **1985**.

[114] **A. Vershinin**, Biological functions of carotenoids - diversity and evolution. *BioFactors*. 10: 99–104, **1999**.

[115] **Zhang-Fan Chen, H. Wang, K. Matsumura, Pei-Yuan Qian**. Expression of calmodulin and myosin light chain kinase during larval settlement of the Barnacle *Balanus amphitrite*. *Plos one*, 7: e31337, **2012**.

[116] **A. Abbott**. Bioadhesives: potential for exploitation. *Journal of Science Progress* 74:131–146, **1990**.

[117] **A. M. Smith, J. A. Callow**. Biological adhesives. Book-Chapter 8, Springer; edition **2006**.

[118] **G. Walker**. The biochemical composition of the cement of two barnacle species, *Balanus hameri* and *Balanus crenatus*. *The Journal of the Marine Biological Association of the United Kingdom* 52: 429–435, **1972**.

[119] **K. Kamino, S. Odo, T. Maruyma**. Cement proteins of the acorn barnacle *Megabalanus rosa*. *Biological Bulletin*. 190: 403–409, **1996**.

[120] **M. J. Naldrett**. The importance of sulfur cross-links and hydrophobic interactions in the polymerization of barnacle cement. *The Journal of the Marine Biological Association of the United Kingdom* 73: 689–702, **1993**.

[121] **M. Wiegemann, B. Watermann**. Peculiarities of barnacle adhesive cured on non-stick surfaces. *Journal of Adhesion Science and Technology*. 17: 1957–1977, **2003**.

[122] **E. R. Holm, B. Orihuela, C. J. Kavanagh, D. Rittschof**. Variation among families for characteristics of the adhesive plaque in the barnacle *Balanus amphitrite*. *Biofouling*. 21: 121–126, **2005**.

[123] **E. R. Holm, C. J. Kavanagh**, **B. Orihuela**, **D. Rittschof**. Phenotypic variation for adhesive tenacity in the barnacle *Balanus amphitrite*. *Journal of Experimental Marine Biology and Ecology*. 380: 61–67, **2009**.

[124] **D. E. Wendt, G. L. Kowalke, J. Kim, I. L. Singer**. Factors that influence elastomeric coating performance: the effect of coating thickness on basal plate morphology, growth and critical removal stress of the barnacle *Balanus amphitrite*. *Biofouling*. 22:1–9, **2006**.

[125] **S. Raman, R. Kumar**. Interfacial morphology and nanomechanics of cement of the barnacle, *Amphibalanus reticulatus* on metallic and non-metallic substrata. *Biofouling*. 27: 569–577, **2011**.

[126] **W. J. Dougherty**. Barnacle Adhesion - Reattachment of the Adult Barnacle Chthamalus-fragilis darwin to Polystyrene Surfaces Followed by Centrifugational Shearing. Journal of Crustacean Biology. 10: 469−478, **1990**.

[127] **G. L. Bowlin**. Encyclopedia of biomaterials and biomedical engineering. Volume 1, 2008.

[128] **M. Wiegemann**. Adhesion in blue mussels (*Mytilus edulis*) and barnacles (*genus Balanus*): Mechanisms and technical applications. *Aquatic Sciences*, 67: 166−176, **2005**.

[129] **W. Yan, S. Pan**. The solubilising effect of denaturation chemicals on the cement of *Balanus reticulatus* Utinomi. Oceanologia et Limnologia Sinica, 12: 125−132, **1981**.

[130] **M. J. Naldrett**. The importance of sulfur cross-links and hydrophobic interactions in the polymerization of barnacle cement. *Journal of marine biology* Association. U.K. 73: 689–702, **1993**.

[131] **H. Nakashima, K. Nishikawa, T. Ooi**. Distinct character in hydrophobicity of amino acid composition of mitochondrial proteins, *Proteins E*: 173–178, **1990**.

[132] **M. J. Naldrett, D. L. Kaplan**. Characterization of barnacle (*Balanus eburneus* and *B. cenatus*) adhesive proteins. *Marine Biotechnolog*. 127: 629–635, **1997**.

[133] **K. Kamino**. Novel barnacle underwater adhesive protein is a charged amino acid–rich protein constituted by a cys-rich repetitive sequence. *Biochemical Journal*. 356: 503–507, **2001**.

[134] **D. E. Barlow, G. H. Dickinson, B. Orihuela, D. Rittschof, K. J. Wahl**. *In situ* ATR-FTIR characterization of primary cement interfaces of the barnacle *Balanus amphitrite*. *Biofouling*. 25: 359–366, **2009**.

[135] **M. Berglin, J. Hedlund, C. Fant, H. Elwing**. Use of surface-sensitive methods for the study of adsorption and cross-linking of marine bioadhesives. *Journal of Adhesion*. 81: 805–822, **2005**.

[136] **M. Wiegemann, T. Kowalik, A. Hartwig**. Noncovalent bonds are key mechanisms for the cohesion of barnacle (*Balanus crenatus*) adhesive proteins. *Marine Biology*. 149: 241–246, **2006**.

[137] **D. M. Fowler, A. V. Koulov, W. E. Balch, J. W. Kelly**. Functional amyloid—from bacteria to humans. *Trends in Biochemical Science*. 32: 217–223, **2007**.

[138] **A. S. Mostaert, C. Giordani, R. Crockett, U. Karsten, R. Schumann, S. P. Jarvis**. Characterisation of amyloid nanostructures in the natural adhesive of unicellular subaerial algae. *Journal of Adhesion*. 85: 465–483, **2009**.

[139] **G. Zandomeneghi, M. R. H. Krebs, M. G. McCammon, M. Fandrich**. FTIR reveals structural differences between native β-sheet proteins and amyloid fibrils. *Protein Science*. 13: 3314–21, **2004**.

[140] **K. Kamino, K. Inoue, T. Maruyama, N. Takamatsu, S. Harayama, Y. Shizuri**. Barnacle cement proteins—importance of disulfide bonds in their insolubility. *Journal of Biological Chemistry*. 275: 27360–27365, **2000**.

[141] **D. B. Ramsay, G. H. Dickinson, B. Orihuela, D. Rittschof, K. J. Wahl**. Base plate mechanics of the barnacle *Balanus amphitrite*. *Biofouling.* 24: 109–118, **2008**.

[142] **M. Wiegemann, B. Watermann**. The impact of desiccation on the adhesion of barnacles attached to non-stick coatings. *Biofouling*. 20: 147–53, **2004**.

[143] **L. Khandeparker, A. C. Anil**. Underwater adhesion: The barnacle way. *International Journal of Adhesion and Adhesives*, 27: 165–172, **2007**.

[144] **F. Peters, M. Epple**. Simulating arterial wall calcification *in vitro*: biomimetic crystallization of calcium phosphates under controlled conditions. *Zeitschrift für Kardiologie*. 90: 81–85, **2001**.

[145] **G. Guillemin, J. L. Patat, J. Fournie, M. Chetail**. The use of coral as a bone graft substitute. *Journal of Biomedical Materials Research*. 5: 557–567, **1987**.

[146] **L. Khandeparker, A. C. Anil, S. Raghukumar**. Relevance of biofilm bacteria in modulating the larval metamorphosis of *Balanus amphitrite*. *FEMS Microbiology Ecology*. 58: 425–438, **2006**.

[147] **Q. J. Ang, J. X. C. Lee, J. H. T. Sng, C. Y. S. Hsu, G. H. Dickinson**. Potential of barnacle cement in dentistry. *Innovation Magazine*. 10: 14–19, **2011**.

[148] **R. R. Despain, K. L. De Vries, R. D. Luntz, M. L. Williams**. Comparison of the strength of barnacle and commercial dental cements. *Journal of Dental Research*, 52: 674–679, **1973**.

[149] **R. W. Phillips**. Bonding agents and adhesives. *Advances into Dental Research*, 2: 150–154, **1988**.

[150] **G. M. Whitesides, M. Bonchcva.** Beyond molecules: self-assembly of mesoscopic and macroscopic components. *Proceeding of the National Academy of the USA (PNAS)*, 99: 4769–4774, **2002**.

[151] **J. H. Waite, M. L. Tanzer**. Polyphenolic Substance of Mytilus- Edulis - Novel Adhesive Containing L-Dopa and Hydroxyproline. *Science*, 212: 1038−1040, **1981**.

[152] **J. P.Visscher**. Reaction of the cyprid larvae of barnacles at the time of attachment. *Biology Bulletin*. 54: 327–335, **1928**.

[153] **D. R. Houghton**, Marine anti-fouling. *Underwater Science and Technology*. 2: 100–105 **1970**.

[154] **W. Suëtaka**. Surface infrared and Raman spectroscopy. Methods and Applications. Methods of Surface Characterization, Vol. 3, XIII, 270 P, **1995**.

[155] **K. Umbach**. Raman: theory and Instrumentation. http://www.ccmr.cornell.edu/igert/modular/docs/Raman_Scattering.pdf Accessed 12.12.2013.

[156] **T. Jue**, Biomedical Applications of Biophysics. *Handbook of Modern Biophysics*, Humana Press, Volume 3, **2010**.

[157] **R. Salzer, and H. W. Siesler**. (eds) (**2009**) Index, in Infrared and Raman Spectroscopic Imaging, Wiley-VCH Verlag GmbH & Co. KGaA, Weinheim, Germany. doi: 10.1002/9783527628230.index.

[158] **Lewis, I. R., and Edwards**, H. Handbook of Raman spectroscopy: from the research laboratory to the process line. CRC Press, 28, **2001**.

[159] Selection Rules: http://www.raman.de/htmlEN/basics/selectEng.html Accessed 12.12.2013.

[160] Combined Atomic Force Microscopy & Raman Spectroscopy – TERS and Co-Located AFM-Raman Systems, *The A to Z of Nanotechnology (Azonano.com)*: http://www.azonano.com/article.aspx?ArticleID=2943 Accessed 12.12.2013.

[161] **Bruker**. Flex Focus Description. http://www.bruker.com/fileadmin/user_upload/1-Products/Infrared_Spectrospcopy/Raman/FlexFocus/Conventional_confocal_microscope_optics.jpg Accessed 12.12.2013.

[162] **P. R. Carey**. Raman and resonance Raman spectroscopy. In Modern Physical Methods in Biochemistry, Part B, ed. ANeiberger, LMvan Deenan, Dordrecht: Elsevier, 27–64, **1988**.

[163] **R. Tuma**. Raman spectroscopy of proteins: from peptides to large assemblies. *Journal of Raman Spectroscopy*. 36: 307–19, **2005**.

[164] **W. L. Peticolas**. Raman-spectroscopy of DNA and proteins. In Biochemical Spectroscopy, ed. KSauer, San Diego: Academic, 389–416, **1995**.

[165] **J. T. Pelton, L. R. McLean**. Spectroscopic methods for analysis of protein secondary structure. *Analytical Biochemistry*. 277: 167–76, **2000**.

[166] **J. Bandekar**. Amide modes and protein conformation. *Biochimica Biophysica Acta (BBA),* 1120: 123–43, **1992**.

[167] **W. L. Peticolas**. Raman-spectroscopy of DNA and proteins. In Biochemical Spectroscopy, ed. KSauer, San Diego: Academic, 389–416, **1995**.

[168] **K. Tsuji, J. Injuk, R.V. Grieken**. X-Ray Spectrometry: Recent Technological Advances. **2004**.

[169] KIT - ANKA -Synchrotron: ANKA - Beamlines - Hard X-ray Spectroscopy – FLUO. http://www.anka.kit.edu/english/979.php Accessed 12.12.2013.

[170] **R. F. Egerton**. Physical Principles of Electron Microscopy. An Introduction to TEM, SEM and AEM. *Springer*, **2005**.

[171] Background information - What is scanning electron microscopy? My Scope: http://www.ammrf.org.au/myscope/sem/background/#detail. Accessed 12.12.2013.

[172] **J. B. Pawley**. Handbook of Biological Confocal Microscopy, *Springer*, 3rd ed., **2006**.

[173] **S. Wilhelm, B. Groebler, M. Gluch, H. Heinz**. Microscopy from Carl Zeiss. Confocal Laser Microscopy. Principles, ZEISS.

[174] Keyence. VK Viewer Reference Manual. Color 3D Laser Microscope. VK-9700K/VK-8700K.

[175] **M. Berjot, J. Marx, A. J. P. Alix**. Determination of the secondary structure of proteins from the Raman amide I band: The reference intensity profiles method. *Journal of Raman Spectroscopy*. 18: 289–300, **1987**.

[176] **L. Liu, T. P. Mernagh**. Phase transitions and Raman spectra of calcite at high pressures and room temperature. *American Mineralogist*. 75: 801–806, **1990**.

[177] **B. W. Barry, H. G. M. Edwards, A. C. Williams.** Fourier transform Raman and infrared vibrational study of human skin: Assignment of spectral bands. *Journal of Raman Spectroscopy*. 23: 641–645, **1992**.

[178] **G. J. Jr. Thomas**, Raman spectroscopy of protein and nucleic acid assemblies. *Annual Review of Biophysics and Biomolecular Structure*. 28: 1–27, **1999**.

[179] **R. Loudon**. The Raman effect in crystals. *Advances in Physics*. 13: 423–482, **1964**.

[180] **. Winter, F. Noll**. Methoden der biophysikalisch Chemie, Chapter 5. Noll.-Stuttgart: Teubner, **1998**.

[181] **N. B. Colthup, L. H. Daly, S. E. Wibereley**. Introduction to infrared and Raman spectroscopy, 3rd ed.; New York, **1990**.

[182] **D. Lin-Vien, N. B.Colthup, W. G. Fateley, J. G. Grasselli**. Infrared and Raman characteristic frequencies of organic molecules, 1st ed.; San Diego: California, **1991**.

[183] **Z. H. Chi, X. G. Chen, Holtz, S. A. Asher**. UV resonance Raman-selective amide vibrational enhancement: quantitative methodology for determining protein secondary structure. *Biochemistry*. 37: 2854–64, **1998**.

[184] **E. Bourget, D. J. Crisp**. An analysis of growth bands and ridges of barnacle shell plate. *Jourrnal of marine Biology*. 554: 39–461, **1975**.

[185] **W. Kabsch, C. Sander**. Dictionary of protein secondary structure: Pattern recognition of hydrogen-bonded and geometrical features. *Biopolymers*. 22: 2577–2637, **1983**.

[186] **M. Jonathan**. Exon shuffling, and the origins of protein folds. Evolution News and Views. http://www.evolutionnews.org/2013/07/exon_shuffling074401.html. July 15, **2013**.

[187] **L. Brocchieri, S. Karlin**. "Protein length in eukaryotic and prokaryotic proteomes". *Nucleic Acids Research.* 33: 3390–3400, **2005**

[188] **M. Berjot, J. Marx, A. J. P. Alix**. Determination of the secondary structure of proteins from the Raman amide I band: The reference intensity profiles method. *Journal of Raman Spectroscopy*., 18: 289–300, **1987**.

[189] **L. Xie, C. Tsou**. Comparison of Secondary Structures of Insulin and Proinsulin by FTIR. *Journal of protein Chemistry*. 12: 483–487, **1993**.

[190] **N. Gediminas**. Raman spectroscopy in analysis of biomolecules. Encyclopedia of analytical chemistry, Niaura, G. **2008**.

[191] **k. R. Ackermann, J. Koster, S. Schluecker**. Polarized Raman microspectroscopy on intact human hair. *Journal of Biophoton*. 5: 419–424, **2008**.

[192] **M. M. Apetri, N. C. Maiti, M. G. Zagorski, P. R. Carey, V. E. Anderson**. Secondary Structure of α-Synuclein Oligomers: Characterization by Raman and Atomic Force Microscopy. *Journnal of Molecular Biology*. 355: 63–71, **2006**.

[193] **N. A. Nousek**. Shell formation and calcium transport in the barnacle *Chthamalus fragilis. Tissue and Cell*. 16: 433–442, **1984**.

[194] **D. Maruzzo, N. Aldred, A. S. Clare, J. T. Høeg**. Metamorphosis in the cirripede crustacean *Balanus amphitrite*. *In: PloS one.* 7: e37408, **2012**.

[195] **V. Sikirzhytski, N. I. Topilina, S. Higashiya, J. T. Welch, I. K. Lednev**. Genetic engineering combined with deep UV resonance Raman spectroscopy for structural characterization of amyloid-like fibrils. *Journal of the American Chemical Society*. 130: 5852–5853, **2008**.

[196] **A. Elhaddaoui, E. Pigorsch, A. Delacourte, S. Turrell**. Spectroscopic investigations of synthetic beta amyloid peptides of Alzheimer's disease. *Journal of Molecular Structure*. 347: 363–370, **1995**.

[197] **N. I. Bishop**. The β-carotenoid, lutein, is specifically required for the formation of the oligomeric forms of the light harvesting complex in the green alga, scenedesmus obliquus. *Journal of Photochemistry and Biology B*: *Biology*. 36: 279–283, **1996**.

[198] **D. Hockett, P. Ingram, A. LeFurgey**. Strontium and manganese uptake in the barnacle shell: electron probe microanalysis imaging to attain fine temporal resolution of biomineralization activity. *In: Marine environmental research*. 43: 131–143, **1997**.

[199] **D. Holland, G. Walker**. The biochemical composition of the cypris larva of the barnacle *Balanus balanoides* L. *Journal du Conseil*. 36: 162–165, **1975**.

[200] **H. Barnes, W. Klepal, B. Mitchell**. The organic and inorganic composition of some cirripede shells. *Journal of Experimental Marine Biology and Ecology*. 21: 119–127, **1976**.

[201] **E. Bourget, D. J. Crisp**. Factors affecting deposition of the shell in *Balanus balanoides* (L). *Journal of the Mrine Biological association of the U. K*. 55: 231–249, **1975b**.

[202] **S. W. Taylor, D. B. Chase, M. H. Emptage, M. J. Nelson, J. H. Waite**. Ferric ion complexes of a DOPA-containing adhesive protein from Mytilusedulis. *Inorganic Chemistry*. 35: 7572–7577, **1996**.

[203] **S. W. Taylor, J. H. Waite, M. M. Ross, J. Shabanowitz, D. F. Hunt**. trans-2,3-cis-3,4-Dihydroxyproline, a new natu- rally occurring amino acid, is the sixth residue in the tandemly repeated consensus decapeptides of an adhesive protein from Mytilusedulis. *Journal of the American Chemical Society*. 116: 10803–10804, **1994**.

[204] **C. Fant, K. Scott, H. Elwing and F. Höök**. Adsorption behavior and enzymatically or chemically induced cross-linking of a mussel adhesive protein. *Biofouling*. 16: 119–132, **2000**.

[205] **M. J. Sever, J. T. Weisser, J. Monahan, S. Srinivasan, J. J. Wilker**. Metal-mediated cross-linking in the generation of a marine-mussel adhesive. *AngewandteChemie* 116: 454–456, **2004**.

Acknowledgement

Foremost, I would like to express my sincere gratitude to my advisors **Prof. Michel Grunze** and **Prof. Axel Rosenhahn** for their continuous support of my Ph.D. study and research, for their patience, motivation and immense knowledge. Their guidance helped me in all the time of research and writing of this thesis. I could not have imagined having a better advisors and mentors for my Ph.D. study. Additionally, I thank both of them for their numerous wise and consistent corrections of this thesis.

I would like to thank both Heidelberg University and Karlsruhe Institute of Technology (KIT) for providing a benign environment and great facilities to work on this project. The financial support from the European Community's Seventh Framework Programme FP7/2007–2013 under Grant Agreement number 237997 (SEACOAT) is acknowledged, as well as support by the Office of Naval Research (N000141210498) and the Virtual Institute VH-VI403 and the Biointerfaces program of the Helmholtz Society.

I sincerely acknowledge stimulating discussions with **Dr. David Moss** (KIT). I would like to thank **Mr. Stefan Heissler** (KIT) heartfully for his help in mastering the principles of Raman spectrosopy and his great guideness in taming the Raman spectroscopy device and his time and efforts in discussing the results. Moreover, I would like to thank **Dr. Rolf Simon, Dr. David Batchelor** and my colleague **Tobias Senkbeil** for their help, support in XRF experiments and discussion of the results (KIT, ANKA). Additional gratitude goes to **Dr. Carlos Azucena** for his help in SEM.

My sincere thanks goes to **Prof. Anthony S. Clare, Dr. Nick Aldred** and **Mr. Alessio Di Fino** for hospitable welcoming me two times at their Institute (School of Marine Science and Technology, Newcastle University, UK), preparation and shipment of cyprid larva and continuous support in biology questions.

Furthermore, I would like to thanks **Prof. Dr. James Callow** and **Prof. Dr. Maureen Callow** for interesting and fruitful discussions during the SECOAT meetings.

I thank all my IFG colleagues and friends for their help and support during these years.

Finally, I would like to thank my parents for their encouragement and endless support, and providing me good studying and working environment. Great thanks goes to **Alina Spiridonova**, for profound language corrections.

Erklärung

Ich erkläre hiermit an Eides Statt, dass ich die vorliegende Dissertation selbst verfasst und mich dabei keiner anderen als der von mir bezeichneten Quellen und Hilfsmittel bedient habe. Ich habe an keiner anderen Stelle ein Prüfungsverfahren beantragt bzw. die Dissertation in dieser oder anderer Form bereits anderweitig als Prüfungsarbeit verwendet oder einer anderen Fakultät als Dissertation vorgelegt.

Heidelberg, den 30.05.2014 .....

(Tawheed Mohamed)